



**Politecnico
di Torino**

Politecnico di Torino

Master's Degree in Civil Engineering
Academic Year 2022/2023
Graduation Session October 2023

Transfer Learning between Full-Scale Structure Health Monitoring Systems: Application to Oval Masonry Domes

Supervisor:

Prof. Rosario Ceravolo

Candidate:

Cavanni Valeria s296491

Co-Supervisors:

Dr. Giorgia Coletta

Dr. Gaetano Miraglia

Dr. Linda Scussolini

To my mother.

Abstract

Structural Health Monitoring (SHM) is a powerful instrument used by engineers to analyze the actual condition of the structure under observation. The data that can be obtained with SHM systems, whether static or dynamic, are many and, as a result, are difficult to manage by hand. For this reason, researchers in recent years have increasingly begun to work with artificial intelligence (AI) for data processing and interpretation. AI attempts to replicate the logical flow of a human being but, unlike a human, it can process much more data and much faster. Various algorithms, such as Machine Learning (ML) algorithms and Transfer Learning (TL) algorithms have already been introduced in the processing of monitoring data. However, these algorithms require as input a labelled dataset, this means that at each data is necessary to associate a label that define the structural conditions (e.g., ‘damaged’ or ‘undamaged’), this is the learning process of the algorithm. Summing up it is possible to say that the model cannot identify a damage if it has never seen a damage. The need of labelled data is an important limit of these models because it is not possible to deliberately damage the structure to obtain data that can be labelled as ‘damaged’, especially if the structure under investigation is part of Cultural Heritage.

In this view, TL, particularly the branch of Domain Adaptation algorithms, becomes essential. These models share knowledge among different domains, that can represent homogeneous or heterogeneous structures. Since, not much labelled data on the real structure are available, it is possible to obtain them from a calibrated Finite Element Model (FEM) by running several simulations. In this case, the domain obtained from the FEM is called Source Domain, while the domain of the real structure is the Target Domain. However, these two domains cannot be considered as a unique one, indeed no matter how calibrated the model is it will never represent the reality, indeed “*all models are wrong, but some are useful*” [George Box]. This leads to having to use domain adaptation algorithms, in such a way to reduce the ‘distance’ between the two domains. Another possibility, in the case of lack of labelled data for the structure under observation, is to use information and data coming from other structures, that are somehow similar to the one of interest. In this view, the structure under observation represents the Target Domain, while all the other structures make up the Source Domain, which will share its knowledge with the Target one.

In this thesis a TL algorithm is used to understand if a transfer of knowledge is possible between data of the *Sanctuary of Vicoforte* and those of the *Church of Santa Caterina*, two architectural heritage structures both characterized by an oval dome, although of different sizes, and with different plan developments. Therefore,

these two structures define a Heterogeneous Population. Specifically, the transfer learning algorithm used is a Domain Adaptation approach for binary and multi-class classification, known as Kernelized-Bayesian-Transfer-Learning. In this view, a first application is developed to identify damages in different elements of two churches, but only at the level of their finite element models. Subsequently, the same algorithm is used to analyze data coming from the monitoring systems on the two real structures, but in this case the classes concern the temperature states instead of damage conditions, because fortunately no damaged data are available.

Contents

List of Figures	V
List of Tables	X
Introduction.....	1
Chapter 1	3
1. The role of machine learning and transfer learning algorithms for structural health monitoring.....	3
1.1 Structural Health Monitoring.....	3
1.1.1 Introduction.....	3
1.1.2 Definition of damage	4
1.1.3 Vibration-Based Structural Health Monitoring	5
1.1.4 Model-driven and Data-driven approaches for SHM	7
1.1.5 Environmental effects	8
1.2 Machine Learning	9
1.2.1 Machine Learning definitions.....	9
1.2.2 Supervised and Unsupervised ML	10
1.2.3 Underfitting and Overfitting in supervised ML.....	12
1.3 Transfer Learning with Domain Adaptation Algorithm.....	14
1.3.2 Domain Adaptation approaches.....	15
1.4 Prediction errors.....	17
Chapter 2.....	19
2. Transfer learning approaches for structural health monitoring of architectural heritage.....	19
2.1 Population-Based SHM	19
2.1.1 The lack of labelled data for damaged states	20
2.1.2 Homogeneous and Heterogeneous populations.....	21
2.1.3 Transfer Learning between the real structure and its FEM, the case of the Sanctuary of Vicoforte	23
Chapter 3.....	29
3. Kernelized Bayesian Transfer Learning	29
3.1 The concepts behind the algorithm.....	29
3.2 Binary classification problems.....	32
3.2.1 Application of KBTL for binary problem in literature: damage detection.....	37

3.3 Multiclass classification problems.....	41
3.3.1 Application of KBTL for multiclass problem in literature: damage detection.....	43
Chapter 4.....	46
4. Transfer Learning technique (KBTL) applied to oval masonry domes for damage detection	46
4.1 Case study	46
4.1.1 Sanctuary of Vicoforte – Source Domain.....	46
4.1.2 Church of Santa Caterina – Target Domain.....	52
4.2 KBTL applied to data from the finite element models for damage localization.....	60
4.2.1 Domains and Labels.....	60
4.2.2 Results.....	64
4.3 KBTL applied to data from the finite element models for the definition of the damage level: slight, medium and serious	66
4.3.1 Domains and Labels.....	66
4.3.2 Results.....	69
Chapter 5.....	72
5. Transfer learning technique (KBTL) applied to oval masonry domes for the temperature states identification	72
5.1 Case study – Accuracy analysis.....	72
5.1.1 Experimental data from the monitoring system of the Sanctuary of Vicoforte	72
5.1.2 ‘Semi-Experimental’ data for the Church of Santa Caterina.....	73
5.1.3 Domains and Labels.....	79
5.1.4 Accuracy study by varying the number of observations of the source domain, the case of Target 1	82
5.1.5 Accuracy study by varying the number of observations of the source domain, the case of Target 2	87
5.2 Case study – Identification of four temperature classes	94
5.2.1 ‘Semi-Experimental’ data for the Church of Santa Caterina.....	94
5.2.2 Domains and Labels.....	97
5.2.3 Results.....	100
Conclusions.....	105
List of Abbreviations	108
References.....	109

List of Figures

Figure 1: Data-Driven and Model-Driven Methods (Ceravolo, Pistone, Zanotti Fragonara, Masetto, & Abbiati, 2016).....	8
Figure 2: Classification (Left side, (ii)) and Regression (Right side, (i)) (Classificatore vs Regressione quale usare? Machine learning esempi pratici, n.d.)	11
Figure 3: Clustering problem (i) (Machine Learning with ML.NET – Complete Guide to Clustering, n.d.).....	12
Figure 4: Example of Overfitting, right fitting and Underfitting (MathWorks, n.d.)	13
Figure 5: Logical process of the K-fold validation technique (Nellihela, 2022)...	14
Figure 6: An illustration of how DA techniques can increase the accuracy for the prediction in the target domain. The feature distributions of the SD and TD are compared, with the original feature distributions on the left and the new feature distributions on the right (Khan, et al., 2023)	16
Figure 7: Categories for the definition of the heterogeneity within a population (Gardner, Bull, Gosliga, Dervilis, & Worden, 2020)	22
Figure 8: Sanctuary of Vicoforte (GT, 2016)	24
Figure 9: Graphical representation of the Target Domain for the Sanctuary of Vicoforte, representative of the two temperature classes: 3°C and 10°C (Coletta, et al., 2021)	25
Figure 10: Multi-physics model of the Sanctuary of Vicoforte (Coletta, et al., 2021).....	26
Figure 11: Graphical representation of the Source Domina for the Sanctuary of Vicoforte representative of the two temperature classes: 3°C and 10°C (Coletta, et al., 2021)	26
Figure 12: RVM classifier (a) and TCA+RVM classifier (b) for the predictions of the two temperature classes: 3°C and 10°C for the Sanctuary of Vicoforte (Coletta, et al., 2021)	27
Figure 13: Comparison between the first (a) and second (b) natural frequencies experimentally identified and the simplified Frequency-Temperature Model	28
Figure 14: Representation of the conceptual flow for KBTL algorithm (Gardner, Bull, Gosliga, Dervilis, & Worden, 2020).....	31
Figure 15: Graphical model of KBTL for binary classification with all priors, hyperparameters, latent variable and model parameters (Gönen & Margolin, 2014)	32
Figure 16: Experimental shear-structures (Gardner, Bull, Dervilis, & Worden, 2022)	38
Figure 17: Simulated shear-structures: (a) connection among the masses by means of dampers and springs; (b) cantilever component of the simulated structures (Gardner, Bull, Dervilis, & Worden, 2022).....	38
Figure 18: Properties of the six lumped-mass simulated structures (Gardner, Bull, Dervilis, & Worden, 2022)	38

Figure 19: Training and Test dataset for the damage detection, from 1 to 6 are the simulated frames while the 7 th is the experimental one, binary classification (Gardner, Bull, Dervilis, & Worden, 2022).....	39
Figure 20: Training Phase of KBTL for PBSHM, the shear-structures case (Gardner, Bull, Dervilis, & Worden, 2022).....	40
Figure 21: Test Phase of KBTL for PBSHM, the shear-structures case (Gardner, Bull, Dervilis, & Worden, 2022)	40
Figure 22: Graphical Model of KBTL for multiclass classification (Gönen & Margolin, 2014)	43
Figure 23: Training and Test dataset for the damage detection, from 1 to 6 are the simulated frames while the 7 th is the experimental one, multiclass classification (Gardner, Bull, Dervilis, & Worden, 2022).....	44
Figure 24: Training Phase of KBTL for multiclass classification of damages (Gardner, Bull, Dervilis, & Worden, 2022).....	45
Figure 25: Test Phase of KBTL for multiclass classification of damages (Gardner, Bull, Dervilis, & Worden, 2022)	45
Figure 26: Static Monitoring System at the Sanctuary of Vicoforte (2004-2014) (Ceravolo, Coletta, Miraglia, & Palma, 2021).....	48
Figure 27: Dynamic Monitoring System at the Sanctuary of Vicoforte - Accelerometers Location (Ceravolo, Coletta, Miraglia, & Palma, 2021)	48
Figure 28: FEM of the Sanctuary of Vicoforte with the representation in different colors of the nine macro-elements (Ceravolo, De Lucia, Miraglia, & Pecorelli, 2020).....	49
Figure 29: Limited FEM of the Sanctuary of Vicoforte for the Thermal Analysis (Ceravolo, De Lucia, Miraglia, & Pecorelli, 2020)	50
Figure 30: First three mode shape of the Sanctuary of Vicoforte obtained with the FEM, (a) first flexural mode in Y direction, (b) first flexural mode in X direction and (c) first torsional mode. The red curves are representative of the undeformed dome.....	51
Figure 31: External (left) and Internal (right) view of the Church of Santa Caterina, in the upper right corner is shown the dome, while in the bottom right corner the chore (La Chiesa, 2021).....	52
Figure 33: Longitudinal section (left) and Front view (right) of Santa Caterina's Church drawings (Ceravolo, Lenticchia, Miraglia, & Scussolini)	53
Figure 32: Church and Chore of the structure of Santa Caterina's Church (Ceravolo, Lenticchia, Miraglia, & Scussolini).....	53
Figure 34: Mechanical Model of the Church of Santa Caterina	54
Figure 35: Setups of the dynamic campaign at the Church of Santa Caterina. (a) Dome YZ (b) Dome XZ (c)Global and (d) Link (Ceravolo, Lenticchia, Miraglia, & Scussolini).....	55
Figure 36: Model updating of the Church of Santa Caterina to consider the realized strengthening interventions (Ceravolo, Lenticchia, Miraglia, & Scussolini).....	57
Figure 37: Setups for the dynamic monitoring of December 2022, January-March 2023 of the Church of Santa Caterina (Ceravolo, Lenticchia, Miraglia, & Scussolini).....	57

Figure 38: Updated elastic modulus of the six macro-elements of the Church of Santa Caterina (Ceravolo, Lenticchia, Miraglia, & Scussolini)	58
Figure 39: Identified modes after the strengthening intervention of the Church of Santa Caterina (Ceravolo, Lenticchia, Miraglia, & Scussolini)	59
Figure 40: Simulated Data for damage identification for the Church of Santa Caterina	61
Figure 41: Simulated Data for damage identification for the Sanctuary of Vicoforte	61
Figure 42: Target Domain (Church of Santa Caterina) for the damage identification	62
Figure 43: Test Domain (Church of Santa Caterina) for damage identification ...	63
Figure 44: Training Phase of the KBTL multi-class for damage detection	64
Figure 45: Test Phase of the KBTL multi-class for damage detection	65
Figure 46: Data simulated from the FEM of the Church of Santa Caterina, for different level of damage (on the left data from damage at the drum-dome element, on the right data from damage at the basement element)	67
Figure 47: Data simulated from FEM of the Sanctuary of Vicoforte for different level of damage (on the left data from a damage at the drum-dome element, on the right data from damage at the basement element)	67
Figure 48: Data for the Training Phase of the KBTL algorithm for the identification of the damage level	68
Figure 49: Data for the test Phase of the KBTL algorithm for the identification of the damage level	69
Figure 50: Training Phase of KBTL multi-class for the identification of the damage level	70
Figure 51: Test Phase of KBTL multi-class for the identification of the damage level	70
Figure 52: Frequency-temperature relationship for the Sanctuary of Vicoforte. (a) First bending mode f_1 , (b) First bending mode f_2 , (c) First torsional mode f_3 and (d) Spatial representation of these first three frequencies	73
Figure 53: Interpolated data for f_1 of the Church of Santa Caterina	74
Figure 54: Interpolated data for f_2 of the Church of Santa Caterina	74
Figure 55: Interpolated data for f_3 of the Church of Santa Caterina	75
Figure 56: Interpolated data for f_4 of the Church of Santa Caterina	75
Figure 57: Interpolated data for f_5 of the Church of Santa Caterina	76
Figure 58: 'Semi-Experimental' relationship between f_1 [Hz] and Temperature [°C] for the Church of Santa Caterina	77
Figure 59: 'Semi-Experimental' relationship between f_2 [Hz] and Temperature [°C] for the Church of Santa Caterina	77
Figure 60: 'Semi-Experimental' relationship between f_3 [Hz] and Temperature [°C] for the Church of Santa Caterina	78
Figure 61: 'Semi-Experimental' relationship between f_4 [Hz] and Temperature [°C] for the Church of Santa Caterina	78
Figure 62: 'Semi-Experimental' relationship between f_5 [Hz] and Temperature [°C] for the Church of Santa Caterina	79

Figure 63: Different Target Domains for the Accuracy study, (a) Target 2 composed by 30 Observations and (b) Target 1 composed by 300 Observations.	80
Figure 64: Different Source Domains for the Accuracy study, (a) VICO_300, (b) VICO_516 and (c) VICO_901	81
Figure 65: Training Phase of Model 1, on the left side the predictions of the algorithm are shown while on the right the correct labels	82
Figure 66: Test Phase of Model 1, on the left side the predictions of the algorithm are shown while on the right the correct labels	83
Figure 67: Training Phase of Model 2, on the left side the predictions of the algorithm are shown while on the right the correct labels	84
Figure 68: Test phase of Model 2, on the left side the predictions of the algorithm are shown while on the right the correct labels	84
Figure 69: Training Phase of Model 3, on the left side the predictions of the algorithm are shown while on the right the correct labels	85
Figure 70: Test Phase of Model 3, on the left side the predictions of the algorithm are shown while on the right the correct labels	86
Figure 71: Accuracy trend on target domain predictions during the training phase (red) and test phase (blue)	87
Figure 72: Training Phase of Model 1, on the left side the predictions of the algorithm are shown while on the right the correct labels	88
Figure 73: Test Phase of Model 1, on the left side the predictions of the algorithm are shown while on the right the correct labels	88
Figure 74: Training Phase of Model 2, on the left side the predictions of the algorithm are shown while on the right the correct labels	90
Figure 75: Test Phase of Model 2, on the left side the predictions of the algorithm are shown while on the right the correct labels	90
Figure 76: Training Phase of Model 3, on the left side the predictions of the algorithm are shown while on the right the correct labels	91
Figure 77: Test Phase of Model 3, on the left side the predictions of the algorithm are shown while on the right the correct labels	92
Figure 78: Accuracy trend on target domain predictions during the training phase (red) and test phase (blue)	93
Figure 79: Simulated bi-linear frequency-temperature law for the natural frequencies of the Church of Santa Caterina, (a) f1 and (b) f2	95
Figure 80: Simulated bi-linear frequency-temperature law for the natural frequencies of the Church of Santa Caterina, (c) f3, (d) f4 and (e) f5	96
Figure 81: Training and Test dataset for the Church of Santa Caterina in the planes frequency-temperature, the points circled in red are data used for the training of the algorithms, all the other are part of the test dataset	98
Figure 82: Training and Test dataset for the Church of Santa Caterina	99
Figure 83: Source Domain (Sanctuary of Vicoforte), plotted in the planes frequency-temperature, used for the training phase of the KBTL	99
Figure 84: Source Domain plotted in the space f1-f2-f3 used for the training of the KBTL	100
Figure 85: Training Phase of the KBTL model for the classification of four different temperature states	102

Figure 86: Test Phase of the KBTL model for the classification of four different temperature states 102

List of Tables

Table 1: Mistake during training and test phase (MathWorks, n.d.)	13
Table 2: Definition of a Confusion Matrix	17
Table 3: Properties of the macro-elements of the Sanctuary of Vicoforte after the model updating	50
Table 4: Comparison between frequency identified from the signal recorded with the monitoring system and frequency obtained with the FEM updated of the Sanctuary of Vicoforte (Ceravolo, De Lucia, Miraglia, & Pecorelli, 2020).....	51
Table 5: First six natural frequencies and damping ratio identified from the signal recorded during the dynamic campaign of 2010, church of Santa Caterina.....	55
Table 6: Comparison between the frequencies obtained with the updated model of the church of Santa Caterina and the frequencies obtained from the identification process on the signal recorded during the dynamic campaign of 2010	56
Table 7: Frequencies and damping ratio identified from the records of the dynamic tests on the Church of Santa Caterina, December 2022, January-March 2023 (Ceravolo, Lenticchia, Miraglia, & Scussolini).....	58
Table 8: Comparison between the frequencies obtained with the identification process (December 2022) and those obtained from the FEM of the Church of Santa Caterina	59
Table 9: Summary of the Domains used for the damage identification problem ..	63
Table 10: Accuracy for the Target and Source Domains, during both the training and test phases for the damage detection.....	65
Table 11: Accuracy for each class during the Test Phase for the damage detection	66
Table 12: Summary of Labels and number of observations for the identification of the damage level	68
Table 13: Accuracy for the Target and Source Domains, during both the training and test phases for the identification of the damage level	71
Table 14: Accuracy for each class during the Test Phase for the identification of the damage level	71
Table 15: Frequencies for three temperature values from the signal recorded during the dynamic monitoring activities at the Church of Santa Caterina.....	74
Table 16: Number of Observations for the Training and Test Phases for the two types of Target Domains.....	80
Table 17: Number of Observations for the different classes of the three possible Source Domains	81
Table 18: Accuracy for each class of temperature of the test phase of the Model 1	83
Table 19: Accuracy for each class of temperature of the test phase of the Model 2	85
Table 20: Accuracy for each class of temperature of the test phase of Model 3 ...	86
Table 21: Summary of the accuracies obtained during the accuracy analysis for the domain Target 1	86
Table 22: Accuracy of Model 1 with domain Target 2, during training and test phase	89

Table 23: Accuracy for each class of Model 1 with domain Target 2, during test phase	89
Table 24: Accuracy of Model 2 with domain Target 2, during training and test phase	91
Table 25: Accuracy for each class of Model 2 with domain Target 2, during test phase	91
Table 26: Accuracy of Model 3 with domain Target 2, during training and test phase	92
Table 27: Accuracy for each class of Model 3 with domain Target 2, during test phase	92
Table 28: Summary of the accuracies obtained during the accuracy analysis for the domain Target 2	93
Table 29: Number of observations for each class for the Domain of the Church of Santa Caterina used for the Training Phase of a simple ML algorithm, the SVM	97
Table 30: Number of observations for each class for the dataset used for the Training Phase of the KBTL, the dataset is here composed by two Domains, Target and Source	97
Table 31: Number of observations for each class for the test phase of both the algorithm, SVM and KBTL	98
Table 32: Confusion Matrix of the Test Phase of the SVM model, obtained with the MATLAB Toolbox Classification Learner.....	101
Table 33: Confusion Matrix of the Test Phase of the KBTL model.....	103
Table 34: Comparison of the accuracies obtained in the training and test phases of the two models (SVM and KBTL)	104

Introduction

In this thesis, the problem of identifying a structural condition is addressed with the help of artificial intelligence algorithms, particularly Machine Learning and Transfer Learning techniques. Some applications regard Cultural Heritage buildings, specifically masonry churches characterized by oval domes, are here present.

Nowadays there are still few applications in the literature that study the use of artificial intelligence in the field of structural health monitoring of such complex structures, but different studies concerning framed structures are present. Therefore, in the first part of the thesis an introduction to structural health monitoring and artificial intelligences is provided, along with some studies already carried out by third parties on framed structures. In the second part a Transfer Learning with Domain Adaptation is used to perform a transfer of knowledge between two architectural heritage structures.

In order to present the logical flow developed and facilitate the reading of the thesis, a brief description of the individual chapters is here presented.

Chapter 1: An introduction to the Structural Health Monitoring is developed, together with a description of the basic concepts behind Machine Learning Algorithms and Transfer Learning Algorithms.

Chapter 2: Details about the Population-Based Structural Health Monitoring and the differences between homogeneous population and heterogeneous population are reported. Then, a first application, found in the literature, of a Domain Adaptation approach applied to the data of Sanctuary of Vicoforte and those from its calibrated model follows.

Chapter 3: The concepts and the assumptions behind the Kernelized Bayesian Transfer Learning are reported, showing the binary classification problem and the multi-class classification problem, with some application found in the literature on shear-frames. This algorithm is part of the domain adaptation approaches and it allows the transfer of knowledge within a heterogeneous population.

Chapter 4: The Kernelized Bayesian Transfer Learning is used to improve knowledge of the Church of Santa Caterina exploiting knowledge of the Sanctuary of Vicoforte. Specifically, two applications are developed, the first is concerned with recognizing a state of damage (including basement damage or damage to the drum-dome system) or a state of health, starting from the natural frequencies of the structures; while the second is concerned with identifying the level of damage (slight, medium, serious) regardless of where it is located.

Chapter 5: The first steps toward transfer of knowledge between the experimental frequencies of the Sanctuary of Vicoforte and the experimental frequencies of Church of Santa Caterina are developed. In particular, an analysis on different temperature states is presented, as there are no frequencies that represent a damage condition for either of the two structures under consideration.

Chapter 1

The role of machine learning and transfer learning algorithms for structural health monitoring

1.1 Structural Health Monitoring

1.1.1 Introduction

“The terms structural health monitoring (SHM) usually refers to process of implementing a damage detection strategy for aerospace, civil or mechanical engineering infrastructure. This process involves the observation of a structure or mechanical system over time using periodically spaced dynamic response measurements, the extraction of damage-sensitive features from these measurements and the statistical analysis of these features to determine the current state of system health” (Farrar & Worden, 2012).

Structural Health Monitoring (SHM) is a branch of civil engineering that focuses its attention to the monitoring of the existing structures in order to preserve them in

time. The main reason why the monitoring activities play such an important role in the research field is that are essential for the preservation and the maintenance of the architectural heritage structure (AHS), such as historical buildings and monuments, which are a large percentage of the European structures and in particular Italian structures. Such buildings are subjected to natural deterioration of the materials and to natural phenomenon, such as earthquakes. Indeed, it is important to keep in mind that the seismic design is a quite new subject, and that most of the AHS have been designed without considering the seismic excitation. For that reason, it is necessary a monitoring activity in order to define the health status of the structure for the design of the interventions that lead to an improvement of the structural behavior, in particular against dynamic excitations, by following the principle of '*minimum interventions*' (ICOMOS, 2003).

SHM can be summarized in two main phases: (i) diagnosis, that has the purpose of evaluate the actual health condition through the collection of data from monitoring systems installed on the structure with the purpose of locate the damage and define its severity; and (ii) prognosis that leads to the prediction of the future performance by using predictive models and algorithms (Rossi & Bournas, 2023). The diagnosis phase is mainly composed by monitoring activities that consist of different techniques that measure structural parameters of interest (diagnostic characteristics), whose variation can be 'read' as a possible damage under development, hence it is important to individuate it as soon as possible so as to intervene lightly. As described in (Rossi & Bournas, 2023) the conventional SHM Techniques are (i) Direct visual inspections, that involve the examination of the crack patterns and anomalies in order to identify some potential damage mechanisms, (ii) Static monitoring systems that continuously measures stress, strain, deformation and displacement and (iii) Dynamic monitoring systems that lead to the identification of the structure's modal parameters, such as frequencies, mode shapes and damping ratios. It is important to highlight that the outputs of a dynamic monitoring system are more representative of the global behavior of the structure compared to the static ones that are based on local tests, such as crack-meters, pressure cells and load cells which give information related to the point in which they are placed. Anyway, both the monitoring systems are influenced by seasonal cycles and environmental changes, like temperature and humidity, which are reflected in fluctuations of the diagnostic characteristics.

1.1.2 Definition of damage

In (Farrar & Worden, 2012) the damage in structural and mechanical systems is defined as:

“Intentional or unintentional changes to the material and/or geometric properties of these systems, including changes to the boundary conditions and system connectivity, which adversely affect the current or future performance of these systems”.

At the nano and micro scale defects such as inclusions, voids and dislocations may not be defined damage, but in the future could be the starting point for the development of damage. Indeed, these defects can propagate and grow in scale becoming real damage. The failure condition is then reached when the damage propagation has reached a point for which the system is no longer capable of performing the function for which it was designed (Farrar & Worden, 2012).

The crack propagation is one of the typical damage presents in structural element that has to be taken under control in order to avoid the possible failure of the structure. The presence of a crack is generally reflected on some diagnostic characteristics, in particular it implies a reduction of the stiffness that can be read as a reduction of frequency. In addition, with the increment of the crack mouth opening there is evidence of an increasing reduction in stiffness, and so of the frequency. Therefore, thanks to a dynamic monitoring system it could be possible the detection of cracks, and thanks to periodic monitoring system even its growth can be identified. It is important to remember that the dynamic response is more representative of the global structural behavior, this means that it is able to reflect principally damages that occur on a global scale, therefore damages that occur on local scale are less easy to be detect by these types of monitoring.

1.1.3 Vibration-Based Structural Health Monitoring

The dynamic monitoring techniques are also known as Vibration-Based Monitoring and nowadays are one of the most used techniques for the monitoring of the existing structure for three main reasons, firstly are a non-destructive and non-invasive structural health monitoring techniques, secondly the dynamic test setups can be easily installed and removed and finally they can be performed with ambient vibrations. Moreover, starting from the signals measured in site with these approaches, it is possible to derive the natural frequencies and the modes shapes of the structure, through an identification process, which hide information about the global behavior of the structure and about the overall integrity.

The dynamic response of a structure, from which the diagnostic characteristics are identified, can be recorded continuously, periodically, or once in a while. In the case of *permanent monitoring systems*, the accelerometers are permanently installed on the structures, hence it is the most expensive solution, but it allows a *continuous control* of the structure, since the signal are recorded

continuously therefore also the variation induced by temperature, humidity or more in general by the environmental changes can be recognized together with any kind of anomalous behavior. The second case is the one of *periodic monitoring systems* for which the instruments are not permanent installed on the structure but are placed only when the measurements are needed, so the response of the structure is recorded periodically, it is important not to let too much time pass between measurements in order to be able to detect possible anomalies. Finally, when the response is measured once it means that it has been obtained with a *single non-destructive dynamic test*, this turns out to be the cheapest method, but it involves extremely poorer information; indeed, it is difficult to identify environmental effects or behavioral anomalies from it.

Subsequently, all the signals recorded are analyzed to extract the diagnostic characteristics, also known as features, and as function of the vibration parameters used as features, three different methods for the identification of a given structural condition can be used (Yang, Zhang, & Tan, 2021): (i) Frequency Domain Methods, (ii) Time Domain Methods and (iii) Time-Frequency Domain Methods.

The Frequency Domain Methods use modal parameters as frequency, mode shape and damping as features of the problem. Frequencies and mode shapes are the most used modal parameters for SHM, since when a structure is damaged this is reflected in a frequency drop, in particular higher is the frequency more significant is that drop. Frequencies can be used together with the mode shapes since they contain different information, indeed frequencies are more global indicator while the mode shapes are more sensible to local damages therefore, they contain location information, that are generally not ‘visible’ from frequencies. Also damping can be used for SHM system. Ideally, the change of damping due to local damages can be measured since the cracks can increase the friction between interfaces, but in practice this is generally hidden by measurement errors and therefore it is not so used. The frequency domain methods are the most commonly used, due to the fact that the dynamic response in frequency domain is generally more stable. Also in this thesis, this method is used, but only with the natural frequencies identified by the signal records.

The Time Domain Methods directly use the dynamic response of structure in time domain, in particular acceleration and displacement are typically used. These methods can be applied to structures subjected to stabilize environmental excitations, indeed different excitations can induce different dynamic responses, and this can lead to errors during the damage identification.

The Time-Frequency Domain Methods use as diagnostic characteristics parameters that come from both the domains, time and frequency. These methods

are more complex and articulated but are more powerful since they contain the information from the stable frequency domain but also the changes over time. The actual limit of these method are the calculation resources and the space for data storage that they required, for instance are not so commonly used.

1.1.4 Model-driven and Data-driven approaches for SHM

To perform a Vibration-Based Structural Health Monitoring, the procedures available can be classified into two main classes: model-driven methods and data-driven methods.

Data-driven methods are based on the analysis of diagnostic characteristics that can be extrapolated from the results of monitoring activities conducted on the real structure, and by managed them with Machine Learning techniques in such a way to obtain a statistical representation of the system. Generally, the data-driven methods are exploit on the results of permanent or long-term monitoring systems, since a lot of observations are available from them and so a more realistic statical representation can be obtained (Ceravolo, Pistone, Zanotti Fragonara, Masetto, & Abbiati, 2016). However, these methods have a limitation in that by relying on measurements made on the actual structure, they do not allow for data that can represent all damage conditions, but only represent the condition the structure is currently in. Therefore, if the structure is in an undamaged condition, information on possible damaged conditions cannot be obtained with these methods and so it is not easy to develop a process of damage identification.

Model-driven methods are based on the use of updated model of the structure, this required a structural model that is calibrated on results of experimental monitoring activities in order to reduce the distance between the experimental results and those simulated with the model. Indeed, models such as Finite Element Models (FEM), can be very useful to simulate different damage conditions that are not present in the real structure. But it is necessary to keep in mind that a model is only a representation of the reality, and it is always characterized by a certain level of uncertainty, since the parameters that have to be managed in a model are a lot, and it is practically impossible to calibrate all of them on the base of monitoring activities results, indeed a model is always a simplification of the reality. One of the principal limits of the model-driven methods is that, since they are based on the numerical model of the structure is difficult to take into consideration the fluctuation of the diagnostic characteristics induced by the environmental effects and by possible noises that instead are present in the diagnostic characteristics that comes from a data-driven approach.

In Figure 1 the logical flow followed by the two methods is reported. In particular, the data-driven methods take the records from the sensors and with an identification process extract the features, with which patterns are generated that will help the user to make decisions. While the model-driven approach starts with the identification process developed on the signal recorded in site, the results of this phase are used to continuously update the model of the structure, then on this updated model several simulations can be run, performing in this way a sensitivity analysis, for which the behavior of the structure is analyzed by varying some mechanical parameters, for instance by varying the elastic modulus of a component different level of damage can be simulated.

From what is stated above, it can be understood how both methods, data-driven and model-driven, have limitations in their use, however, it can also be seen how one method compensates for the other, which is why the field of SHM is also moving toward so-called *hybrid approaches*, whereby both experimental data and numerical data are used to understand the state the structure is in.

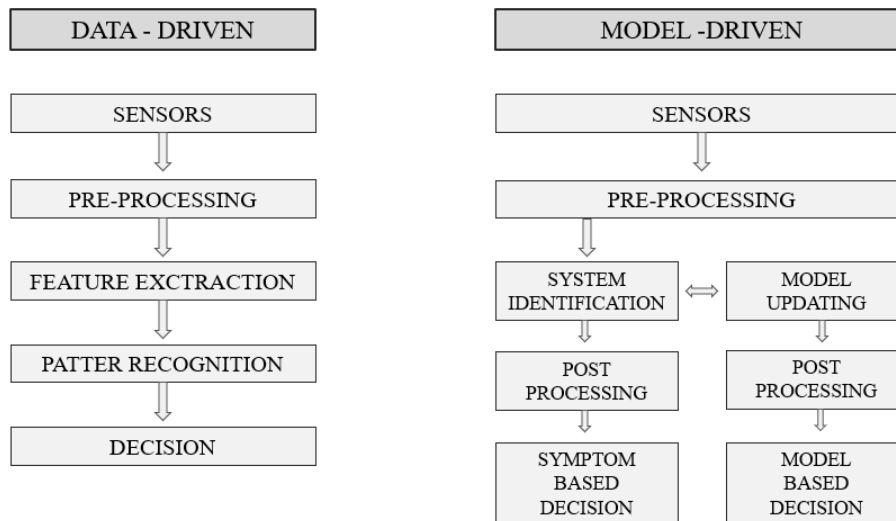


Figure 1: Data-Driven and Model-Driven Methods (Ceravolo, Pistone, Zanotti Fragonara, Masetto, & Abbiati, 2016)

1.1.5 Environmental effects

The environmental effects lead to variation of the diagnostic characteristics that cannot be confused with alteration of that characteristics induced by damages. For instance, the difference between *pathological* and *physiological* variation as to be highlighted. From such terms it can be noted the similarity that exists between a structure and the human body. The physiological variations are related to health structural states, are harmless and reversible and for instance cannot be related to the development of damages or anomalies; on the other hand, a pathological

variation is induced by phenomenon that leads to a deterioration of the structure that can get worse over time and that consequently is not reversible. Therefore, is essential to understand if the variation of the diagnostic characteristics is representative of a physiological or pathological conditions; indeed, attention as to be taken to not confuse a variation induced by a damage with a variation induced by environmental effects, because this would lead to a delay in identifying the deterioration conditions that in the while could worse, thus requiring more invasive interventions in future.

The environmental effects can act on the mass and on the stiffness of the structure and so on the dynamic response in terms of frequencies. The main problem is that, even if these fluctuations are generally harmless, they have to be recognized. However, does not exist a unique relationship between the diagnostic characteristics, such as frequency, and the environmental changes, such as temperature. For that reason, the definition of the environmental effects on the dynamic response of the structure is an open research field. Hence, theoretically for each structure we could find a different frequency-temperature relationship, indeed in literature different model can be found.

1.2 Machine Learning

1.2.1 Machine Learning definitions

The first definition of Machine Learning (ML) has been formulated by Arthur Samuel, that is considered one of the forerunners and founders of the Artificial Intelligence (AI):

“The Machine learning is a field of study that gives computers the ability to learn without being explicitly programmed.”

Another definition related to ML is the one related to the “Well-Posed Learning Problem”, that has been developed by Tom Mitchell:

“A computer program is said to learn from experience E with respect to some class of tasks T and performance measure P , if its performance at tasks T , as measured by P , improves with experience E .”

The experience E is composed by the information that the computer used to make decisions, while the measure P permit to understand if the computer is actually learning something of new in the development of the task T .

Some rigorous definitions follow to introduce the field of Machine Learning.

Definition 1. *'A **feature** is a characteristic that is representative of the system under investigations. The set of all the features defines the feature space χ .'*

Definition 2. *'A **domain** $D = \{\chi, p(X)\}$ is an object that consists of a feature space χ and a marginal probability distribution $p(X)$ over the feature data $X = \{\mathbf{x}_i\}_{i=1}^N \in \chi$, a finite sample from χ .'*

Definition 3. *'A **label** is an identifying number that can be associated with each observation, so as to signal that those data within that observation are representative of a given condition, for instance '0' for a health system and '1' for a damaged one. The set of all the possible labels defines the label space \mathcal{Y} .'*

Definition 4. *'A **task** $\mathcal{T} = \{\mathcal{Y}, f(\cdot)\}$ is an object consists of a label space \mathcal{Y} and a predictive function $f(\cdot)$ which can be inferred from training data $\{\mathbf{x}_i, \mathbf{y}_i\}_{i=1}^N$ where $\mathbf{x}_i \in \chi$ and $\mathbf{y}_i \in \mathcal{Y}$.'*

From a practical point of view these algorithms try to replicate the human learning process. Indeed, when a human being needs to learn something, he needs someone to explain it to him first, and then he can begin to exploit that given thing learned. For example, a child before he can distinguish a bicycle from a motorcycle needs an adult to show him the differences, only then the child will be able to recognize them independently. The same thing happens with this type of algorithms, the first phase in which we provide it data and information to learn a given task is called the training phase, while to verify that the algorithm is able to process that task even on data different from those provided to it as input, a test phase is developed. Therefore, this type of algorithms are divided in two phases: (i) training phase and (ii) test phase. During the (i) training phase the algorithm, starting from the input dataset, tries to learn a defined task; while, during the (ii) test phase a new dataset (that takes the name of test dataset, composed by data that were not present in the training dataset) is provided to the algorithm, which tries to make predictions about this new data based on what it learned in the previous phase. In relation to the child's example, it can be said that during the training phase different motorcycles and bicycles are shown to the child and someone told him which are bicycles, and which are motorcycles, while in the test phase new bicycles and motorcycles are shown to the child and he has to tell us which are the bicycles, and which are the motorcycles.

1.2.2 Supervised and Unsupervised ML

The ML algorithms can be classified in two typologies, supervised and unsupervised algorithms. The main difference between these two concern the type

of data that are provided to the algorithm, in particular if the dataset is labelled or not labelled.

The Supervised algorithms are ML problems that are provided of a labelled dataset for the training phase, in order to classified data or predict outcomes. The supervised learning can be subdivided into two types of problems, depending on the result to which they lead: (i) Regression or (ii) Classification. (i) The Regression problems are problems for which a continuous variable is predicted, starting from a certain input value. Indeed, the algorithm tries to define the best fitting curves of the labelled data provided, that means the curves that best approximate the data. With these algorithms different fitting curves can be found, however, particular attention has to be paid in order to avoid curves that “*approximate too well*” the data of the training phase, because if something like this happens the risk is to have a model that is too much adapted to the input data and so it will not be able to give accurate predictions (Delua, 2021). Some common regressions are linear logistic and polynomial regression. (ii) The Classification problems are algorithm that assign a label (or class) to each data, this means that in this case the output is discrete. A typical example of application of a classification algorithm in SHM is to define if a given diagnostic characteristic, that in the ML field takes the name of *feature*, such as frequency, is describing a damaged condition or a health one. To these two conditions two different labels, such as '0' and '1', are assigned and then the algorithm output will be a label, '0' or '1', for each frequency. In Figure 2 a graphical representation of a classification and a regression problem is proposed.

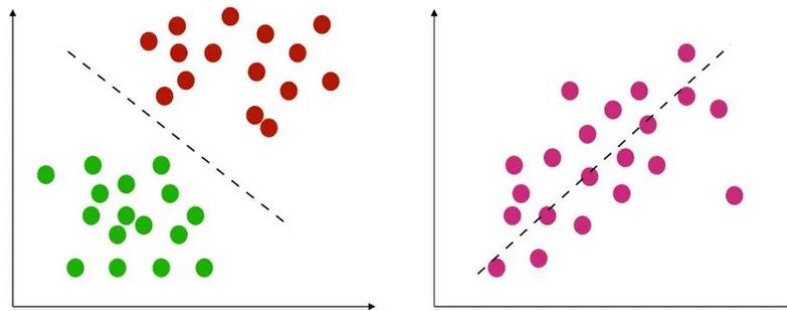


Figure 2: Classification (Left side, (ii)) and Regression (Right side, (i)) (Classificatore vs Regressione quale usare? Machine learning esempi pratici, n.d.)

The Unsupervised algorithms are ML problems that are not provided of a labelled dataset for the training phase. From a practical point of view the data of the provided dataset are labelled with a unique label, that is equivalent to not label them. Starting from these data, the algorithm tries to find some hidden path without the human intervention (Delua, 2021). Also, in this case different algorithms typologies exist: (i) Clustering; (ii) Association and (iii) Dimensionality reduction. (i) The algorithms of clustering are very common, and they try to group unlabelled data

starting from their similarities or their differences, in Figure 3 an example is reported. (ii) The algorithm of association uses different rules in order to find a relationship between the variables of the given unlabeled dataset. And, finally, (iii) the dimensionality reduction algorithms are used when the number of features (or dimensions) in the given dataset is too high, these algorithms are generally used in the pre-processing of data, in order to reduce them but maintaining their integrity (Delua, 2021).

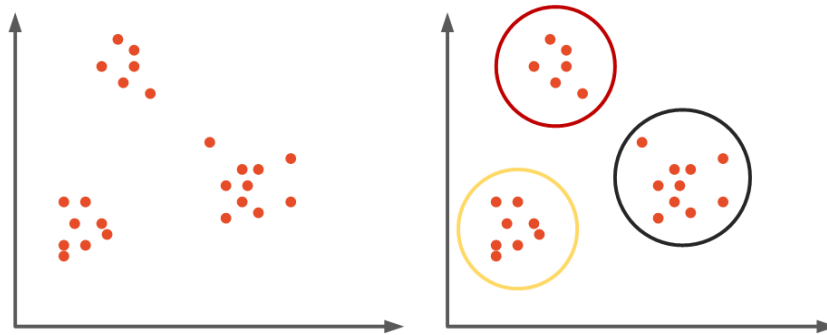


Figure 3: Clustering problem (i) (*Machine Learning with ML.NET – Complete Guide to Clustering, n.d.*)

1.2.3 Underfitting and Overfitting in supervised ML

During the training phase an algorithm can reach a condition of underfitting, right fitting or overfitting. The right fitting condition is the one that as to be reached by the algorithm, in order to avoid errors in the prediction phase on new data.

The Overfitting is the phenomenon for which the model obtained with a ML algorithm is too much adapted to the training dataset that is not able to work in a proper way with new data. The overfitting can occur when (MathWorks, n.d.):

1. The Machine Learning Model is too complex, it is too much adapted to the training data that do not generalize well.
2. The size of the training dataset is too small for the complexity of the model.

The overfitting can be generally managed, by acting on the complexity of the model or improving the training dataset.

The Underfitting is, conceptually, the opposite of the overfitting, therefore is typical of too simple ML model on the training dataset, that indicates a too small degree of the polynomial used for the classification or the regression. A possible

solution to this problem is to increase the features number and consequently the polynomial degree, increasing in this way the complexity of the algorithm. The overfitting and the underfitting are conditions that can occurs in both classification and regression problems. In Figure 4, a visual example of these conditions is presented.

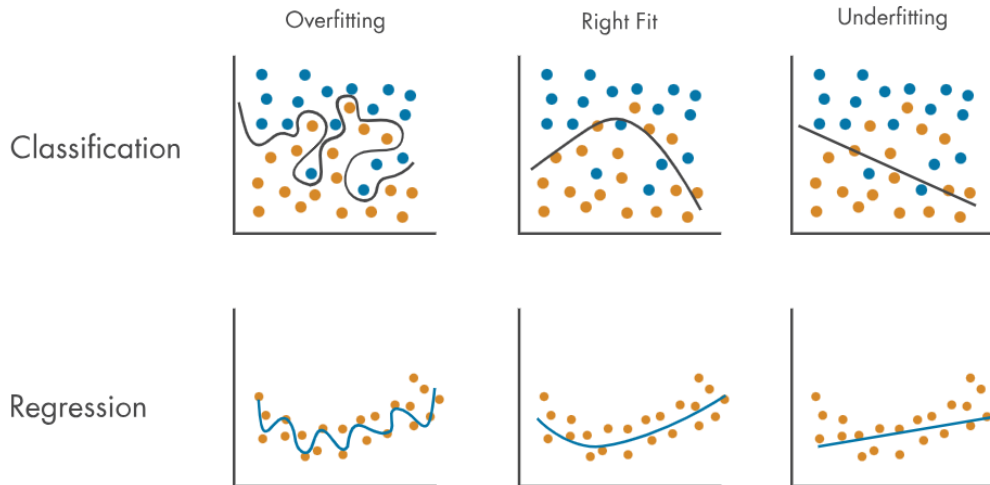


Figure 4: Example of Overfitting, right fitting and Underfitting (MathWorks, n.d.)

Generally, overfitting is more difficult to be detected on training dataset with respect to the underfitting, indeed the overfitting is simpler identified during the test phase, since in these cases the accuracy¹ in the test phase is strongly smaller than the one of the training phase. In Table 1, the mistake level in the predictions is defined as function of the model conditions (overfitting, exact fitting and underfitting).

<i>Mistake</i>		<i>Model Conditions</i>		
		<i>Overfitting</i>	<i>Exact Fit</i>	<i>Underfitting</i>
<i>Phase</i>	Training	Low	Low	High
	Test	High	Low	High

Table 1: Mistake during training and test phase (MathWorks, n.d.)

In order to avoid overfitting problems, the model can be validated before using it on the test dataset.

¹ Accuracy: it is the ratio of the number of observations that were correctly predicted to the number of total observations for which the algorithm had to generate a prediction.

The Model validation is generally performed by testing the model on a separate test dataset, that takes the name of validation dataset, before introducing new data, that means the real test dataset. One of the most common techniques for the model validation is the *Cross-validation technique* also known as *K-fold validation*. In (Nellihela, 2022) the K-fold validation is described as follows. The training dataset is split into K subsamples, by trying to create subsamples of equal size and ensuring that K is smaller or equal to the number of elements in the dataset. Then different iterations are performed, at the i^{th} iteration the i^{th} subsample is used as test dataset, while all the other are considered as training dataset, the model is trained, and the error is evaluated for the test dataset previously defined. These iterations are performed until all the subsamples have been used as test dataset; finally, the error rate in the prediction is defined as the average of all the error rate individuated at each iteration. In Figure 5 a visual representation of this process is shown.

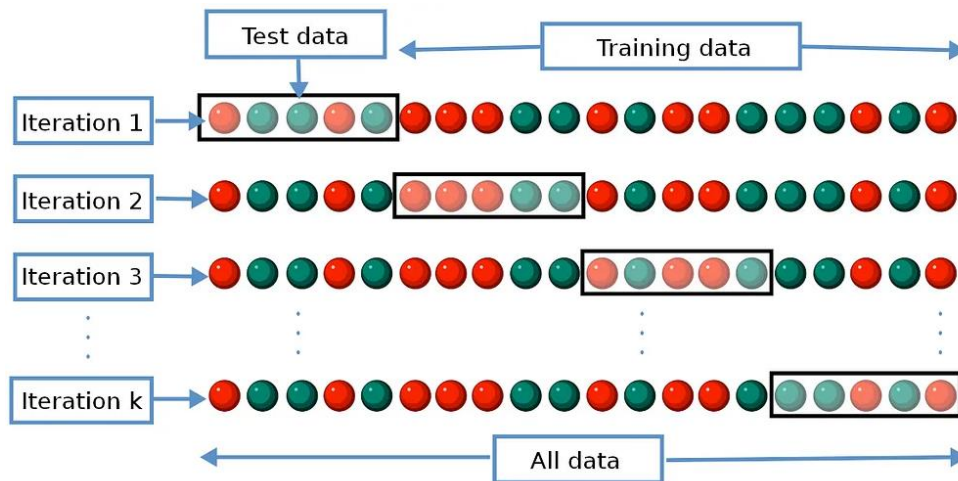


Figure 5: Logical process of the K-fold validation technique (Nellihela, 2022)

1.3 Transfer Learning with Domain Adaptation Algorithm

1.3.1 Transfer Learning Definition

The transfer learning (TL) has been introduced as a *fine-tuning approach* in order to use a pre-existing neural network in a different setting than the one for which the network was originally designed. This could be performed, for instance in the deep neural network by replacing some layers, generally the last ones, and by re-training the neural network with the new training dataset. Nowadays, a second TL category is available that is represented by the Domain Adaptation approaches that are the most common methods used in SHM applications.

1.3.2 Domain Adaptation approaches

Domain Adaptation (DA) is a TL technique based on the improvement of the performance of a model trained on a given domain that contains insufficient data by using knowledge that has been learned by the model from another domain with adequate labelled data. These two domains are defined as target domain and source domain, respectively. The Target Domain is the reference domain for which network is trained, but which contains too few data to obtain accurate predictions and it can be composed of labelled or partially labelled data. The Source Domain is the domain of labelled data that is exploited to increase performance on making prediction of data belonging to the target domain. With this in mind, transfer learning may be an important resource for SHM, as it would allow information and knowledge to be shared among similar structures. Some strict definitions follow in order to introduce the concepts behind these types of algorithms (Gardner, Bull, Gosliga, Dervilis, & Worden, 2020).

The *source domain dataset* can be defined as:

$$D_s = \{\mathbf{x}_{s,i}, \mathbf{y}_{s,i}\}_{i=1}^{N_s} \text{ where } \mathbf{x}_{s,i} \in \mathcal{X}_s \text{ and } \mathbf{y}_{s,i} \in \mathcal{Y}_s$$

And the *target domain dataset* as:

$$D_t = \{\mathbf{x}_{t,i}, \mathbf{y}_{t,i}\}_{i=1}^{N_t} \text{ where } \mathbf{x}_{t,i} \in \mathcal{X}_t \text{ and } \mathbf{y}_{t,i} \in \mathcal{Y}_t$$

Where N_s and N_t are the number of observations in the source domain and target domain respectively and generally:

$$0 \leq N_t \ll N_s$$

Definition 5. ‘*Transfer Learning with Domain Adaptation*, given a source domain D_s and a task \mathcal{T}_s , and a target domain D_t and a task \mathcal{T}_t , is the process of improving the target predictive function $f_t(\cdot)$ in \mathcal{T}_t by using knowledge from D_s and \mathcal{T}_s , whilst assuming $D_s \neq D_t$ and $\mathcal{T}_s \neq \mathcal{T}_t$.’

Starting from the definitions above, it is possible to understand the ‘mechanisms’ behind Domain Adaptation Approaches, indeed it can be summarized in two main steps: (i) Domain Adaptation to move to the Shared Latent Space the starting domains and (ii) ML in the Shared Latent Space. The step (i) is what can be practically define as Domain Adaptation, indeed the two domains are different, for instance they can show different data distribution, for which an adaptation of these domains is required before performing on these data a ML algorithm, such as a classification. Therefore, the heart of Domain Adaptation

approaches is to minimize the distance between the data distributions of the target and source domain, in order to exploit the source domain to obtain an improvement in the prediction accuracy of the domain under investigation (target domain). Generally, this is performed by a translation or projection of the two domains into a Shared Latent Space, usually represented by the letter \mathcal{H} . Since the dimensional reduction of the domains and their projection in the latent subspace is often the results of an optimization process, the axes of this Latent Subspace do not have a real physical meaning but are only a different representation of the information given by the original domains. Once the distance between the two domains has been reduced, an ML algorithm is introduced within the shared latent space (ii) in order to develop a classifier that in the future will be able to generalize for data different from those provided during the training.

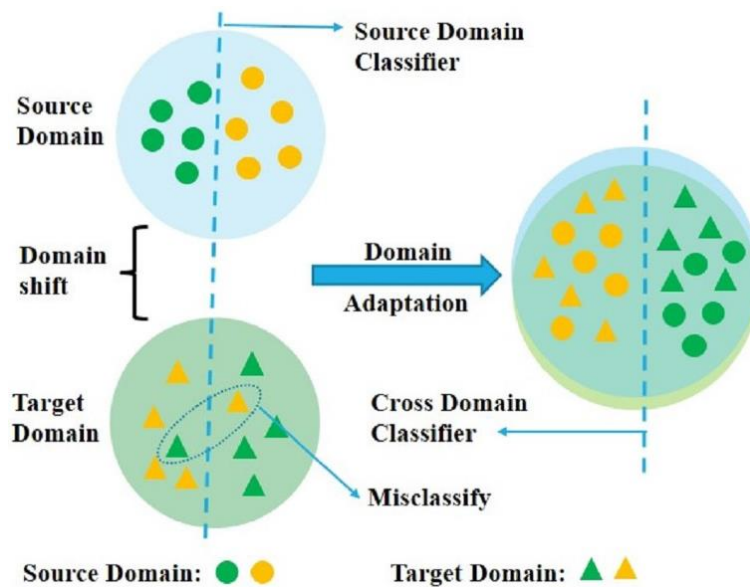


Figure 6: An illustration of how DA techniques can increase the accuracy for the prediction in the target domain. The feature distributions of the SD and TD are compared, with the original feature distributions on the left and the new feature distributions on the right (Khan, et al., 2023)

Several Domain Adaptation methods can be defined depending on factors like, the availability of labelled data for target domain, the feature spaces of the two domains and the path that is used to reduce the distance between the two. The main used DA approaches are: Supervised DA and Semi-Supervised DA. A Supervised DA can be performed when a Labelled Target Domain is available; while, when the Target Domain is only partially labelled the DA is of Semi-Supervised type. Then, different DA (supervised or un-supervised) are developed on the base of the features spaces of the two domains. In particular, Homogeneous DA are algorithms applied in the case in which the source and the target domain have the same feature space, and therefore a single feature space can be considered for both. While

Heterogeneous DA algorithms are applied when the target and source domain have a different feature space dimensionality (Kundu, 2022). In this thesis only Supervised DA have been used, with possible inconsistent feature between the domains (Heterogeneous DA).

1.4 Prediction errors

From a practical point of view, it is practically impossible to obtain a ML or TL model that can predict all the data correctly, having 100% of accuracy, especially in the test phase. As a result, the model will surely provide incorrect predictions; with this in mind, it becomes essential to know how to classify such errors. The output of all these algorithms are predictions that can be classified as: (i) True Positive (TP), (ii) True Negative (TN), (iii) False Positive (FP) and (iv) False Negative (FN). Among these four possibilities, the first two define how the algorithm has classified in the proper way the positive class (i) and the negative class (ii), while the second two show how the algorithm has performed a mistake in the predictions. A FP is reached when a data that belongs to the positive class is classified by the algorithm as a data that belongs to the negative one; while a FN is reached when a data that belongs to the negative class is classified by the algorithm as a data that belongs to the positive one. Thanks to these four definitions, for each model, it is possible the definition of the *Confusion Matrix*, where the number of data predicted are reported and classified as TP, TN, FP and FN, in Table 2 a schematic representation of this type of matrices is reported.

Confusion Matrix

Number of observations of TP	Number of observations of FP
Number of observations of FN	Number of observations of TN

Table 2: Definition of a Confusion Matrix

If the ML or TL is applied for SHM it can be understood that the positive class characterized the undamaged condition while the negative one the damaged one. Starting from these definitions, different conclusions can be drawn. Firstly, the worst mistake that an algorithm can perform is the FN, indeed in this case it is confusing a damaged state with an undamaged one, while the FP is less problematic. Indeed, let's suppose that a dynamic SHM activity has been developed in order to verify the actual state of the structure under investigation, so that if damage is present, it is possible to intervene quickly and let's assume that the algorithm that

has been used for the classification of the data ‘does not see’ a damaged state, that means the production of FNs. If something like this occurs, it follows that the user will not see the damage and therefore will not develop any intervention carried out to restore the structure. In addition, the risk is that the model will not be able to see the damage for quite some time, and therefore the damage may develop unnoticed. When the model finally perceives the damage condition, it may be very advanced and difficult to treat. This is the reason why, in SHM the FN may be very hostile. On the other hand, if the algorithm generates an error of the FP type, the consequences are strongly different. Indeed, in such a circumstance the algorithm is confusing an undamaged condition with a damaged one, so it could be said that the error exists but for the benefit of safety. The consequences in such circumstances are economic and not structural, indeed if these models identify a damage further site investigations are required in order to better understand the damaged state. However, if it is a FP prediction once at the site it will be realized that damage is not present, so an additional expense for these additional tests was required when theoretically it was not needed.

It can be concluded that, especially in SHM the number of false negatives is to be reduced as much as possible. In this view, the *meta-optimization* of the models plays an important role, i.e., knowing that errors will be present we can try to act on the hyper-parameters² of the algorithm so that in the test phase these errors are more FP than FN.

² Hyper-Parameters: are input parameters of algorithms that are managed by the user; indeed, they can be modified until the model that best performs for that task for which it was generated is obtained.

Chapter 2

Transfer learning approaches for structural health monitoring of architectural heritage

2.1 Population-Based SHM

One of the main requests of ML classifier algorithms is that they need at least some data for each considered labels, therefore also of the damage conditions. This is because these algorithms learn as a human do during his entire life. A human initially needs someone who tell him that that given condition is a harm condition, while that other condition is a healthy condition before he can distinguish between them independently, and the same is needed by these algorithms. In this perspective the theory of Population-Based Structural Health Monitoring (PBSHM) becomes relevant.

In conventional SHM, the algorithm learnt from a training dataset composed by observations that have been recorded from a single structure. However, this training dataset can be limited and incomplete, one of the main reason ways it could be incomplete is the lack of labelled data for damage states. To overcome this problem PBSHM can be used, for which data coming from other similar structures (other real structures or finite element models) are used to improve the performance of the algorithm for the prediction on future measurements. These ‘additional’

structures and the analyzed structure form a *population*, as function of the type of structures present and on the base of the similarity among them the population can be classified as homogeneous or heterogeneous population.

This PBSHM is based on (i) transfer of knowledge and (ii) mapping. With (i) it may be possible to obtain a quite complete damage-label dataset by combining labels from all structures in a population. Then, by mapping (ii) this ‘complete knowledge’ onto a consistent space, it will be possible to generate a general machine learning method for the complete population in order to perform future prediction (Gardner, Bull, Gosliga, Dervilis, & Worden, 2020). In both cases, homogenous and heterogeneous populations benefit in the knowledge transfer have been demonstrated.

2.1.1 The lack of labelled data for damaged states

Nowadays, many studies can be found in literature where ML and TL are used to predict damage conditions in structure; however, most of these structures are ordinary structures, such as regular framed buildings. In these cases, finding data of a damaged condition is relatively simple, indeed, Finite Element Model (FEM) can be quite close to the reality and so can be used to simulate many damage conditions, or “*disposable structures*” in scale can be constructed in order to simulate on its different damage scenarios, without causing damage on the analyzed structure. However, when these algorithms have to be applied on AHS the damage data retrieval is not so easy, therefore the lack of labelled data for damaged states represents the most important obstacle that has to be overcome.

The AHS are often characterized by irregularities in plane and in elevation, uncertainty in the material properties and in the geometries, which makes the realization of truthful FEM complex. The only way to obtain a model that can be considered as representative of the reality is to perform a calibration of the model as result of a quite extensive investigation campaign. If a corroborated model is available a TL algorithm can be used between the model domain, which would represent the source domain and real structure domain, or rather the target domain. Generally, between these two domains, from model and real structure, is required a TL algorithm instead of a ML algorithm, because no matter how calibrated the model is, it can never be an accurate copy of reality, inevitably some factors will always be overlooked.

AHS, such as Churches, can be similar to each other, even if is practically impossible to find two identical churches. Anyways, if two AHSs are similar, one might consider using the already acquired knowledge of one to improve that of the

other. In this thesis, first steps in this direction are shown. In particular, the two structures compared will be two churches, the *Sanctuary of Vicoforte* (Vicoforte, CN) characterized by the world's largest masonry oval dome and the *Church of Santa Caterina* (Casale Monferrato, AL) whose structure is also characterized by a masonry oval dome, even if of smaller dimensions.

2.1.2 Homogeneous and Heterogeneous populations

'A population, in the context of PBSHM, is a group of structures (the smallest being a group of two structures) that provide information required for performing health monitoring.'

This is the general definition of *population* present in (Gardner, Bull, Gosliga, Dervilis, & Worden, 2020). However, this is a general definition that can be further divided into two categories: homogeneous and heterogeneous populations, as function of the dissimilarity within the population:

'Homogenous population is one in which each structure in the population can be deemed nominally identical for a given context. A heterogeneous population is thus a group of non-identical, and therefore different structures.'

In the above definition the term '*context*' has been used, therefore there is a strictly relationship between the homogeneity/heterogeneity and the context for which the structures have been defined as part of a homogenous or heterogenous populations. Thus, two structures can be defined as nominally identical for a given context, and non-identical for another. This means that a *spectrum of heterogeneity* can be defined, with an increment in the similarity until reaching the homogenous population. A method for quantify these differences is based on the use of Irreducible Element models and Attributed Graphs, details can be found in (Gosliga, Gardner, Bull, Dervilis, & Worden, 2021), here only a summary is reported. This approach highlighted three main fields that can introduce differences within the structures:

1. Geometry: in terms of shape, size and scaling of the structure in the population (e.g., population composed by aluminum plates all with different length, width and thickness).
2. Material: in terms of different material properties in the population (e.g., population composed of two plates with the same geometry one in aluminum and one in steel).

3. Topology: in terms of the graphical representations of each structure in the population (e.g., two aluminum plates with the same geometry but one is a cantilever while the other is fixed along two sides).

These three categories can be separated or even overlapped, creating in this way different typologies of heterogeneity, in Figure 7 a representation of this is shown.

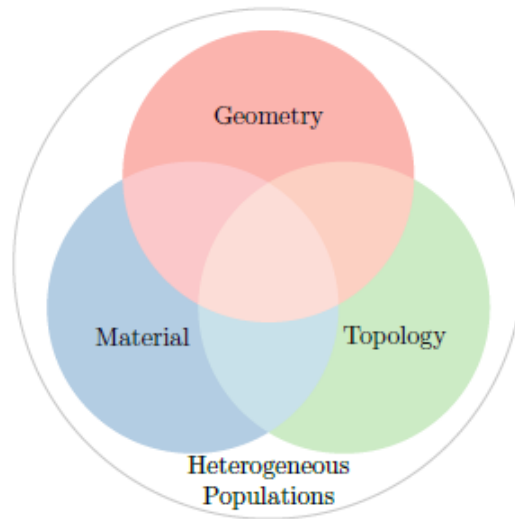


Figure 7: Categories for the definition of the heterogeneity within a population (Gardner, Bull, Gosliga, Dervilis, & Worden, 2020)

It is also necessary to highlight that differences observed in data can also occur due to categories that are different from the three described above. For instance, how the data acquisition is developed can induce some heterogeneity within the population, as different sensors placement is reflected in different data distributions. The following definitions are extrapolated from (Gardner, Bull, Gosliga, Dervilis, & Worden, 2020).

Definition 4. *'Homogenous Transfer Learning assumes that the feature and the label spaces represent the same attributes $\chi_s = \chi_t$ and $\mathbf{y}_s = \mathbf{y}_t$, and therefore that the dimensions of the feature space are equal $\mathbf{d}_s = \mathbf{d}_t$.'*

Definition 5. *'Heterogenous Transfer Learning assumes that the feature spaces are not equivalent $\chi_s \neq \chi_t$ and often that the source and target domains share no common features, meaning $\mathbf{d}_s \neq \mathbf{d}_t$. In addition, heterogenous transfer learning can also assume that $\mathbf{y}_s \neq \mathbf{y}_t$.'*

2.1.3 Transfer Learning between the real structure and its FEM, the case of the Sanctuary of Vicoforte

In this section a study carried out on the *Sanctuary of Vicoforte* for the identification of temperature states through the use of Transfer Learning with Domain Adaptation approach is reported since it represents, conceptually, the starting point for *Chapter 4* and *Chapter 5*. The study that is returning here has been developed and published by (Coletta, et al., 2021). In this study, as domain adaptation approach, the Transfer Component Analysis (TCA) has been used to reduce the distance between data distributions from a continuous monitoring dataset collected on the real structure and data obtained from its corresponding FEM. This application of DA aims to improve the recognition of different environmental conditions, in particular the temperature variations that are reflected in changes in the dynamic parameters (in this case frequencies). In future, this algorithm or similar, may be used for the damage detection.

TCA algorithm is a homogenous transfer learning that learn some transfer components for each domain to transfer them in a Reproducing Kernel Hilbert Space (RKHS) by using the Maximum Mean Discrepancy criterion as embedding criterion. Thanks to the transfer to the RKHS the two domains, source and target, will be closer to each other, due to the minimization of the distance between the density of the domains. The main hypotheses on the basis of this algorithm are that: (i) the features space and (ii) the label spaces are the same for both the domain (since it is a homogenous transfer learning), (iii) the diagnostic features are differently distributed (different marginal distribution) but (iv) the conditional distribution of the two domains is the same. These four hypotheses can be summarized with the following expressions:

$$X_s = X_t \text{ (i) and } Y_s = Y_t \text{ (ii)}$$

$$P(X_s) \neq P(X_t) \text{ (iii) but } P(Y_s|X_s) = P(Y_t|X_t) \text{ (iv)}$$

This study has been developed on data acquired from the permanent dynamic monitoring realized on the Sanctuary, that represent a monumental building of the 17th century with the largest oval masonry dome in the world. In addition, a calibrated numerical model of this construction exists, and so the transfer learning has been performed between the data from the monitoring systems and those simulated on the FEM. As previously defined, the TCA is a homogenous transfer learning, hence the structures that represent the two domains must be considered as homogenous. In this case, the two domains are obtained from the real structure (Target Domain) and its Finite Element Model (Source Domain) that has been

calibrated on the base of the results obtained through the monitoring systems, therefore they can be considered identical in typology, geometry and material.

The Target Domain is composed by features and labels. The features, in terms of frequencies, have been obtained from the dynamic monitoring system applied to the structure; while the labels in terms of temperature associated to the measured frequency have been obtained from the measurement performed by the meteorological station of Mondovì (the closed one to the Sanctuary). Each observation is composed by the first three experimental frequencies, namely the first two bending frequencies in the directions of the minor axis and the major axis of the dome and the first torsional frequency. Each observation is labelled with a temperature class, defined as the average temperature recorded at the meteorological station on the day of the acquisition of the signal from which the modal frequency has been obtained. Among all these samples, only the observations related to 3°C and 10°C have been used as training dataset of the target domain. The data recorded at 10°C belong to the Class 1; while the data recorded at 3°C belong to the Class 2. In particular this dataset is composed by 32 observations for the class 1 and 69 observations for the class 2, for a total number of observations equal to 101. In Figure 8, a photo of the Sanctuary is shown, while in Figure 9 the Target Domain is plotted in the space $f1 [Hz] - f2 [Hz] - f3 [Hz]$ where it is possible to individuate the two classes, class 1 (10°C) in blue and class 2 (3°C) in green. From this plot what can be noted is the partially overlapping that exist between the two classes, that can introduce poor accuracy in the classification with a simple ML algorithm, that could be amplified by the possible overfitting due to the smallness of the dataset.



Figure 8: Sanctuary of Vicoforte (GT, 2016)

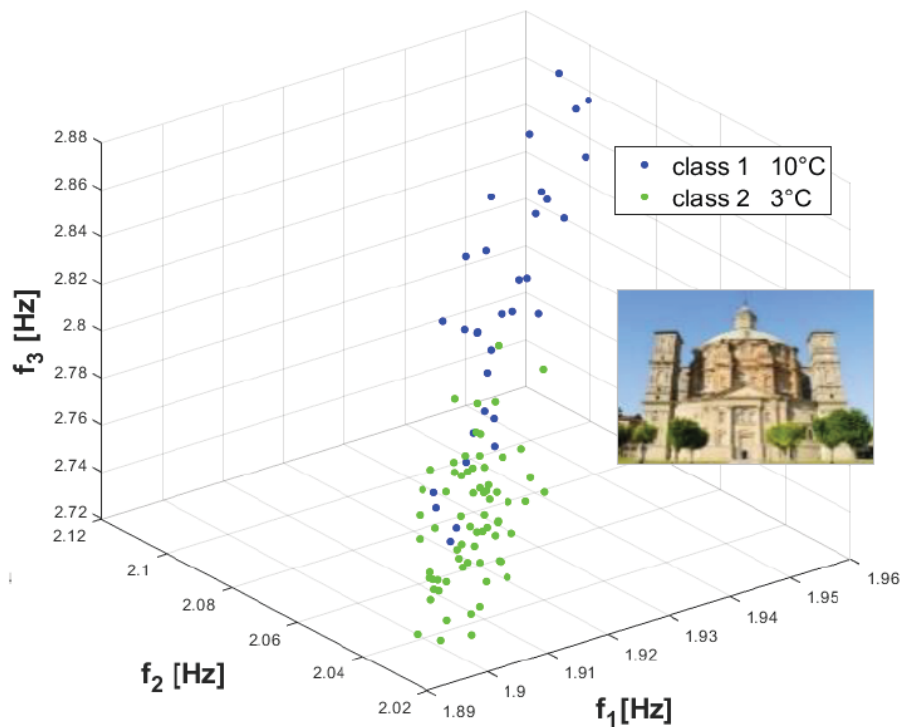


Figure 9: Graphical representation of the Target Domain for the Sanctuary of Vicoforte, representative of the two temperature classes: 3°C and 10°C (Coletta, et al., 2021)

The Source Domain is represented by data obtained by simulation on the FEM of the Sanctuary of Vicoforte, that is a numerical multi-physics model (Figure 10). In order to obtain the frequencies for the two temperature classes 3°C and 10°C, the FEM eigenvalue problem have been solved 100 times, 50 times for the class 1 e the other 50 for the class 2. To provide the variation of the mechanical parameters induce by a given temperature a Gaussian distribution has been associated with the elastic modulus of each macro-element. The mean value has been set equal to the calibrated one, with a variance based on literature values and on the variability of the experimental results obtained. Each eigenvalue analysis has been performed by assigning a random value of the elastic modulus extrapolated from that Gaussian distribution. From each eigenvalue analysis only the first three frequencies of the Sanctuary, namely the first two bending modes in the y (minor axes) and x direction (major axes) and the first torsional mode, have been selected and used to generate the Source Domain. In Figure 11 the plot of the Source Domain in the space $f_1 [Hz] - f_2 [Hz] - f_3 [Hz]$ is shown. What can be observed is that the two classes do not have any overlapped regions, hence there is a difference between data from Target Domain and data from Source Domain, difference that may be justified by the fact that the FEM is not influenced by any external phenomena, that can introduce additional variations of the frequencies, unlike the real structure.

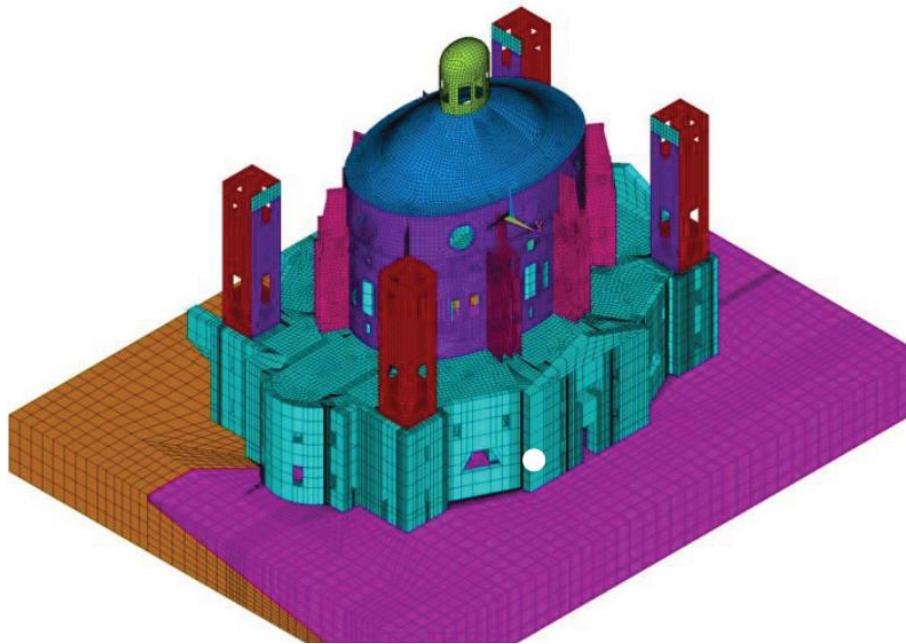


Figure 10: Multi-physics model of the Sanctuary of Vicoforte (Coletta, et al., 2021)

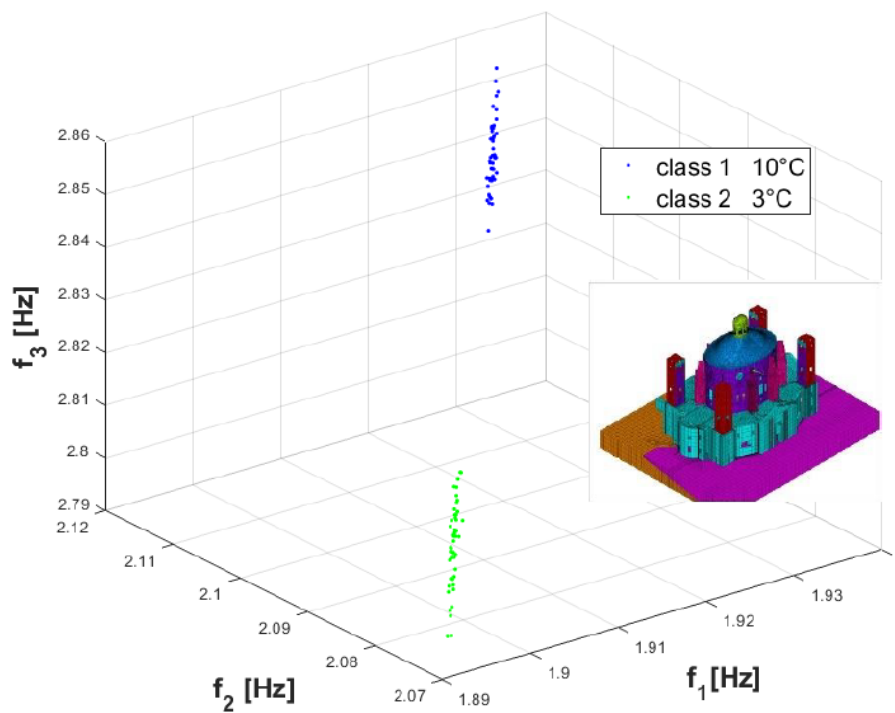


Figure 11: Graphical representation of the Source Domina for the Sanctuary of Vicoforte representative of the two temperature classes: 3°C and 10°C (Coletta, et al., 2021)

At first a simple ML algorithm, the Relevance Vector Machine (RVM), has been trained on a training dataset composed by both the domains without performing any domain adaptation to minimize the distance between the two distributions. In Figure 12(a) the training dataset and some predictions are represented, the data that are not externally circled are the ones used for the training, while the others have been used as test. With this model an accuracy of 62.8 % has been reached.

Secondly, a TCA has been performed before the application of the RVM, the results are shown in Figure 12(b). With this second approach an accuracy of 79.1 % as been reached, hence the application of TCA lead to an improvement of almost the 20 %.

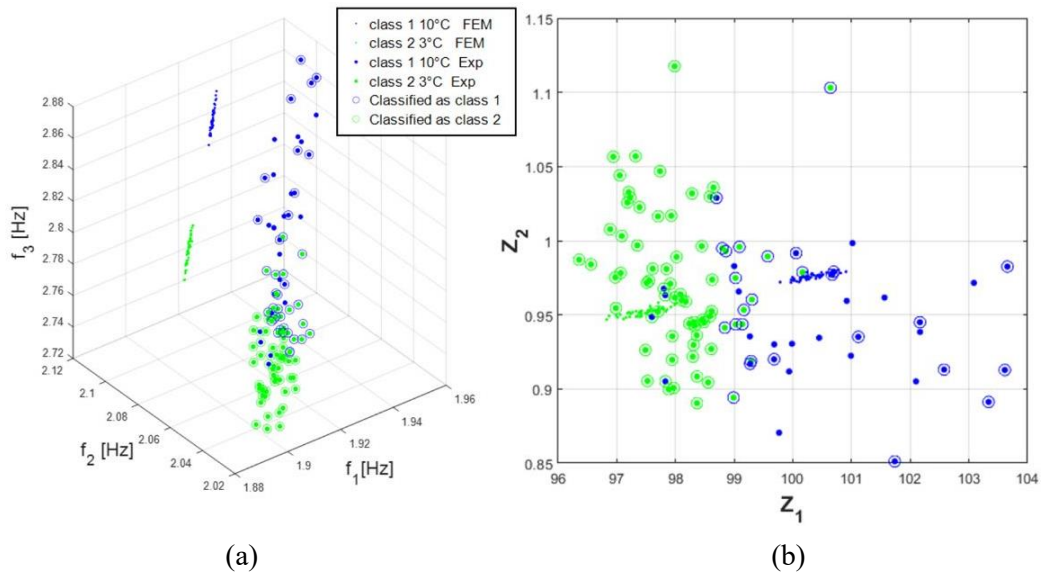


Figure 12: RVM classifier (a) and TCA+RVM classifier (b) for the predictions of the two temperature classes: 3°C and 10°C for the Sanctuary of Vicoforte (Coletta, et al., 2021)

In addition, in the same paper (Coletta, et al., 2021) a simplified Frequency-Temperature Model has been developed, in particular the natural frequencies of the system as the temperature varies, $f_k(T)$, for the k^{th} vibrating mode can be defined as:

$$f_k(T) \approx f_{0,k} \sqrt{1 + \alpha_{H_2O}(T)T}$$

Where $f_{0,k}$ is the fictitious 0 Kelvin frequency for the k^{th} mode. In Figure 13 the first two natural frequencies experimentally identified are compared with the model Frequency-Temperature described above.

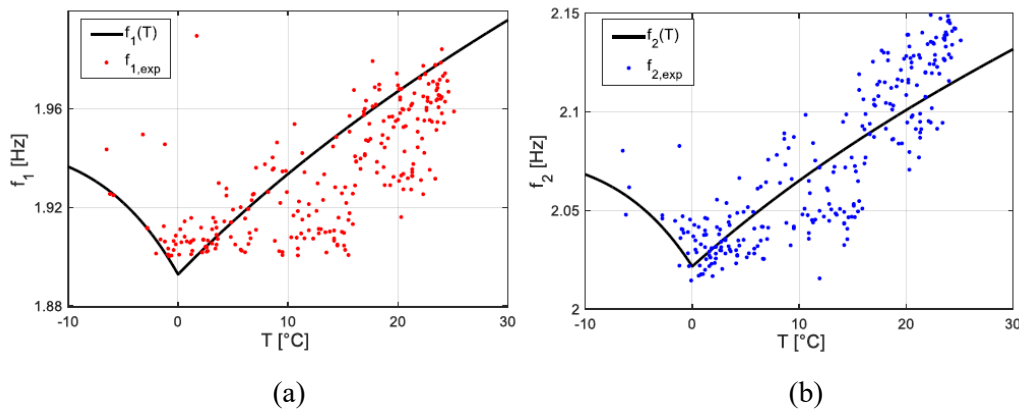


Figure 13: Comparison between the first (a) and second (b) natural frequencies experimentally identified and the simplified Frequency-Temperature Model

Therefore, it can be seen that the temperatures have a bi-linear trend, decreasing for negative temperatures and increasing for positive temperatures; this aspect will be taken up in *Chapter 5* where the frequencies of a second church will be simulated considering this bi-linearity. However, as previously mentioned, there is no unambiguous law temperature-frequency, in particular different types of behavior can be found in the literature for positive temperatures (increasing or decreasing), but in the case of negative temperatures a decreasing trend with increasing temperature has always been shown. Thus for negative temperatures, increasing frequencies are observed as the temperatures decrease, reflecting a possible increase in stiffness.

Chapter 3

Kernelized Bayesian Transfer Learning

3.1 The concepts behind the algorithm

The Kernelized Bayesian Transfer Learning (KBTL) is a population based SHM, that works considering the theory behind DA approaches, hence it tries to use the labelled information across the population of structures to create a ML model that may be able to generalize across the complete population. This algorithm is a *heterogeneous transfer learning algorithm*, since it admits a different feature set for each domain within the population, this means that it admits the *feature inconsistency*. This property of KBTL is quite important because it permits to use structures for which the feature spaces have different dimension. Practically speaking, in most of the cases the features are the natural frequencies of the structure, and so under this hypothesis each domain can have a different number of natural frequencies. Consequently, the range of structures that can be used increases with respect to the homogenous transfer learning that required the same feature space for each structure.

This TL has been introduced by Gönen and Margolin in 2014 (Gönen & Margolin, 2014). The Kernelized Bayesian Transfer Learning is a supervised learning algorithm that tries to share information across multiple datasets from different systems in order to generate a classification model (linear classifier) in a

generalized latent subspace. The definitions of domain and task are briefly restated (Gardner, Bull, Dervilis, & Worden, 2022):

'A domain $\mathbf{D} = \{\mathcal{X}, p(\mathbf{X})\}$ is an object that consists of a feature space \mathcal{X} and a marginal probability distribution $p(\mathbf{X})$ over a finite sample of feature data $\mathbf{X} = \{\mathbf{x}_i\}_{i=1}^N \in \mathcal{X}$.'

'A task $\mathcal{T} = \{\mathcal{Y}, f(\cdot)\}$ is the combination of a label space \mathcal{Y} and a predictive function $f: \mathcal{X} \rightarrow \mathcal{Y}$.'

This model assumes T domains $\{D_t\}_{t=1}^T$ with inconsistent feature spaces $\{\mathcal{X}_t\}_{t=1}^T$. Each domain has an associated task $\{\mathcal{T}_t\}_{t=1}^T$ with consistent label spaces $\mathcal{Y}_t = \mathcal{Y}_k \forall t, k \in 1:T$, and so a global and unique label space \mathcal{Y} can be assumed. Each domain has N_t finite feature observations $X_t = \{\mathbf{x}_{t,i} \in \mathcal{X}_t\}_{i=1}^{N_t}$ at which correspond a finite set of label observations $Y_t \in \mathcal{Y}$. For each domain/task pair, there is a specific kernel function $k_t(\cdot, \cdot)$ that defines the correlation between datapoints of the t domain, hence each domain is represented by its own kernel matrix $K_t = k_t(X_t, X_t)$. The algorithm can be divided into two main steps:

- (i) It projects data points from the different tasks into a shared subspace, \mathcal{H} , using a kernel-based dimensionality reduction model for each task.
- (ii) It performs a discriminative classifier in the shared latent subspace.

The first stage has been designed to manage the inconsistent feature spaces. Considering two domains D_t and D_k with dimensions d_t and d_k , with $d_t \neq d_k$, these two domains have to be projected in the shared latent subspace through a dimensional reduction to the dimension \mathcal{R} of the latent subspace \mathcal{H} . In particular, at first the feature extraction is performed using the input kernel matrices $\{K_t \in \mathbb{R}^{N_t \times N_t}\}_{t=1}^T$ and the task-specific projection matrices, defined as optimal linear projection matrix $\{A_t \in \mathbb{R}^{N_t \times \mathcal{R}}\}_{t=1}^T$ learned by the algorithm, one for each domain. After the projection, a representation of the datapoints in the shared latent subspace \mathcal{H} is obtained for each task $\{H_t = A_t^T K_t \in \mathbb{R}^{\mathcal{R} \times N_t}\}_{t=1}^T$.

The second stage is composed by the classification part that calculates the predicted outputs in the shared latent subspace \mathcal{H} with a linear discriminant:

$$f_t = H_t^T \boldsymbol{\omega} + \mathbf{1}b \quad \forall t \in 1:T$$

Where $\mathbf{1}$ is a vector of ones. The classifier parameters are represented in the formulation above by the bias $\{b \in \mathbb{R}^{1 \times 1}\}$ and the weights vector $\{\boldsymbol{\omega} \in \mathbb{R}^{\mathcal{R} \times 1}\}$ that

3.2 Binary classification problems

As previously defined, the algorithm is summarized in two main steps: (i) to find the representations of the domains in the latent subspace by using the kernel matrices and the task-specific projection matrices and (ii) to perform a binary classification in the subspace using a unique set of classification parameters.

In Figure 15 a graphical model of kernelized Bayesian transfer learning for binary classification with all the priors, hyperparameters, latent variables and model parameters is shown.

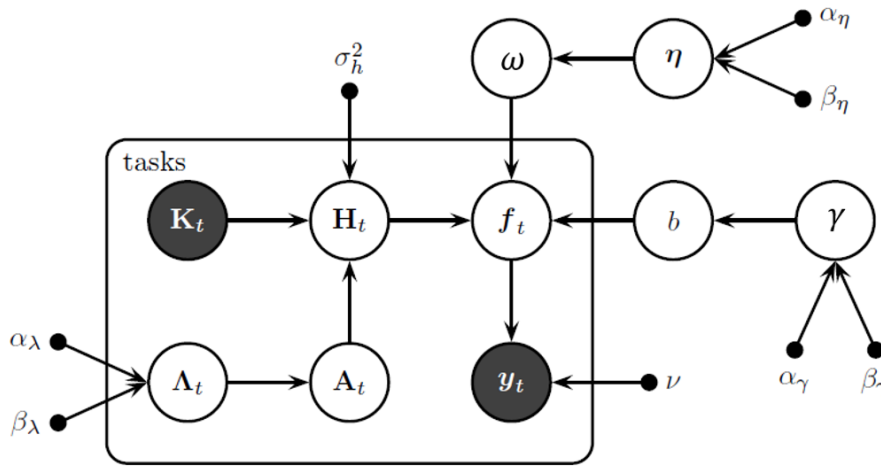


Figure 15: Graphical model of KBTL for binary classification with all priors, hyperparameters, latent variable and model parameters (Gönen & Margolin, 2014)

In the imagine above it is possible to individuate the priors: (i) the matrix of priors $\{\Lambda_t \in \mathbb{R}^{N_t \times \mathcal{R}}\}$ of the task-specific projection matrix A_t ; (ii) the vector of priors $\{\boldsymbol{\eta} \in \mathbb{R}^{\mathcal{R} \times 1}\}$ of the weights vector $\boldsymbol{\omega}$ and (iii) the prior γ for the bias parameter b . These priors are summarized in $\Xi = \{\gamma, \boldsymbol{\eta}, \{\Lambda_t\}_{t=1}^T\}$. For these three priors, three sets of hyperparameters are defined as $\{\alpha_\lambda, \beta_\lambda\}$, $\{\alpha_\eta, \beta_\eta\}$ and $\{\alpha_\gamma, \beta_\gamma\}$, that for a faster representation are summarized in $\zeta = \{\alpha_\eta, \beta_\eta, \alpha_\gamma, \beta_\gamma, \alpha_\lambda, \beta_\lambda\}$. The variance of the latent subspace is introduced as σ_h^2 . Finally, the latent variables and the model parameters are collected in $\Theta = \{b, \boldsymbol{\omega}, \{f_t, A_t, H_t\}_{t=1}^T\}$.

The first step of the algorithm is a projection with a dimensionality reduction in the latent subspace, that is performed with a kernel-based dimensionality reduction, whose distributional assumptions are:

$$\begin{aligned} \lambda_{t,s}^i &\sim \mathcal{G}(\lambda_{t,s}^i; \alpha_\lambda, \beta_\lambda) & \forall(t, i, s) \\ a_{t,s}^i | \lambda_{t,s}^i &\sim \mathcal{N}(a_{t,s}^i; 0, (\lambda_{t,s}^i)^{-1}) & \forall(t, i, s) \\ h_{t,i}^s | \mathbf{a}_{t,s}, \mathbf{k}_{t,i} &\sim \mathcal{N}(h_{t,i}^s; \mathbf{a}_{t,s}^\top \mathbf{k}_{t,i}, \sigma_h^2) & \forall(t, i, s) \end{aligned}$$

Where the superscript index represents the rows, while the subscript index the columns. For what concerns the distributions, $\mathcal{N}(\cdot, \boldsymbol{\mu}, \boldsymbol{\Sigma})$ represents the normal distribution with mean vector $\boldsymbol{\mu}$ and the covariance matrix $\boldsymbol{\Sigma}$, while $\mathcal{G}(\cdot, \alpha, \beta)$ represents the gamma distribution with shape parameter α and scale parameter β . The additional distributional assumptions related to the binary classification are as follows:

$$\begin{aligned}
 \gamma &\sim \mathcal{G}(\gamma; \alpha_\gamma, \beta_\gamma) \\
 b|\gamma &\sim \mathcal{N}(b; 0, \gamma^{-1}) \\
 \eta_s &\sim \mathcal{G}(\eta_s; \alpha_\eta, \beta_\eta) && \forall s \\
 \omega_s|\eta_s &\sim \mathcal{N}(\omega_s; 0, \eta_s^{-1}) && \forall s \\
 f_{t,i}|b, \boldsymbol{\omega}, \mathbf{h}_{t,i} &\sim \mathcal{N}(f_{t,i}; \boldsymbol{\omega}^\top \mathbf{h}_{t,i} + b, 1) && \forall (t, i) \\
 y_{t,i}|f_{t,i} &\sim \delta(f_{t,i} y_{t,i} > \nu) && \forall (t, i)
 \end{aligned}$$

Where the predicted outputs $\{\mathbf{f}_t\}_{t=1}^T$, similar to the discriminant outputs in Support Vector Machine (SVM) algorithm, are introduced to make the inference procedures efficient. The *non-negative margin parameter* ν is introduced to create a low-density region between the two classes, conceptually similar to the SVM margin, and to solve the scaling ambiguity. Finally, $\delta(\cdot)$ represents the Kronecker delta function that returns 1 if the argument is true and 0 in the other cases.

In order to obtain an efficient inference mechanism³, Gönen and Margolin (Gönen & Margolin, 2014) have formulated a deterministic variational approximation, that use a lower bound on the marginal likelihood using an ensemble of factored posteriors to find the joint parameter distribution. In this first part general formulations are described, then the specific ones for the binary problem are shown.

In this model, the factorable ensemble approximation of the required posterior is written as:

$$\begin{aligned}
 p(\boldsymbol{\Theta}, \mathbf{E}|\{\mathbf{K}_t, \mathbf{y}_t\}_{t=1}^T) &\approx q(\boldsymbol{\Theta}, \mathbf{E}) = \\
 &= \prod_{t=1}^T [q(\boldsymbol{\Lambda}_t)q(\mathbf{A}_t)q(\mathbf{H}_t)]q(\gamma)q(\boldsymbol{\eta})q(b, \boldsymbol{\omega}) \prod_{t=1}^T q(\mathbf{f}_t)
 \end{aligned}$$

All the factors in the ensemble are defined as their full conditional distribution:

$$q(\boldsymbol{\Lambda}_t) = \prod_{i \in \mathcal{I}_t} \prod_{s=1}^{\mathcal{R}} \mathcal{G}(\lambda_{t,s}^i; \alpha(\lambda_{t,s}^i), \beta(\lambda_{t,s}^i))$$

³ Variational inference is the process by which a neural network predicts for a data item received as input.

$$\begin{aligned}
q(\mathbf{A}_t) &= \prod_{s=1}^{\mathcal{R}} \mathcal{N}(\mathbf{a}_{t,s}; \mu(\mathbf{a}_{t,s}), \Sigma(\mathbf{a}_{t,s})) \\
q(\mathbf{H}_t) &= \prod_{i \in \mathcal{J}_t} \mathcal{N}(\mathbf{h}_{t,i}; \mu(\mathbf{h}_{t,i}), \Sigma(\mathbf{h}_{t,i})) \\
q(\gamma) &= \mathcal{G}(\gamma; \alpha(\gamma), \beta(\gamma)) \\
q(\boldsymbol{\eta}) &= \prod_{s=1}^{\mathcal{R}} \mathcal{G}(\eta_s; \alpha(\eta_s), \beta(\eta_s)) \\
q(b, \boldsymbol{\omega}) &= \mathcal{N}\left(\begin{bmatrix} b \\ \boldsymbol{\omega} \end{bmatrix}; \mu(b, \boldsymbol{\omega}), \Sigma(b, \boldsymbol{\omega})\right) \\
q(\mathbf{f}_t) &= \prod_{i \in \mathcal{J}_t} \mathcal{TN}(f_{t,i}; \mu(f_{t,i}), \Sigma(f_{t,i}), \rho(f_{t,i}))
\end{aligned}$$

Where:

- ~ $\alpha(\cdot), \beta(\cdot), \mu(\cdot)$ and $\Sigma(\cdot)$ are respectively, the shape parameter, the scale parameter, the means vectors, and the covariance matrix for their arguments.
- ~ $\mathcal{TN}(\cdot; \mu(\cdot), \Sigma(\cdot), \rho(\cdot))$ represents the truncated normal distribution with the mean vector $\boldsymbol{\mu}$, the covariance matrix $\boldsymbol{\Sigma}$ and the truncation rule $\rho(\cdot)$ such that $\mathcal{TN}(\cdot; \mu(\cdot), \Sigma(\cdot), \rho(\cdot)) \propto \mathcal{N}(\cdot; \mu(\cdot), \Sigma(\cdot))$ if $\rho(\cdot)$ is true, in the other cases $\mathcal{TN}(\cdot; \mu(\cdot), \Sigma(\cdot), \rho(\cdot)) = 0$.
- ~ \mathcal{J}_t indicates the indices of datapoints in task t .

The marginal likelihood is bounded with the Jensen's inequality:

$$\begin{aligned}
\log p(\{\mathbf{y}_t\}_{t=1}^T | \{\mathbf{K}_t\}_{t=1}^T) \\
\geq E_{q(\boldsymbol{\Theta}, \boldsymbol{\Xi})}[\log p(\{\mathbf{y}_t\}_{t=1}^T, \boldsymbol{\Theta}, \boldsymbol{\Xi} | \{\mathbf{K}_t\}_{t=1}^T)] - E_{q(\boldsymbol{\Theta}, \boldsymbol{\Xi})}[\log q(\boldsymbol{\Theta}, \boldsymbol{\Xi})]
\end{aligned}$$

Then, this bound is optimized by iteratively maximizing it with respect to each factor until convergence. The approximate posterior distribution for a particular factor τ is defined as,

$$q(\tau) \propto \exp(E_{q(\{\boldsymbol{\Theta}, \boldsymbol{\Xi}\} \setminus \tau)}[\log p(\{\mathbf{y}_t\}_{t=1}^T, \boldsymbol{\Theta}, \boldsymbol{\Xi} | \{\mathbf{K}_t\}_{t=1}^T)])$$

Where $E_{q(\cdot)}[g(\cdot)]$ is the posterior expectation, that later will be described for simplicity as $\langle g(\cdot) \rangle$.

For this model, this resulting approximate posterior distribution of each factor follows the same distribution of the factor itself.

In this section the formulations for the *Binary Problem* are shown. For the binary classification approximate posterior distribution of the precision priors are:

$$\begin{aligned}\alpha(\lambda_{t,s}^i) &= \alpha_\lambda + \frac{1}{2} \\ \beta(\lambda_{t,s}^i) &= \left(\frac{1}{\beta_\lambda} + \frac{\langle (a_{t,s}^i)^2 \rangle}{2} \right)^{-1} \\ \alpha(\gamma) &= \alpha_\gamma + \frac{1}{2} \\ \beta(\gamma) &= \left(\frac{1}{\beta_\gamma} + \frac{\langle b^2 \rangle}{2} \right)^{-1} \\ \alpha(\eta_s) &= \alpha_\eta + \frac{1}{2} \\ \beta(\eta_s) &= \left(\frac{1}{\beta_\eta} + \frac{\langle \omega_s^2 \rangle}{2} \right)^{-1}\end{aligned}$$

Where $\langle g(\cdot) \rangle$ is the posterior expectation.

The approximate posterior distributions of the task-specific projection matrix A_t for the binary problem are:

$$\begin{aligned}\Sigma(\mathbf{a}_{t,s}) &= \left(\text{diag}(\langle \lambda_{t,s} \rangle) + \frac{\mathbf{K}_t \mathbf{K}_t^\top}{\sigma_h^2} \right)^{-1} \\ \mu(\mathbf{a}_{t,s}) &= \Sigma(\mathbf{a}_{t,s}) \left(\frac{\mathbf{K}_t \langle (h_t^s)^\top \rangle}{\sigma_h^2} \right)\end{aligned}$$

And the approximate posterior distribution of the hidden representation for each data point can be updated as:

$$\begin{aligned}\Sigma(\mathbf{h}_{t,i}) &= \left(\frac{\mathbf{I}}{\sigma_h^2} + \langle \omega \omega^\top \rangle \right)^{-1} \\ \mu(\mathbf{h}_{t,i}) &= \Sigma(\mathbf{h}_{t,i}) \left(\frac{\langle A_t^\top \rangle \mathbf{k}_{t,i}}{\sigma_h^2} + \langle f_{t,i} \rangle \langle \omega \rangle - \langle b \omega \rangle \right)\end{aligned}$$

In this last formulation is highlighted how the classifier parameters, weights vector and bias, are shared across the tasks.

Then, the joint approximate posterior distribution of b and ω are defined as,

$$\Sigma(b, \omega) = \begin{bmatrix} \langle \gamma \rangle + \sum_{t=1}^T N_t & \sum_{t=1}^T \mathbf{1}^\top \langle \mathbf{H}_t^\top \rangle \\ \sum_{t=1}^T \langle \mathbf{H}_t \rangle \mathbf{1} & \text{diag}(\langle \eta \rangle) + \sum_{t=1}^T \langle \mathbf{H}_t \mathbf{H}_t^\top \rangle \end{bmatrix}$$

$$\mu(b, \boldsymbol{\omega}) = \Sigma(b, \boldsymbol{\omega}) \begin{bmatrix} \sum_{t=1}^T \mathbf{1}^\top \langle \mathbf{f}_t \rangle \\ \sum_{t=1}^T \langle \mathbf{H}_t \rangle \langle \mathbf{f}_t \rangle \end{bmatrix}$$

From these formulations it is possible to note how the model transfer information between the tasks, indeed they update $q(b, \boldsymbol{\omega})$ all together.

Finally, the approximate posterior distributions of the predicted output are:

$$\begin{aligned} \Sigma(f_{t,i}) &= 1 \\ \mu(f_{t,i}) &= \langle \boldsymbol{\omega}^\top \rangle \langle \mathbf{h}_{t,i} \rangle + \langle b \rangle \\ \rho(f_{t,i}) &= f_{t,i} y_{t,i} > \nu \end{aligned}$$

For the predictions, the predictive equations are obtained by substituting the true posteriors with the approximate posterior distributions, this implies the substitution of $p(\mathbf{A}_t | \{\mathbf{K}_u, \mathbf{y}_u\}_{u=1}^T)$ with its approximate posterior distribution $q(\mathbf{A}_t)$. Hence, the predictive distribution of the representation in the latent subspace $\mathbf{h}_{t,*}$ for new datapoints $\mathbf{x}_{t,*}$ is,

$$p(\mathbf{h}_{t,*} | \mathbf{k}_{t,*}, \{\mathbf{K}_u, \mathbf{y}_u\}_{u=1}^T) = \prod_{s=1}^{\mathcal{R}} \mathcal{N}(h_{t,s}^s; \mu(\mathbf{a}_{t,s})^\top \mathbf{k}_{t,*}, \sigma_h^2 + \mathbf{k}_{t,*}^\top \Sigma(\mathbf{a}_{t,s}) \mathbf{k}_{t,*})$$

While the predictive distribution of the predicted output $f_{t,*}$ can be found by substituting $p(b, \boldsymbol{\omega} | \{\mathbf{K}_t, \mathbf{y}_t\}_{t=1}^T)$ with its approximate posterior distribution $q(b, \boldsymbol{\omega})$:

$$\begin{aligned} p(f_{t,*} | \mathbf{h}_{t,*}, \{\mathbf{K}_u, \mathbf{y}_u\}_{u=1}^T) &= \\ &= \mathcal{N}\left(f_{t,*}; \mu(b, \boldsymbol{\omega})^\top \begin{bmatrix} 1 \\ \mathbf{h}_{t,*} \end{bmatrix}, 1 + [1 \quad \mathbf{h}_{t,*}] \Sigma(b, \boldsymbol{\omega}) \begin{bmatrix} 1 \\ \mathbf{h}_{t,*} \end{bmatrix}\right) \end{aligned}$$

And the predictive distribution of the class label $y_{t,*}$ is defined using the predicted output distribution as,

$$p(y_{t,*} = +1 | f_{t,*}, \{\mathbf{K}_u, \mathbf{y}_u\}_{u=1}^T) = \mathcal{Z}_{t,*}^{-1} \Phi\left(\frac{\mu(f_{t,*}) - \nu}{\Sigma(f_{t,*})}\right)$$

Where $\mathcal{Z}_{t,*}$ is the normalization coefficient calculated for the test datapoints, and $\Phi(\cdot)$ is the standardized normal cumulative distribution function.

3.2.1 Application of KBTL for binary problem in literature: damage detection

In this section an application of KBTL proposed by (Gardner, Bull, Dervilis, & Worden, 2022) to demonstrate the applicability of this model for the population based SHM is reported. For this application, a heterogeneous population of shear-structures has been used, specifically consisting of numerical and experimental frames, each with a different number of storeys. The set of features, for each frame of the population is composed by n bending natural frequencies, with n number of storeys of the given frame, this implies inconsistent feature spaces for the different structures.

For the algorithm a radial-basis function kernel (RBF kernel) has been used. The RBF kernel of two input feature vectors (x and x') is defined as,

$$K(x, x') = e^{-\frac{\|x-x'\|^2}{2\sigma^2}} = e^{-\gamma\|x-x'\|^2} \text{ with } \gamma = \frac{1}{2\sigma^2} > 0$$

Where $\|x - x'\|^2$ is the squared Euclidean distance, while γ is a free parameter used to tune the equation determined with the median heuristics approach (Gretton, et al., 2012).

The population is composed of seven shear-structures, one of them is an experimental frame (Figure 16), while the other six are lumped-mass models in bending. Each simulated structure is composed by n masses $\{m_i\}_{i=1}^n$, stiffness $\{k_i\}_{i=1}^n$ and damping coefficients $\{c_i\}_{i=1}^n$ connected as in Figure 17(a). Each mass is characterized by a length l_m , width w_m and a density ρ . The stiffness elements have been designed as four cantilever beam, hence the stiffness assigned to the i^{th} spring is $\{k_i\}_{i=1}^n = 4k_b = 4 \cdot \frac{3EI}{l_b^3}$, where E is the elastic modulus, I the second moment of inertia and l_b the beam length. While the damping coefficients have been directly specified and not derived from a physical model. To obtain different observations for these simulated frames, a random value of E , ρ and c has been extract from base distributions. The properties of these six frames are summarized in Figure 18.



Figure 16: Experimental shear-structures (Gardner, Bull, Dervilis, & Worden, 2022)

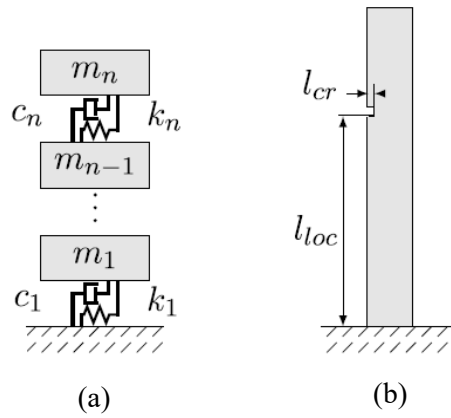


Figure 17: Simulated shear-structures: (a) connection among the masses by means of dampers and springs; (b) cantilever component of the simulated structures (Gardner, Bull, Dervilis, & Worden, 2022)

D	DOF d_i	Beam geometry $\{l_b, w_b, t_b\}$ mm	Mass geometry $\{l_m, w_m, t_m\}$ mm	Elastic modulus E GPa	Density ρ kg/m ³	Damping c N s/m
1	4	{185, 25, 6.35}	{350, 254, 25}	\mathcal{N} (71, 1.0×10^{-9})	\mathcal{N} (2700, 10)	\mathcal{G} (50, 0.1)
2	8	{200, 35, 6.25}	{450, 322, 35}	\mathcal{N} (70, 1.2×10^{-9})	\mathcal{N} (2800, 22)	\mathcal{G} (8, 0.8)
3	10	{177, 45, 6.15}	{340, 274, 45}	\mathcal{N} (72, 1.3×10^{-9})	\mathcal{N} (2550, 25)	\mathcal{G} (25, 0.2)
4	3	{193, 32, 5.55}	{260, 265, 32}	\mathcal{N} (75, 1.5×10^{-9})	\mathcal{N} (2600, 15)	\mathcal{G} (20, 0.3)
5	5	{165, 46, 7.45}	{420, 333, 46}	\mathcal{N} (73, 1.4×10^{-9})	\mathcal{N} (2650, 20)	\mathcal{G} (45, 0.1)
6	3	{175, 40, 6.05}	{400, 310, 41}	\mathcal{N} (69, 1.1×10^{-9})	\mathcal{N} (2750, 18)	\mathcal{G} (20, 0.2)

Figure 18: Properties of the six lumped-mass simulated structures (Gardner, Bull, Dervilis, & Worden, 2022)

For what concern the experimental structure it has been constructed with aluminum 6082 with three storeys, hence three natural frequencies for each observation have been considered. The natural frequencies have been obtained thanks to an electrodynamic shaker that induced a white-noise excitation to the first storey and to three uniaxial accelerometers, one at each floor, that have measured the response.

The damage condition has been obtained by introducing in the experimental frame a crack at the midpoint of the beam of the first storey, with a width equal to half of the beam width. While, in the simulated frames, the same damage has been obtained with a reduction of EI , in particular the stiffness of the spring representing the first storey has been reduced as,

$$k_r = 3 \left(\frac{3EI}{l_b^3} \right) + k_d$$

Where k_d is the tip stiffness of a cantilever beam with a crack located at l_{loc} from the base and of a width l_{cr} as shown in Figure 17(b).

Each domain has been composed by a different number of observations, as it is shown in Figure 19. The two classes are, ‘ $y = 0$ ’ that denote the undamaged state and ‘ $y = 1$ ’ that denote the presence of a crack at the first storey.

From an algorithm point of view, the labels have been converted into ‘ $+1$ ’ and ‘ -1 ’. A point belongs to:

$$\begin{cases} +1 & \text{if } p(y_{t,*} = +1 | f_{t,*}, D) \geq 0,5 \\ -1 & \text{if } p(y_{t,*} = +1 | f_{t,*}, D) < 0,5 \end{cases}$$

Domain	Training		Testing	
	$y = 0$	$y = 1$	$y = 0$	$y = 1$
1	110	25	1000	1000
2	60	20	1000	1000
3	70	50	1000	1000
4	120	10	1000	1000
5	200	25	1000	1000
6	100	10	1000	1000
7 ^a	3	3	2	2

Figure 19: Training and Test dataset for the damage detection, from 1 to 6 are the simulated frames while the 7th is the experimental one, binary classification (Gardner, Bull, Dervilis, & Worden, 2022)

In Figure 20, the results of the training phase are shown, and it can be noted that the latent space dimension chosen by the authors is $\mathcal{R} = 2$ and the margin between the two classes is highlighted by the central continuous line. The figure is divided into two plots, the one on the left represents the training dataset in the latent subspace \mathcal{H} with colors representing the predictions performed by the model and the one on the right that shows the training set in the latent subspace \mathcal{H} but with colors that describe the labels provided as input. In Figure 21 an analogous

representation is shown, but in this case test dataset is plotted. In both these last two figures the experimental frame can be recognized since it is represented with the larger dot \bullet , while the six simulated frames are represented by \times , \square , \star , $*$, \diamond and Δ , respectively. From the test phase, an *accuracy* greater than 92 % is identified for all domains. This demonstrates how KBTL's algorithm can be a powerful instrument for PBSHM in problem of binary classification, allowing the use of data from a range of structures, which may not be perfectly equal to the one for which the SHM has been carried out.

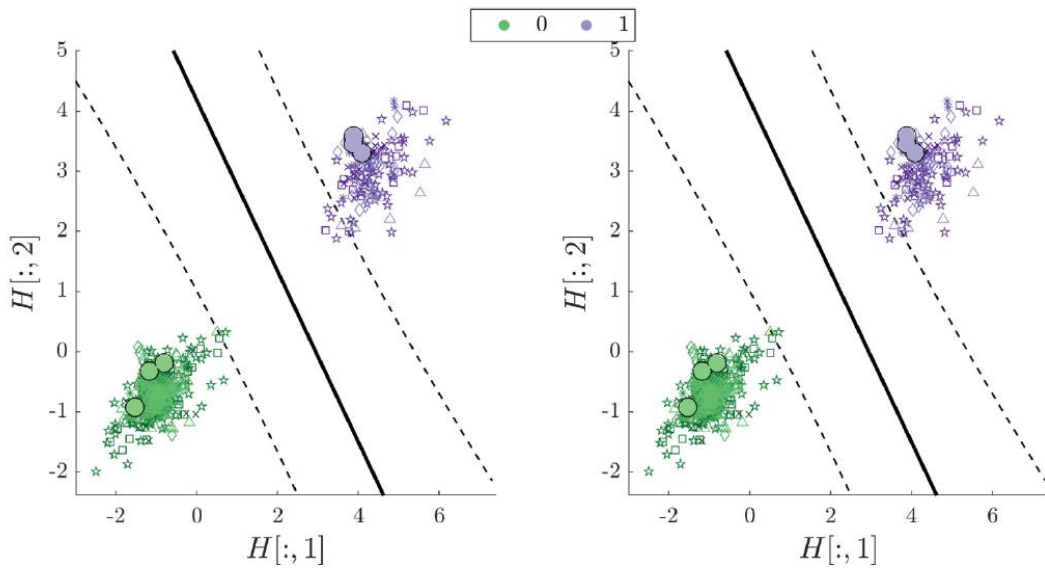


Figure 20: Training Phase of KBTL for PBSHM, the shear-structures case (Gardner, Bull, Dervilis, & Worden, 2022)

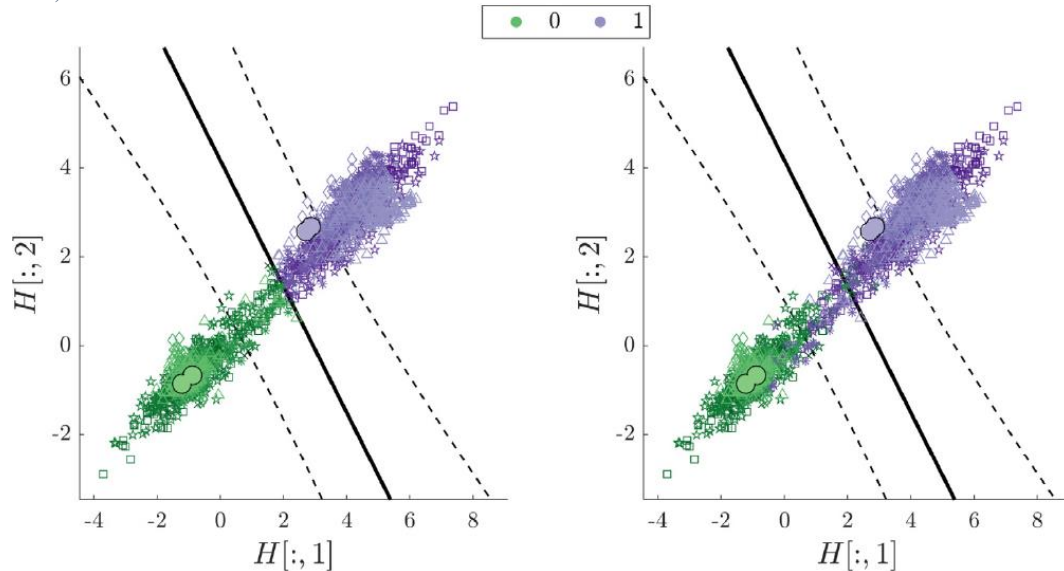


Figure 21: Test Phase of KBTL for PBSHM, the shear-structures case (Gardner, Bull, Dervilis, & Worden, 2022)

3.3 Multiclass classification problems

A multi-class classification implies that the number of classes is strictly greater than 2 ($K > 2$). To perform this type of classification the method defines a shared latent subspace for all the classes, and inside of this subspace a classifier of type *one-versus-all* is applied (Gönen & Margolin, 2014). A one-versus-all classification means that each class has its own classifier that separates it from the other classes. Consequently, a first difference with the binary classification problem can be highlighted, since in this case the classifier parameters, weights and bias, are not shared among the classes, but each class has its own set of classifier parameters $\{b_c \in \mathbb{R}, \boldsymbol{\omega}_c \in \mathbb{R}^{\mathcal{R}}\}$, with their corresponding priors. This means that, for each data the probability that it belongs to the class c is computed, then the data will be labelled by the class for which the highest probability has been computed. In Figure 22 a graphical model of KBTL for multiclass classification is shown.

The distributional assumptions are different from the ones of the binary problem, the new ones are listed below.

$$\begin{aligned}
 \gamma_c &\sim \mathcal{G}(\gamma_c; \alpha_\gamma, \beta_\gamma) && \forall c \\
 b_c | \gamma_c &\sim \mathcal{N}(b_c; 0, \gamma_c^{-1}) && \forall c \\
 \eta_{c,s} &\sim \mathcal{G}(\eta_{c,s}; \alpha_\eta, \beta_\eta) && \forall (c, s) \\
 \omega_{c,s} | \eta_{c,s} &\sim \mathcal{N}(\omega_{c,s}; 0, \eta_{c,s}^{-1}) && \forall (c, s) \\
 f_{t,c,i} | b_c, \boldsymbol{\omega}_c, \mathbf{h}_{t,i} &\sim \mathcal{N}(f_{t,c,i}; \boldsymbol{\omega}_c^\top \mathbf{h}_{t,i} + b_c, 1) && \forall (t, c, i) \\
 y_{t,c,i} | f_{t,c,i} &\sim \delta(f_{t,c,i} y_{t,c,i} > \nu) && \forall (t, c, i)
 \end{aligned}$$

The approximate posterior distributions of the precision priors are defined as,

$$\begin{aligned}
 \alpha(\gamma_c) &= \alpha_\gamma + \frac{1}{2} \\
 \beta(\gamma_c) &= \left(\frac{1}{\beta_\gamma} + \frac{\langle b_c^2 \rangle}{2} \right)^{-1} \\
 \alpha(\eta_{c,s}) &= \alpha_\eta + \frac{1}{2} \\
 \beta(\eta_{c,s}) &= \left(\frac{1}{\beta_\eta} + \frac{\langle \omega_{c,s}^2 \rangle}{2} \right)^{-1}
 \end{aligned}$$

Then, the joint approximate posterior distribution of b_c and $\boldsymbol{\omega}_c$ are defined as,

$$\Sigma(b_c, \boldsymbol{\omega}_c) = \begin{bmatrix} \langle \gamma_c \rangle + \sum_{t=1}^T N_t & \sum_{t=1}^T \mathbf{1}^\top \langle \mathbf{H}_t^\top \rangle \\ \sum_{t=1}^T \langle \mathbf{H}_t \rangle \mathbf{1} & \text{diag}(\langle \boldsymbol{\eta}_c \rangle) + \sum_{t=1}^T \langle \mathbf{H}_t \mathbf{H}_t^\top \rangle \end{bmatrix}$$

$$\mu(b_c, \boldsymbol{\omega}_c) = \Sigma(b_c, \boldsymbol{\omega}_c) \begin{bmatrix} \sum_{t=1}^T \mathbf{1}^\top \langle \mathbf{f}_{t,c} \rangle \\ \sum_{t=1}^T \langle \mathbf{H}_t \rangle \langle \mathbf{f}_{t,c} \rangle \end{bmatrix}$$

And the approximate posterior distributions of the predicted output are:

$$\Sigma(f_{t,c,i}) = 1$$

$$\mu(f_{t,c,i}) = \langle \boldsymbol{\omega}_c^\top \rangle \langle \mathbf{h}_{t,i} \rangle + \langle b_c \rangle$$

$$\rho(f_{t,c,i}) = f_{t,c,i} y_{t,c,i} > \nu$$

The approximate posterior distribution of the hidden representation for each data point can be updated as:

$$\Sigma(\mathbf{h}_{t,i}) = \left(\frac{\mathbf{I}}{\sigma_h^2} + \sum_{c=1}^K \langle \boldsymbol{\omega}_c \boldsymbol{\omega}_c^\top \rangle \right)^{-1}$$

$$\mu(\mathbf{h}_{t,i}) = \Sigma(\mathbf{h}_{t,i}) \left(\frac{\langle \mathbf{A}_t^\top \rangle \mathbf{k}_{t,i}}{\sigma_h^2} + \sum_{c=1}^K \langle f_{t,c,i} \rangle \langle \boldsymbol{\omega}_c \rangle - \langle b_c \boldsymbol{\omega}_c \rangle \right)$$

While the equations of the task-specific projection matrices and their priors remain the same of the ones declared in the binary problem.

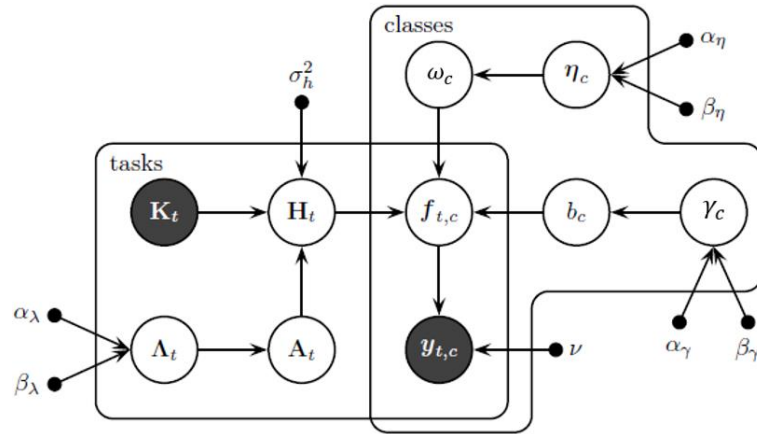


Figure 22: Graphical Model of KBTL for multiclass classification (Gönen & Margolin, 2014)

3.3.1 Application of KBTL for multiclass problem in literature: damage detection

In this section an application proposed by (Gardner, Bull, Dervilis, & Worden, 2022) on the application of KBTL with multiclass classification to the SHM is proposed. This application has been carried out in order to demonstrate the effectiveness of this method in the field of population based SHM. For this application, the same shear-structures of *subchapter 3.2.1* have been used, therefore for their detailed description is referred to that paragraph. Remember that in total seven domains have been used, of which six are simulated with models while one is experimental.

The label space \mathcal{Y} is different from the one of the previous case, indeed in this case four classes are present and $\mathcal{Y} = \{ '0', '1', '2', '3' \}$. The four different classes are related to a different storey on which the crack has been introduced, label '0' corresponds to an undamaged condition, label '1' to a crack located on a beam of the first storey, label '2' to a crack located on a beam of the second storey and label '3' to a crack located on a beam of the third floor. The observations have been obtained as in the previous case, for the experimental frame by introducing a crack of length equal to half of the beam width at the beam midpoint and for the simulated frames by reducing the stiffness of the storey in which the crack is introduced. In Figure 23 the number of observations of all labels for each domain (from 1 to 6 are simulated frames, while the 7th one is the experimental frame), what can be highlighted is that for label '3' the training domain of the experimental frame does not have observations. Indeed, this algorithm is able to generate a model that can predict all four classes for all domains, even though input observations covering all classes were not provided for some of them.

Domain	Training				Testing			
	$y = 0$	$y = 1$	$y = 2$	$y = 3$	$y = 0$	$y = 1$	$y = 2$	$y = 3$
1	120	60	60	0	1000	1000	1000	1000
2	50	20	25	20	1000	1000	1000	1000
3	55	30	30	25	1000	1000	1000	1000
4	70	45	1	45	1000	1000	1000	1000
5	140	1	70	70	1000	1000	1000	1000
6	200	50	50	1	1000	1000	1000	1000
7 ^a	3	3	3	0	2	2	2	0

Figure 23: Training and Test dataset for the damage detection, from 1 to 6 are the simulated frames while the 7th is the experimental one, multiclass classification (Gardner, Bull, Dervilis, & Worden, 2022)

In Figure 24, the results of the training phase are shown, and it can be noted that the latent space dimension chosen by the authors is $\mathcal{R} = 2$ and the margin between two classes is highlighted by a central continuous line. The figure is divided into two plots, the one on the left represents the training dataset in the latent subspace \mathcal{H} with colors representing the predictions performed by the model while the right one shows the training set in the latent subspace \mathcal{H} but with colors that describe the labels provided as input. The predictions are performed assigning at each data the label for which the highest probability has been computed. In Figure 25 an analogous representation is shown, but in this case test dataset is plotted. In both these last two figures the experimental frame can be recognized since it is represented with the larger dot \bullet , while the six simulated frames are represented by \times , \square , \star , $*$, \diamond and Δ , respectively. From the test phase, an *accuracy* greater than 92 % is identified for all domains. This demonstrates how KBTL's algorithm can be a powerful instrument for PBSHM in problem of binary classification, allowing the use of data from a range of structures, which may not be perfectly equal to the one for which the SHM is being carried out.

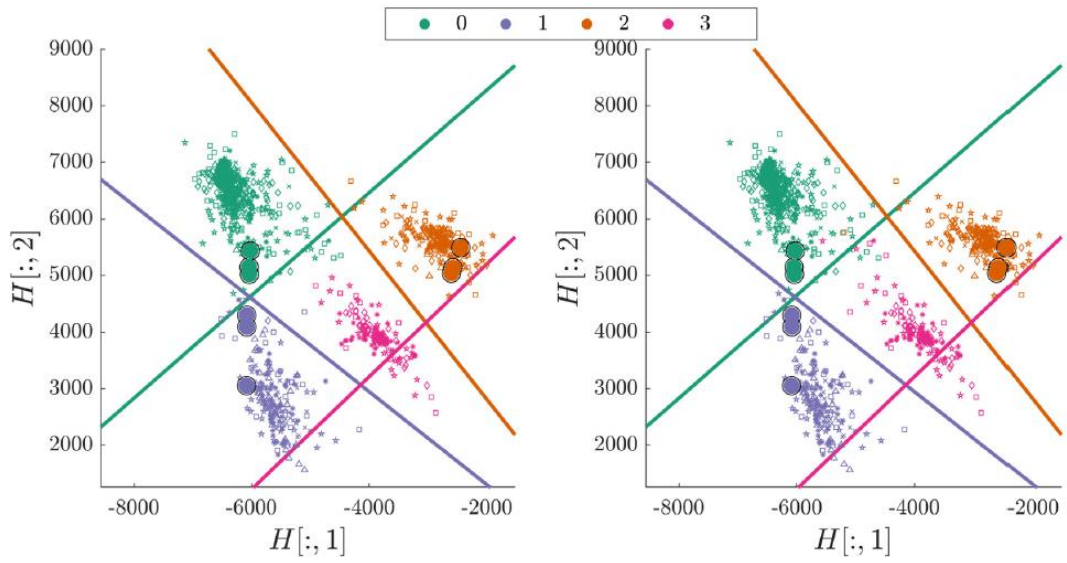


Figure 24: Training Phase of KBTL for multiclass classification of damages (Gardner, Bull, Dervilis, & Worden, 2022)

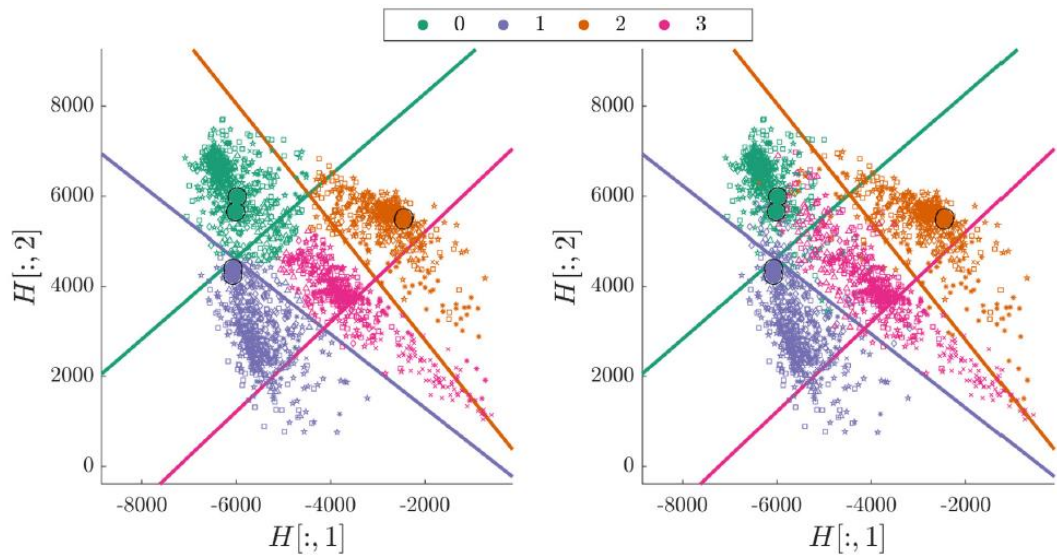


Figure 25: Test Phase of KBTL for multiclass classification of damages (Gardner, Bull, Dervilis, & Worden, 2022)

Chapter 4

Transfer Learning technique (KBTL) applied to oval masonry domes for damage detection

4.1 Case study

In this chapter an application about damage detection is presented. In particular a transfer of knowledge between two churches is used in order to verify if data coming from a church different from the one under analysis are useful for the damage identification. Since no damaged data are available for the two real structures, this application is performed only at the level of the FEM of the two churches.

4.1.1 Sanctuary of Vicoforte – Source Domain

The Sanctuary of Vicoforte is characterized by the world's largest oval-shaped masonry dome and its construction started at the end of the 16th century under the project of Ascanio Vitozzi. However, construction had some interruptions, until the 18th century, when it has been resumed by Francesco Gallo, with whom the dome has been erected. This dome is characterized by internal axes of 37.15 *m* and 24.80 *m*. In the first years after the construction the structure suffers of different

structural problems, reason why in 1983 some strengthening interventions have been performed. Then in 1987, a severe cracking configuration has been observed in the drum-dome system, therefore a new system composed by 56 tie-bars tensioned has been introduced in addition to the existing system of circumferential iron rings located between dome and drum that was close to the yielding condition.

On this structure a static monitoring activity of ten years, from November 2004 to November 2014, has been developed, from which it has been possible to obtain information about the seasonal influence of the temperature and to assess the damage state of the building as well as verifying the effectiveness of previously added strengthening systems (Ceravolo, De Marinis, Pecorelli, & Zanotti Fragonara, 2017). This static monitoring system can be subdivided into two main groups: the first one was composed by instruments for the measurements of stress, strains and crack width (load cells, wire gauges and crack meters), while the second one was composed by instruments for the measurement of the environmental conditions (thermometers) (Ceravolo, Coletta, Miraglia, & Palma, 2021). In Figure 26 a representation in plan of the thermometers (T), the wire gauges (E0), the load cells (LC) and the crack meters (CM) is shown. Nevertheless, since the static monitoring system is able to provide only local information about the structural health, starting from December 2015 a permanent monitoring system has been installed in order to record the dynamic response of the Sanctuary, in particular three orthogonal accelerometers have been located at the base of the crypt to measure to ground acceleration, while a set of nine accelerometers, along longitudinal and transverse direction, have been located at different levels of the lantern-dome-drum system. All the twelve accelerometers used are mono-axial piezoelectric accelerometers, in Figure 27 a visual representation of their location in the Sanctuary is shown. The acquisition system was set in order to record data for 20 minutes every hour when the ground horizontal accelerations, measured by the three accelerometers at the base of the crypt, exceed a pre-set value. The pre-set value has been chosen as $0.042g$, based on the seismic hazard of the area defined by the Italian Regulations. Starting from these recorded accelerations, the modal parameters of the Sanctuary can be obtained using an automatic modal identification procedure that use an algorithm that is part of the Stochastic Subspace Identification techniques.

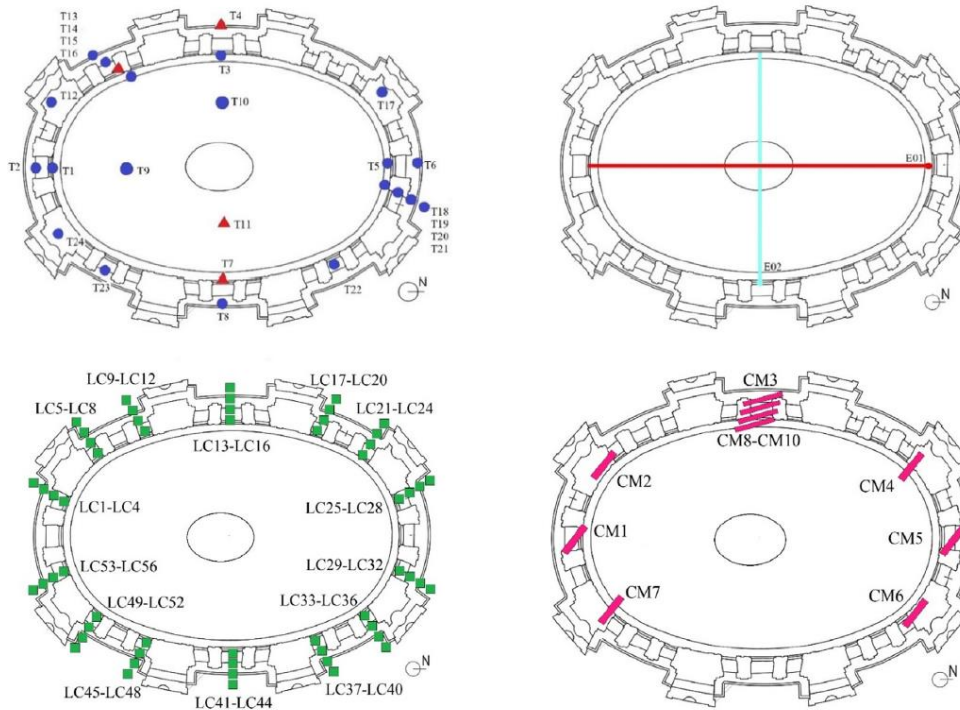


Figure 26: Static Monitoring System at the Sanctuary of Vicoforte (2004-2014) (Ceravolo, Coletta, Miraglia, & Palma, 2021)

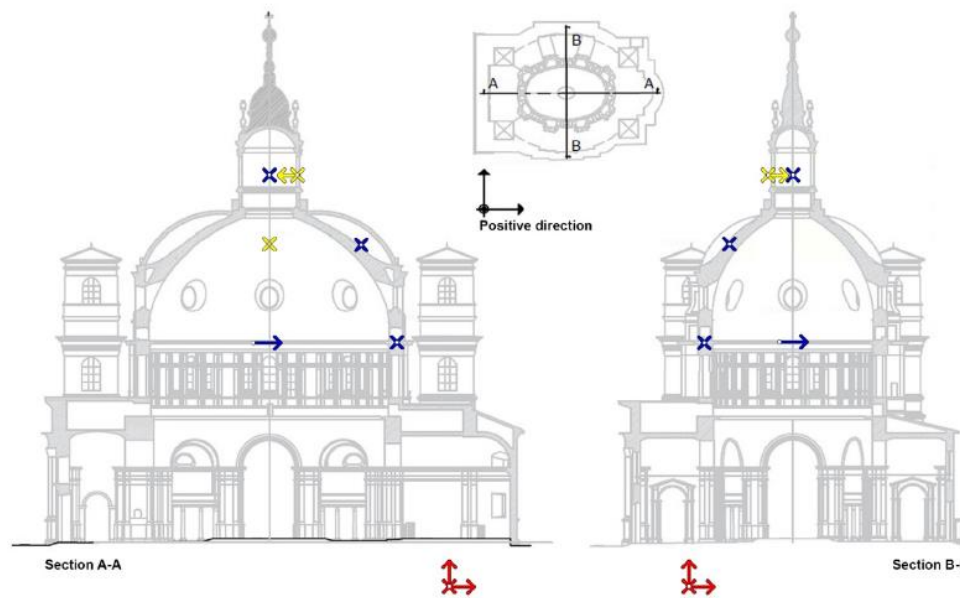


Figure 27: Dynamic Monitoring System at the Sanctuary of Vicoforte - Accelerometers Location (Ceravolo, Coletta, Miraglia, & Palma, 2021)

A Finite Element Model (FEM) of the Sanctuary is available and it is composed by nine homogenous macro-elements: seven for the structure (lantern, dome, drum, basement, buttresses, belltowers, and iron ties) and two for the soil (marl and clay), in Figure 28 these nine macro-elements are highlighted. For what concern the elements used for the modelling, shell elements have been used to model the lantern, the dome, the drum and the buttresses, the tie-bars of the strengthening system have been modelled with a 2-node beam elements, while the soil foundation and pillars have been modelled using 8-node hexahedral solid elements (Ceravolo, De Lucia, Miraglia, & Pecorelli, 2020). This model has been thermo-elastic updated using the Multiphysics data obtained from the monitoring activities, in particular the input data has been the temperature distribution of the drum-dome system related to the force acting in the tie-bars obtained with a thermal analysis of only a partial finite element model of the Sanctuary. This partial model was composed by the upper macro-elements, such as the lantern, the dome, the drum and the buttresses, as can be observed in Figure 29, and for both steel and masonry an isotropic thermal conductivity has been considered. In Table 3 the updated properties of the model, in terms of Elastic Modulus, Poisson's Ratio and density are reported.

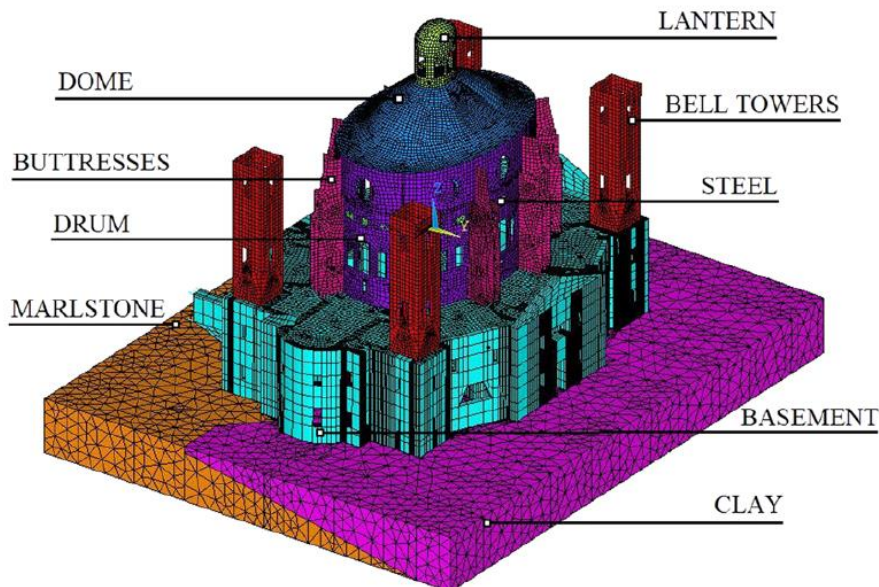


Figure 28: FEM of the Sanctuary of Vicoforte with the representation in different colors of the nine macro-elements (Ceravolo, De Lucia, Miraglia, & Pecorelli, 2020)

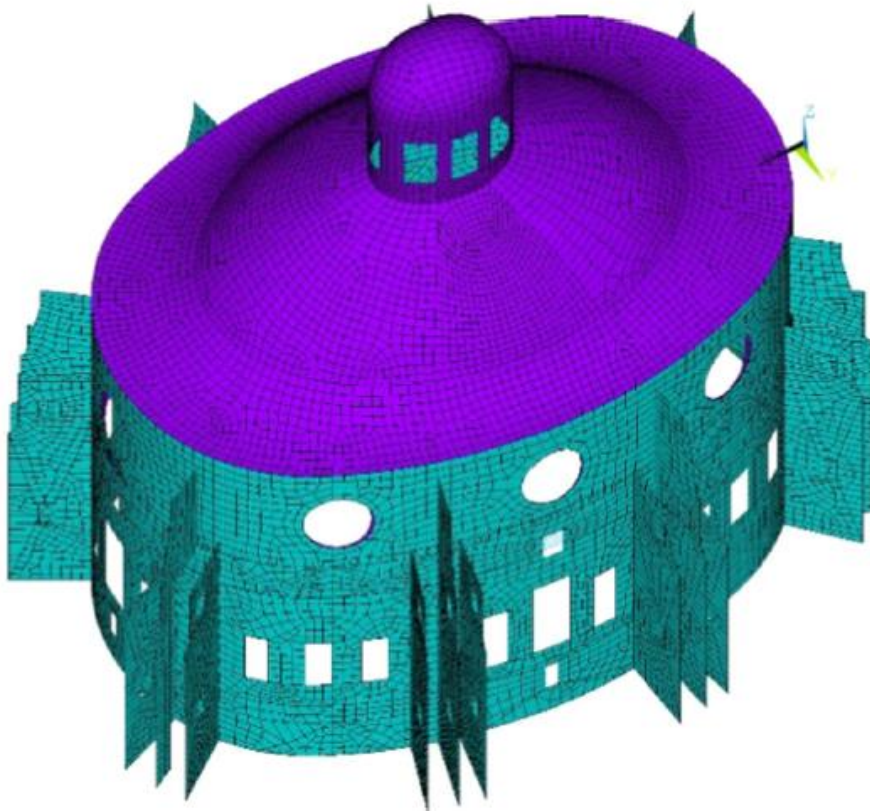


Figure 29: Limited FEM of the Sanctuary of Vicoforte for the Thermal Analysis (Ceravolo, De Lucia, Miraglia, & Pecorelli, 2020)

Macro-element	E [GPa]	ν [-]	ρ [kg/m ³]
Belltowers	4.50	0.35	1800
Basement	2.00	0.35	1800
Buttresses	5.50	0.30	1700
Clay	0.75	0.35	1900
Dome	5.50	0.35	1800
Drum	2.30	0.35	1700
Lantern	5.60	0.35	1800
Marlstone	5.60	0.35	2100
Steel	210	0.30	7800

Table 3: Properties of the macro-elements of the Sanctuary of Vicoforte after the model updating

Finally, in Figure 30 the FEM mode shapes of the first three modes are shown. The first modes are the first flexural mode in Y direction (that means the direction of the minor axis) the first flexural mode in X direction (that means the direction of the major axis) and the first torsional mode around Z. A comparison between the

frequencies obtained by the monitoring activities (as mean value over a year) and the ones obtained with the model (numerical frequencies) has been obtained for different modes (Ceravolo, De Lucia, Miraglia, & Pecorelli, 2020), the results are reported in Table 4.

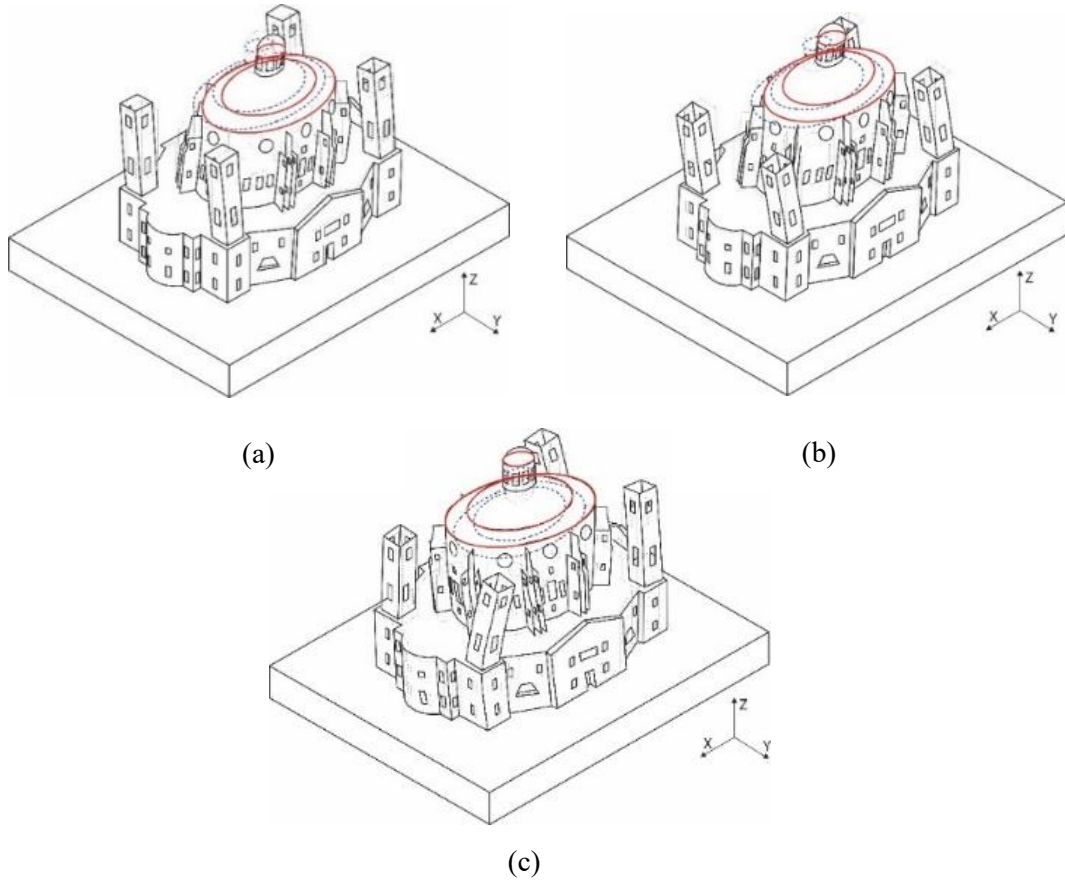


Figure 30: First three mode shape of the Sanctuary of Vicoforte obtained with the FEM, (a) first flexural mode in Y direction, (b) first flexural mode in X direction and (c) first torsional mode. The red curves are representative of the undeformed dome.

Mode	f_{ID} [Hz]	$f_{FEM, updated}$ [Hz]	Error [%]
1st bending Y	1.93	1.93	0.00
1st bending X	2.09	2.11	-0.96
1st torsional	2.84	2.84	0.00
2nd bending Y	3.60	3.89	-8.06
2nd bending X	3.96	4.17	-5.30

Table 4: Comparison between frequency identified from the signal recorded with the monitoring system and frequency obtained with the FEM updated of the Sanctuary of Vicoforte (Ceravolo, De Lucia, Miraglia, & Pecorelli, 2020)

4.1.2 Church of Santa Caterina – Target Domain

The Church of Santa Maria delle Grazie, also known as Church of Santa Caterina, is an important example of baroque religious architecture located in Casale Monferrato (AI). In the 18th century an extension of the church voted to Santa Maria delle Grazie was designed and partly built by Giovanni Battista Scapitta, who died during the construction phase, which was later supposedly completed by Giacomo Zanetti. In Figure 31 the external and internal view of the structure is presented. The Church is characterized by the typical aspect of a monastery church, indeed it present two halls, the external one that is open to the public, the actual church, and the internal one that is open only to the nuns and takes the name of choir; in Figure 33 this subdivision is shown. The external church has a Greek cross plan in whose central room eight large columns, connected by arches, are present to sustain the above dome and lantern system set on a drum. Both the dome and the drum have an elliptical shape, with the major axis of 14 meters and the minor axis of 10 meters, then the drum is placed at 13 meters and spreads 7 meters in height, where eight sides windows are located, while the dome has a height of 5 meters. The oval dome presents eight ribs connected to the columns of the drum and it is covered by a thin layer of copper plates fixed to the external masonry. Then above the dome a lantern is located at approximately 26 meters of height and spreads 6 meters in height, along which eight windows are placed. The principal façade of Piazza Castello has a total height of 13 meters of which 6 meters are above the drum, hence this last section behaves like a cantilever. In Figure 32 some drawings of the Church are reported for a visual identification of the parts.



Figure 31: External (left) and Internal (right) view of the Church of Santa Caterina, in the upper right corner is shown the dome, while in the bottom right corner the choir (La Chiesa, 2021)

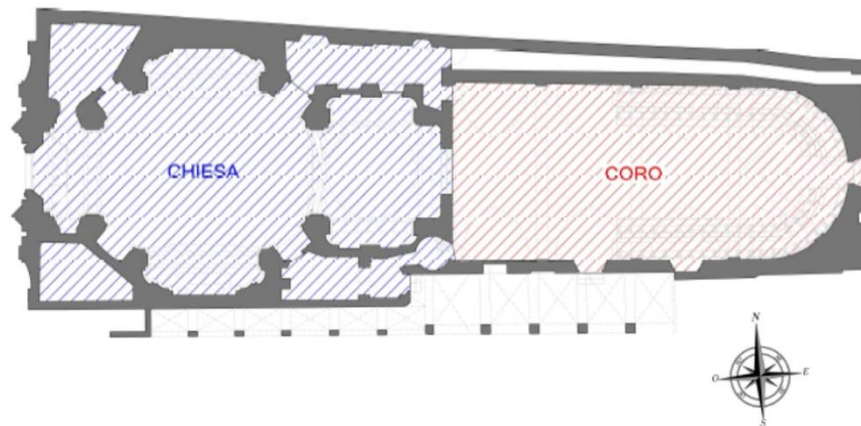


Figure 33: Church and Chore of the structure of Santa Caterina's Church (Ceravolo, Lenticchia, Miraglia, & Scussolini)



Figure 32: Longitudinal section (left) and Front view (right) of Santa Caterina's Church drawings (Ceravolo, Lenticchia, Miraglia, & Scussolini)

Thanks to a series of visual inspections, an extended state of damage all over the church has been identified, particularly damaged appear to be the drum-dome system, the lantern and the principal façade. This state of damage was induced by several factors, among which humidity was fundamental.

Based on the results obtained in the 2010 with the dynamic test campaign a first preliminary geometric model and the consequent mechanical model of the structure have been realized as shown in Figure 34 (Ceravolo, Lenticchia, Miraglia, & Scussolini). As for the model of the Sanctuary of Vicoforte, also this model has been developed by dividing the structure in macro-elements, in this case six, among which we find the basement/foundation, the drum-dome system, the lantern, the façade and the external walls. For what concerns the material a linear elastic isotropic behavior and a homogeneity throughout the structure has been considered,

with elastic modulus equal to 2500 MPa , Poisson ratio equal to 0.40 and a density of 2000 kg/m^3 . While, the elements used for the mesh of this model are mono-dimensional and bi-dimensional elements, in particular a 2-nodes beam element has been used for the thick columns at the base, for the thin columns of the lantern and for the ribs of the drum-dome systems; while, a 4-nodes shell element has been used for the arches and for the walls composing the base, the façade, the lantern, the drum-dome system and the external walls. Finally, the structure has been assumed as clamped at the base and its interaction with soil has been neglected, while the interaction with the choir has been considered as rigid, since the choir has not been modelled due to the leakage of information. This is the primary model that has been used to identify the structural elements the most effect the dynamic behavior of the church and on the base of these results a dynamic campaign has been designed and has been carried out on the 23rd, 24th, 27th, 28th and 29th of September 2010. For this monitoring campaign, four measure points has been designed, three of these have been used to obtain the mode shapes in the three main directions, translation in X direction, translation in Y direction and rotation around Z, while the fourth one has been designed to link the channels during the signal processing phase. The different setups (measure points) are, the Dome YZ (it analyzed the section parallel to the plane YZ in the direction orthogonal to the principal axis of the structure), the Dome XZ (it analyzed the section parallel to the plane XZ in the direction parallel to the principal axis of the structure), the Global (similar to the Dome XZ, but extended to the choir) and the link. In Figure 35 the drawings of the structure with the different setups are reported and it is possible to note that each setup was composed by 18 acquisition channels.

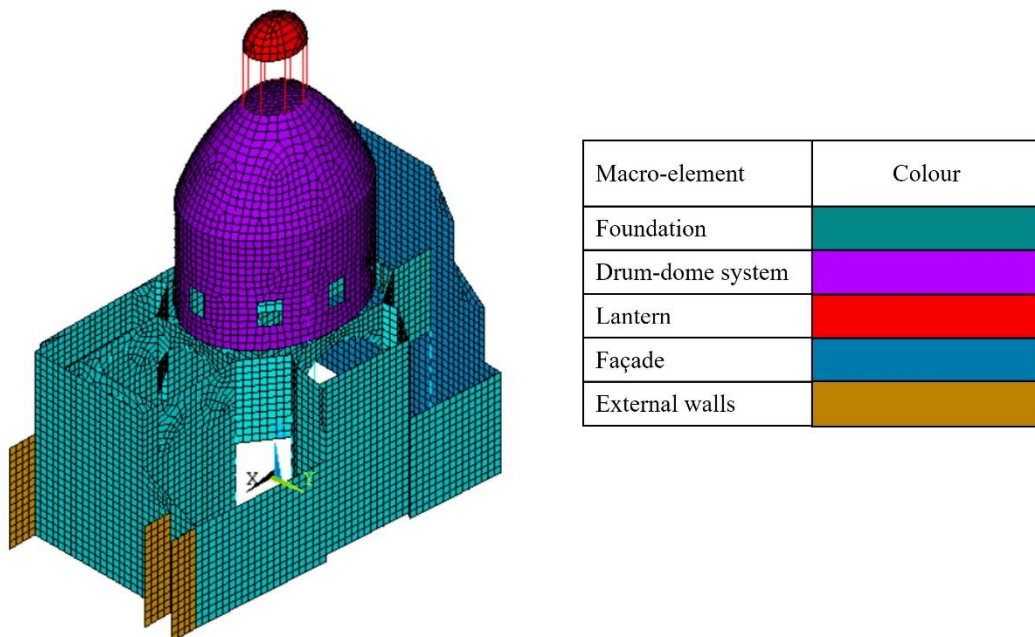


Figure 34: Mechanical Model of the Church of Santa Caterina

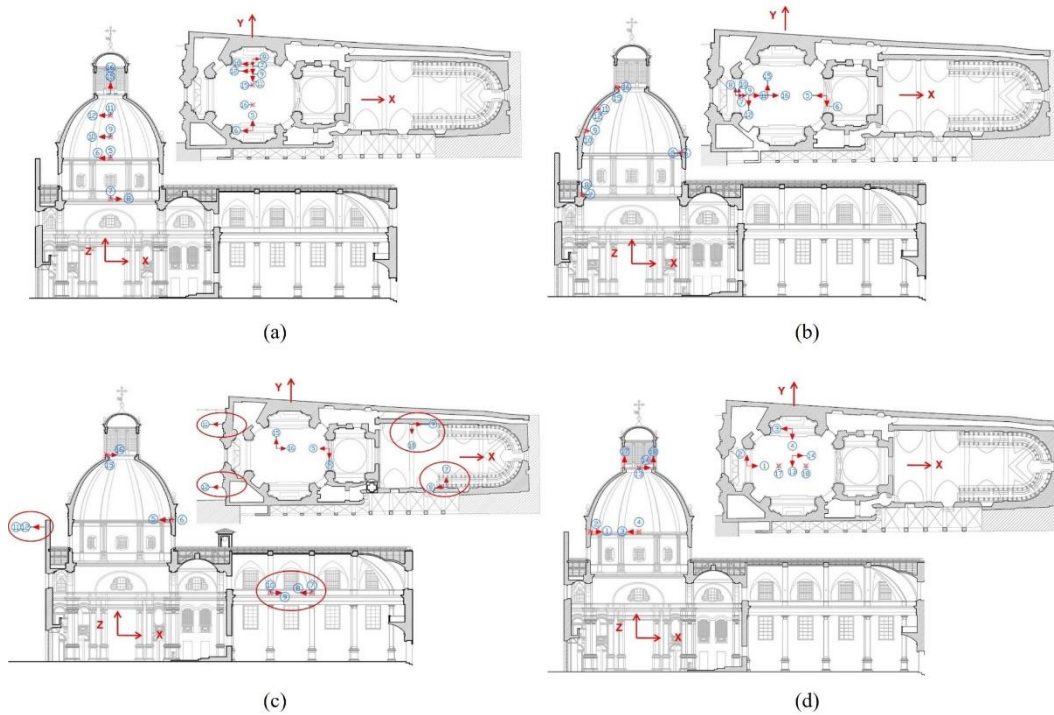


Figure 35: Setups of the dynamic campaign at the Church of Santa Caterina. (a) Dome YZ (b) Dome XZ (c) Global and (d) Link (Ceravolo, Lenticchia, Miraglia, & Scussolini)

Starting from the signal recorded in this campaign a linear dynamic identification of the structure, in terms of frequencies, mode shapes and damping ratios, has been carried out in the time domain with an algorithm, generally defined as “Canonical Variate Analysis”. The first six natural frequencies and damping ratio identified with this process are collected in Table 5.

<i>Identifier</i>	<i>Description</i>	f [Hz]	ζ [%]
1	Transverse global mode and chorus in-phase with the dome. The lantern moves transversally.	3.03	1.93
2	Local facade mode. Small movements of the lantern.	3.33	0.63
3	Transverse mode with torsional components and chorus, counter-phase to the dome. The lantern moves mainly transversally.	3.97	4.23
4	Longitudinal global mode of the drum-dome system. The lantern moves mainly longitudinally.	4.40	3.17
5	Transverse mode with high components of the lantern. The lantern moves transversally.	5.11	3.14
6	Torsional global mode and chorus counter-phase to the dome.	5.39	0.86

Table 5: First six natural frequencies and damping ratio identified from the signal recorded during the dynamic campaign of 2010, church of Santa Caterina

Finally, the model updating of the preliminary model, described above, has been carried out thanks to the information (natural frequencies and mode shapes) obtained from the dynamic campaign of 2010. In Table 6 is reported the comparison between the frequencies obtained from the experimental campaign and the frequencies obtained from the updated model.

<i>Identifier</i>	<i>Mode number in FEM (2010)</i>	<i>Freq. FEM (2010) [Hz]</i>	<i>Freq. ID. (2010) [Hz]</i>	<i>Error [%]</i>
1	1	2.94	3.03	2.97
2	2	3.53	3.33	-6.01
3	3	4.29	3.97	-8.06
4	4	4.30	4.40	2.27

Table 6: Comparison between the frequencies obtained with the updated model of the church of Santa Caterina and the frequencies obtained from the identification process on the signal recorded during the dynamic campaign of 2010

Thanks to the initial visual inspections and to the update models, the high vulnerability of the façade and the lantern has been confirmed, therefore a strengthening intervention has been designed and realized on the structure. For what concern the lantern, sixteen L-shaped profiles have been placed along the eight columns and three C-shaped profiles have been installed on the lintel and in correspondence of the windows, to create a sort of circular cage to guarantee a better global behavior of the system. While, for the façade a metal frame has been connected to the tympanum (the cantilever portion of the façade) in the inner side. The system tympanum-metal frame behaves like a parallel collaborating system; indeed, the metal frame collaborates to increase the compressive strength of the masonry. In addition, this frame allows a redistribution of the horizontal seismic actions, with consequent reduction of the seismic response in both in-plane directions. Since these interventions have induced a variation in the response of the structure, also the model has required an additional updating to take them into account, in particular the two systems have been modelled as it is shown in Figure 36.

After the realization of these strengthening interventions a dynamic test campaign during December 2022 and from January 2023 to March 2023 has been developed with the same procedure of the campaign of 2010, to verify the effectiveness of these interventions, to obtain continuously records and to obtain information to design a permanent dynamic monitoring system, in particular for the lantern and the façade (the most critical elements). In this case the setups were composed by, three accelerometers placed at the top of the lantern to record the lateral and torsional vibration of the element. In particular, two accelerometers have been used to capture the accelerations in the transverse directions and the other to acquire the longitudinal acceleration, as it is shown in Figure 37.

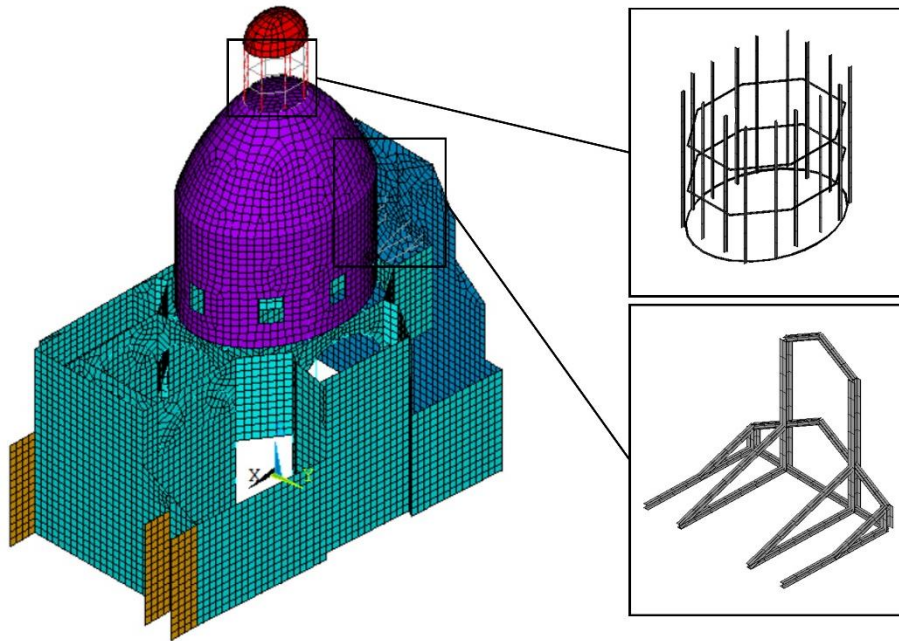


Figure 36: Model updating of the Church of Santa Caterina to consider the realized strengthening interventions (Ceravolo, Lenticchia, Miraglia, & Scussolini)

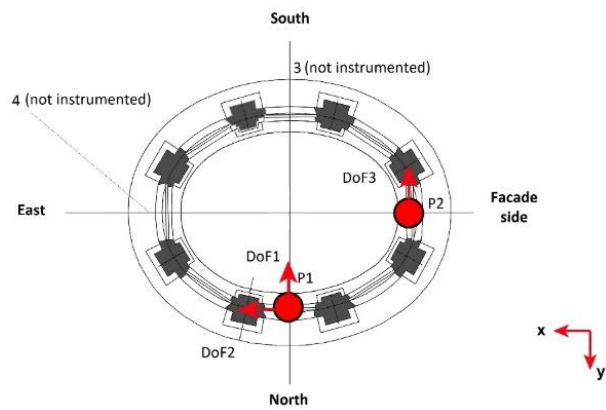


Figure 37: Setups for the dynamic monitoring of December 2022, January-March 2023 of the Church of Santa Caterina (Ceravolo, Lenticchia, Miraglia, & Scussolini)

Thanks to an identification process, as in 2010, six stable modes for the lantern have been detected, the results are reported in Table 7.

<i>Identifier</i>	<i>Description</i>	f [Hz]	ζ [%]
1	Lantern moves transversally.	3.05	2.00
2	The lantern moves mainly transversally with small longitudinal effects.	3.45	1.60
3	The lantern moves mainly transversally with smaller components in longitudinal direction.	4.06	1.50
4	The lantern moves mainly longitudinally with smaller components in transverse direction.	4.49	1.50
5	The lantern moves transversally, and very little in the longitudinal direction.	5.19	1.50
6	The lantern moves equally in the transverse and longitudinal directions.	5.51	1.20

Table 7: Frequencies and damping ratio identified from the records of the dynamic tests on the Church of Santa Caterina, December 2022, January-March 2023 (Ceravolo, Lenticchia, Miraglia, & Scussolini)

Then, as done in the 2010, a model updating considering the results of the last dynamic tests campaign has been performed. During this process, the elastic modulus of the materials has been modified in different steps (each module could vary within a predefined range) until the frequencies obtained with the model and those obtained from the experimental campaign have been sufficiently similar. In Figure 38 the final updated values of the macro-elements elastic modules are shown.

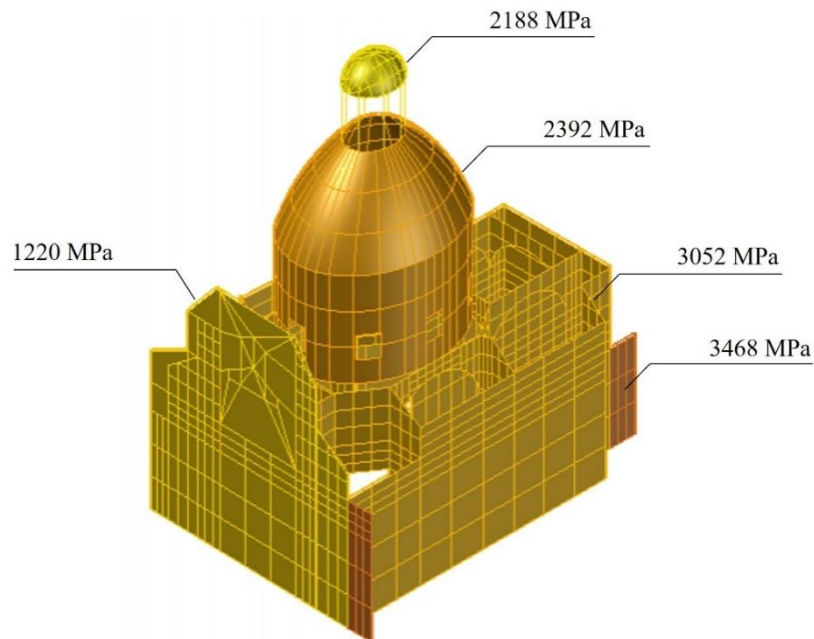


Figure 38: Updated elastic modulus of the six macro-elements of the Church of Santa Caterina (Ceravolo, Lenticchia, Miraglia, & Scussolini)

Finally, in Table 8 the comparison between the frequencies obtained with the identification process and those obtained from the FEM of the church are reported, while in Figure 39 the modes simulated on the FEM are shown.

<i>Identifier</i>	<i>Mode number in FEM (2022)</i>	<i>Freq. FEM (2022) [Hz]</i>	<i>Freq. ID. (2022) [Hz]</i>	<i>Error [%]</i>
1	1	2.93	3.05	3.93
2	2	3.14	3.45	8.98
3	4	4.12	4.06	-1.48
4	5	4.81	4.49	-7.13

Table 8: Comparison between the frequencies obtained with the identification process (December 2022) and those obtained from the FEM of the Church of Santa Caterina

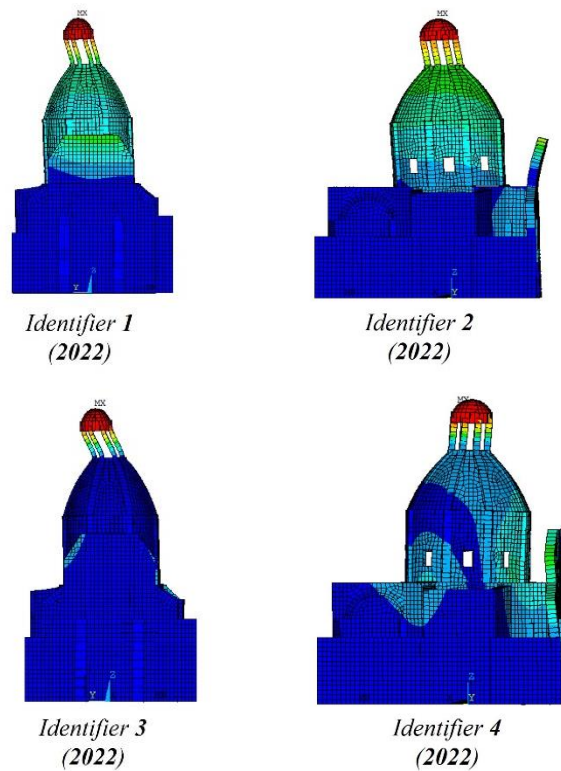


Figure 39: Identified modes after the strengthening intervention of the Church of Santa Caterina (Ceravolo, Lenticchia, Miraglia, & Scussolini)

4.2 KBTL applied to data from the finite element models for damage localization

4.2.1 Domains and Labels

Starting from the two FEM models of the two churches, data representing a damage state have been simulated. In particular, the two models have in common two different macro-elements, the drum-dome element and the basement element, therefore a variation of the elastic modulus of these two macro-elements has been imposed to both the models, and for each value of the modulus the natural frequencies of the structures have been obtained. In both the models, 100 analyses have been performed by varying the elastic modulus of the drum-dome macro-element and other 100 analyses by varying the elastic modulus of the basement macro-element.

The elastic modulus for each analysis has been obtained by pre-multiplying the calibrated value, for a value belonging to the range $[0.5, 1.0]$, that implies a reduction of the elastic modulus of the actual condition of at most 50 %.

For each structures the natural frequencies have been obtained. For the Sanctuary of Vicoforte the first three natural frequencies, first bending frequency in Y direction ($f_1[Hz]$), first bending frequency in X direction ($f_2[Hz]$) and first torsional frequencies ($f_3[Hz]$) are used as the features of the Source Domain for the problem of damage detection. While, for the Church of Santa Caterina the first bending frequency in the longitudinal direction ($f_1[Hz]$) is used as data related to the variation of the drum-dome elastic modulus and the first bending frequency in the transverse direction ($f_2[Hz]$) as data related to the variation of the basement elastic modulus, that together define the Target Domain. This domain has less features with respect to the Source Domain, since the torsional component is prevalently related to the lantern, and it is not so evident as in Vicoforte, and in addition some coupling problems are present and therefore only one frequency can be identified as function of where the damage is located. The frequencies have been divided in 3 classes, that define the three labels of the problem. If the frequencies of an observation are representative of a drum-dome damage the *label '0'* is assigned, if they represent a basement damage the *label '1'* is assigned, and regardless of which element the elastic modulus has been reduced to, if the reduction is less than the 10 %, *label '2'* has been assigned, which represents a slight altered condition or even a health one. In Figure 40 the visual representation of the simulated frequencies as function of the reduction imposed to the elastic modulus for Santa Caterina is shown, analogously in Figure 41 the frequencies of Vicoforte are shown.

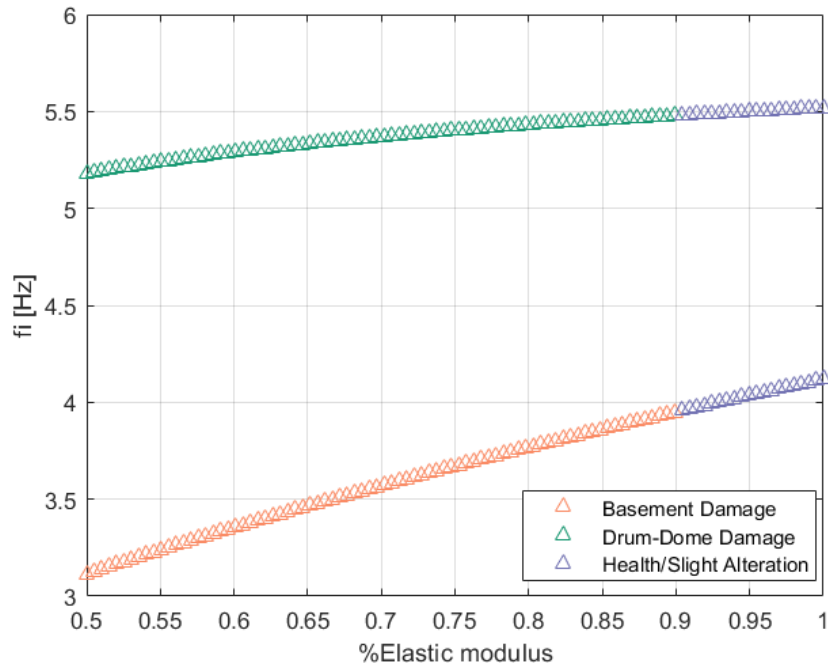


Figure 40: Simulated Data for damage identification for the Church of Santa Caterina

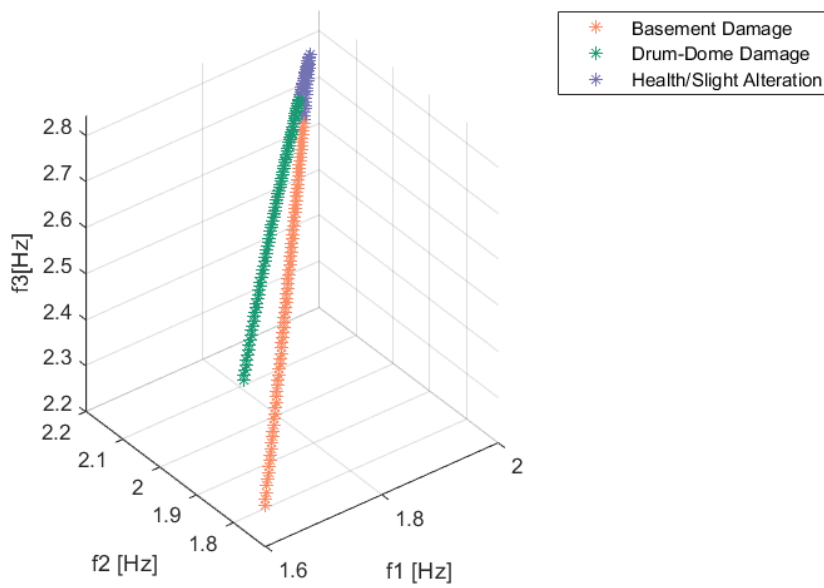


Figure 41: Simulated Data for damage identification for the Sanctuary of Vicoforte

Theoretically, since the data are obtained with FEM of the structures, whatever damage condition could be simulated, but if we work with real structure this cannot be done, since the structure cannot be appositely damaged to record a frequency that could describe it. For instance, even if this application is developed on the base of data acquired from the models, it is supposed to have only few data related to the damage conditions of the Church of Santa Caterina and more information from the Sanctuary of Vicoforte, therefore in this view is evident how the Church of Santa Caterina is the Target Domain, while the Sanctuary of Vicoforte the Source Domain. Here, the domain adaptation is used to improve the knowledge of the Church of Santa Caterina by exploiting information that comes from the Sanctuary of Vicoforte. Hence, the Source Domain is actually represented by Figure 41, while the actual Target Domain, composed by 25 observations, 10 for the *label '0'*, 10 for the *label '1'* and 5 for the *label '2'*, is shown in Figure 42, these observations have been chosen more or less in the middle of each classes in order to be in the worst condition, indeed in this way the algorithm does not have information about the limits of each class from the domain of the Church of Santa Caterina. The remaining simulated data from the Church of Santa Caterina are then used as Test Domain (Figure 43), to verify for how many new data (data that were not used during the training phase) the algorithm is able to assign the correct labels, so the correct damaged/undamaged condition. In this condition whereby few data are available for the structure under investigation (in this case the Church of Santa Caterina), a simple ML model inferred in its domain will most likely tend toward overfitting, so it will become too much adapt to the training data that will no longer be able to generalize for new data, for this reason the domain adaptation is used, indeed a *'larger'* training dataset (data from both the structures) will help the algorithm to define a classifier that will be able to generalize better for new data.

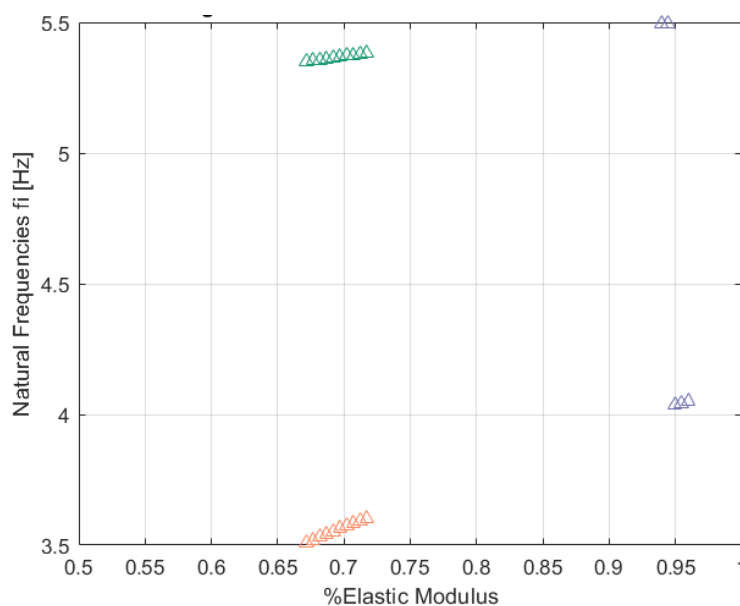


Figure 42: Target Domain (Church of Santa Caterina) for the damage identification

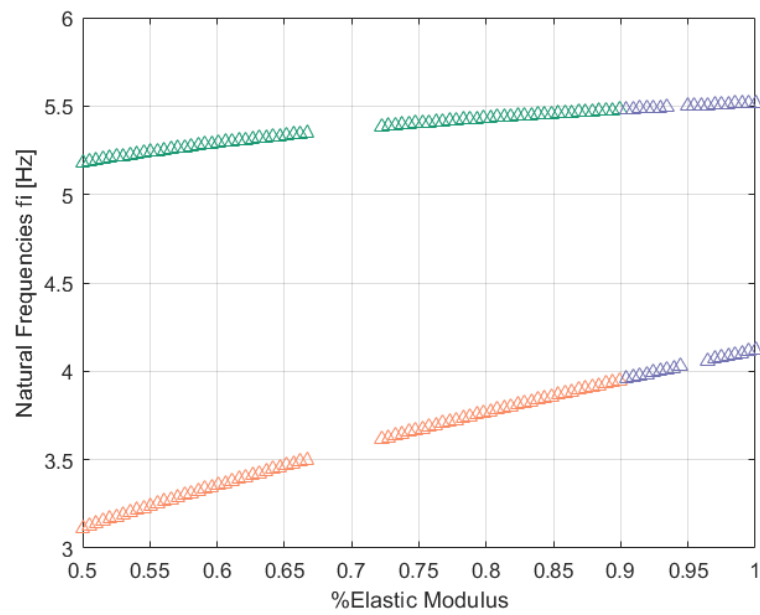


Figure 43: Test Domain (Church of Santa Caterina) for damage identification

In the following table a summary of the Target and Source Domain composition is shown.

OBSERVATIONS						
<i>Domains</i>	<i>Training Phase</i>			<i>Test Phase</i>		
	<i>Labels</i>			<i>Labels</i>		
	<i>y = 0</i>	<i>y = 1</i>	<i>y = 2</i>	<i>y = 0</i>	<i>y = 1</i>	<i>y = 2</i>
Target <i>(Church of Santa Caterina)</i>	10	10	5	70	70	35
Source <i>(Sanctuary of Vicoforte)</i>	80	80	40	0	0	0

Table 9: Summary of the Domains used for the damage identification problem

4.2.2 Results

Since the labels are three, a multi-class KBTL has been applied to the training dataset, composed by Source and Target Domain to infer a classifier. A dimension $\mathcal{R} = 2$ of the latent subspace is chosen in order to have a visual representation of the model. In Figure 44 the results of the training phase are shown, here the two domains for the training phase, are dimensional reduced and projected in the latent subspace where a linear discriminant is inferred. It is possible to distinguish the two domains and the three classes, indeed the Sanctuary of Vicoforte is represented by the star *, while the Church of Santa Caterina by the triangle Δ , then the three classes can be identified by the different colors, green for *label '0'* (damage at the drum-dome macro-element), orange for *label '1'* (damage at the basement macro-element) and purple for *label '2'* (health condition or slight alteration). In the figure two plots are visible, indeed the one on the left shows the domains projected in the latent subspace where each data is colored as function of the prediction performed by the algorithm (*'predicted labels'*), while the one on the right shows the same domains projected but with the data colored as function of the labels provided to the algorithm as input together with the frequencies, therefore are the *'correct labels'*.

In Figure 45 the test phase is shown, since the domain of the Sanctuary of Vicoforte is used only to increase the knowledge of the Church of Santa Caterina, the test is performed only on data representative of this last structure, for this reason only triangles Δ are present. As in the previous figure the two plots show, the one on the left the *'predicted labels'* while the one on the right the *'correct labels'*.

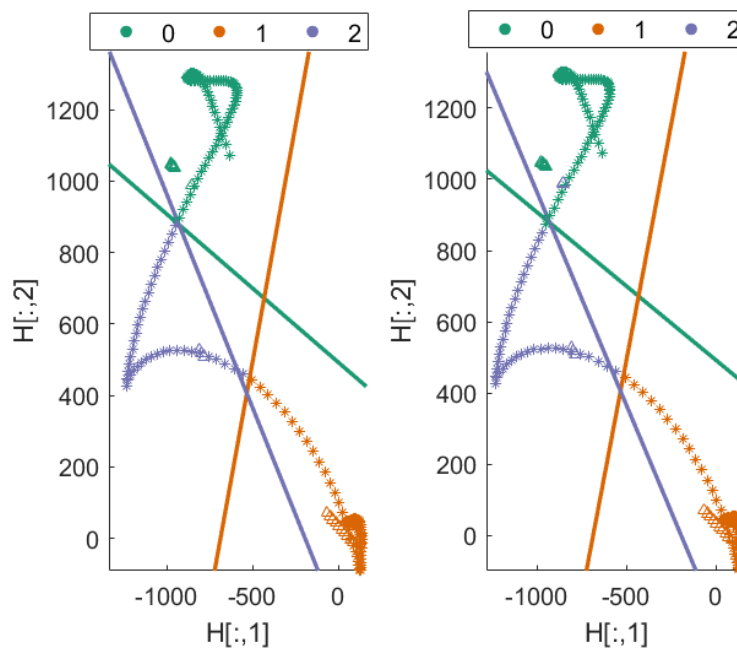


Figure 44: Training Phase of the KBTL multi-class for damage detection

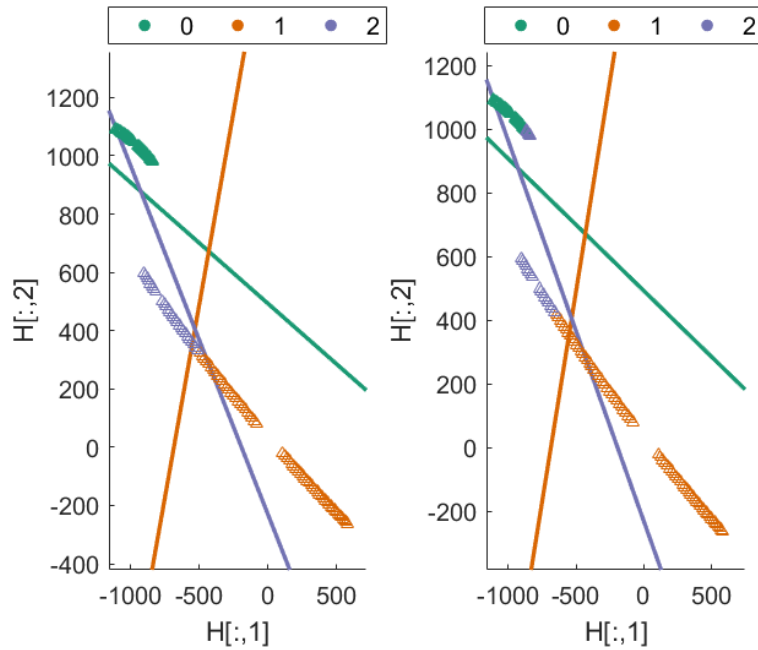


Figure 45: Test Phase of the KBTL multi-class for damage detection

Since the ‘correct labels’ are available for all the data, for both training and test phase, the accuracy of the algorithm can be computed as,

$$accuracy = \frac{\text{number of observations for which } y_{\text{predicted}} = y_{\text{correct}}}{\text{total number of observations}}$$

the values are shown in Table 10. What can be observed is that although few data for the Target Domain are provided to the algorithm a quite good accuracy in the test phase is obtained, hence thanks to the presence of data from the Sanctuary of Vicoforte the algorithm is able to generalize well also for the data representative of the Church of Santa Caterina.

<i>ACCURACY</i>		
<i>Domains</i>	<i>Training Phase</i>	<i>Test Phase</i>
Target (Church of Santa Caterina)	92.00 %	84.00 %
Source (Sanctuary of Vicoforte)	99.50 %	-

Table 10: Accuracy for the Target and Source Domains, during both the training and test phases for the damage detection

It is also possible, during the test phase, to compute the accuracy for each class, the results are reported in Table 11, from which can be observe that there are quite good

accuracy for the first two classes, that are representative of a damage condition, while the third one has less accuracy, this theoretically could be a problem. However, in this case the class that is confused is the one representative of a health state or at most of a slight alteration, and it is confused with a damage condition (damage at the drum-dome macro-element or at the basement macro-element) this means that this error is characterized by what can be called *False Positive*. A false positive is obtained when a data that, for instance, is representing an undamaged condition is confused with a damaged one, hence there is the error but in a safety condition. If something like this happens in the reality, the consequence could be an 'unnecessary' economic expense because further investigations would be required to verify a damage that in reality does not exist. This could be accepted, while what cannot be accept is a *false negative*, that means when a damage condition is confused with a health one, if this happens the identification of the damage may occur only in the future when the damage will be more severe and thus more reflected in the frequencies. Hence, false negatives lead to a delay in damage identification, which in the field of structural health monitoring of architectural heritage buildings could be detrimental. Fortunately, in this application only few data (10 observations) representative of a damage at the basement are confused with a health state or a slight state of alteration.

<i>ACCURACY</i>		
<i>Target Domain (Church of Santa Caterina)</i>		
<i>Class 1 - label '0'</i> <i>(Drum-dome damage)</i>	<i>Class 2 - label '1'</i> <i>(Basement damage)</i>	<i>Class 3 - label '2'</i> <i>(Health state)</i>
100%	85.71 %	48.57 %

Table 11: Accuracy for each class during the Test Phase for the damage detection

4.3 KBTL applied to data from the finite element models for the definition of the damage level: slight, medium and serious

4.3.1 Domains and Labels

Starting from the same data, simulated with the FEM of the structures, used in the previous *subchapter 4.2*, a second application is developed. In this second case, the aim is to create an algorithm that is able to define the level of the damage, no matter where it is located, therefore the features used are the same of the previous case but

the labels change. Three levels of damage are assumed, defined according to reduction imposed to the elastic modulus during the simulation. For data related to elastic modulus belonging to the interval $[0.81E, 0.90E]$ the *label '0'* is assigned, to the interval $[0.71E, 0.80E]$ the *label '1'* and to the interval $[0.50E, 0.70E]$ the *label '2'*. Hence, the *label '0'* is representative of slight damages, the *label '1'* of medium damages and the *label '2'* of serious damages. In the next two figures the data simulated on the two FEM are represented highlighting the three classes with three different colors, green for *label '0'*, orange for *label '1'* and purple for *label '2'*.

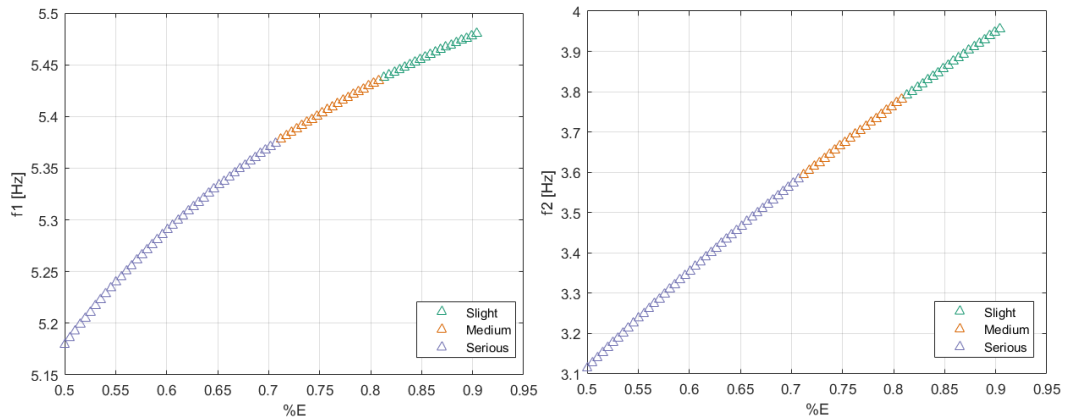


Figure 46: Data simulated from the FEM of the Church of Santa Caterina, for different level of damage (on the left data from damage at the drum-dome element, on the right data from damage at the basement element)

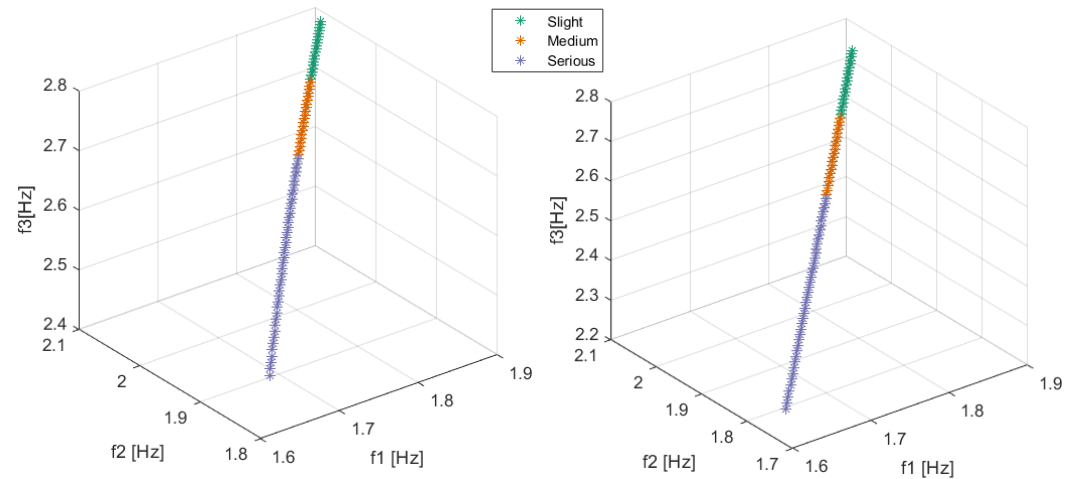


Figure 47: Data simulated from FEM of the Sanctuary of Vicoforte for different level of damage (on the left data from a damage at the drum-dome element, on the right data from damage at the basement element)

Also in this case, the Source Domain is considered as composed by all the data shown in Figure 47, while the Target Domain is considered as composed by only some data, in order to simulate the poor knowledge of the structure, therefore in Figure 48 the data used for the training phase of the algorithm for the target domain

is shown. Indeed, if in the reality some una-tantum dynamic tests are performed, and so is not present a periodic monitoring system, only frequencies representing the damage at that time can be derived, therefore only 5 observations for the *label '0'*, 10 observations for the *label '1'* and 10 observations for the *label '2'* are used for the training, these observations have been chosen more or less in the middle of each classes in order to be in the worst condition, indeed in this way the algorithm does not have information about the limits of each class from the domain of the Church of Santa Caterina. Finally, all the data that are not part of this domain are used later as test domain (Figure 49) to verify the accuracy of the algorithm. In Table 12 a summary of the observations for each class is shown.

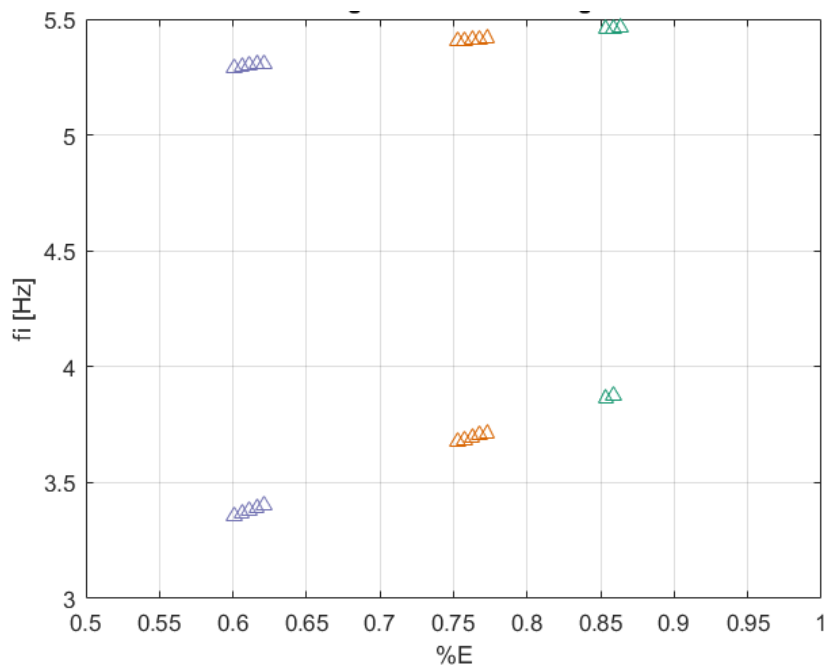


Figure 48: Data for the Training Phase of the KBTL algorithm for the identification of the damage level

OBSERVATIONS						
<i>Domains</i>	<i>Training Phase</i>			<i>Test Phase</i>		
	<i>Labels</i>			<i>Labels</i>		
	<i>y = 0</i>	<i>y = 1</i>	<i>y = 2</i>	<i>y = 0</i>	<i>y = 1</i>	<i>y = 2</i>
Target <i>(Church of Santa Caterina)</i>	10	10	5	33	30	74
Source <i>(Sanctuary of Vicoforte)</i>	38	40	84	0	0	0

Table 12: Summary of Labels and number of observations for the identification of the damage level

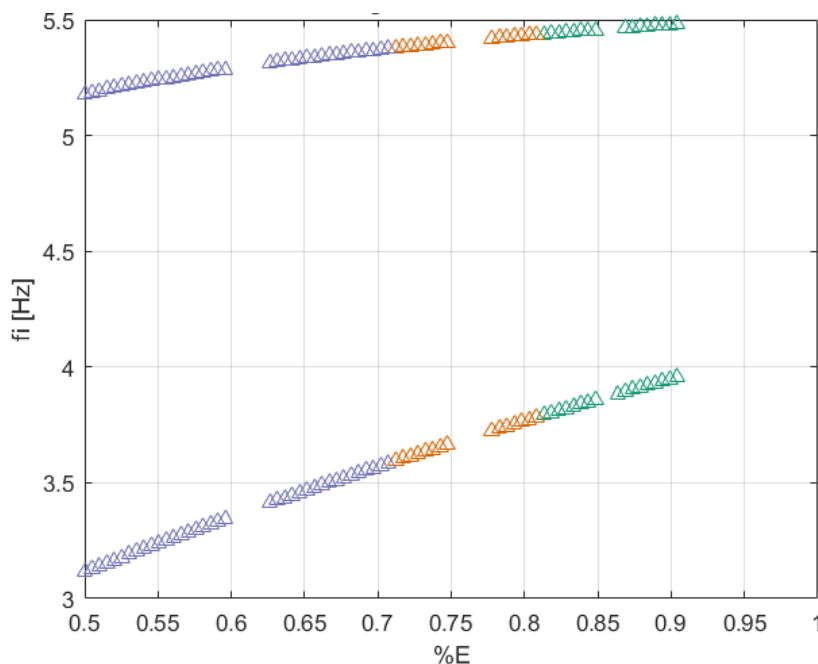


Figure 49: Data for the test Phase of the KBTL algorithm for the identification of the damage level

4.3.2 Results

Since the labels are three, a multi-class KBTL has been applied to the training dataset, composed by Source and Target Domain, to infer a classifier. A dimension $\mathcal{R} = 2$ of the latent subspace is chosen in order to have a visual representation of the model. In Figure 50 the results from the training phase of the algorithm are shown. Here the two different domains can be identified by the two different symbols, the star * for the Source Domain (Sanctuary of Vicoforte) and the triangle Δ for the Target Domain (Church of Santa Caterina), while the three classes can be identified by the different colors, green for *label '0'* (slight damage), orange for *label '1'* (medium damage) and purple for *label '2'* (serious damage). In the figure two plots are visible, indeed the one on the left shows the domains projected in the latent subspace where each data is colored as function of the prediction performed by the algorithm (*'predicted labels'*), while the one on the right shows the same domains but with the data colored as function of the labels provided to the algorithm as input together with the frequencies, therefore are the *'correct labels'*.

In Figure 51 the test phase is shown, since the domain of the Sanctuary of Vicoforte is used only to increase the knowledge of the Church of Santa Caterina, the test is performed only on data representative of this last structure, for this reason only triangles Δ are present. As in the previous figure the two plots show, the one on the left the *'predicted labels'* while the one on the right the *'correct labels'*.

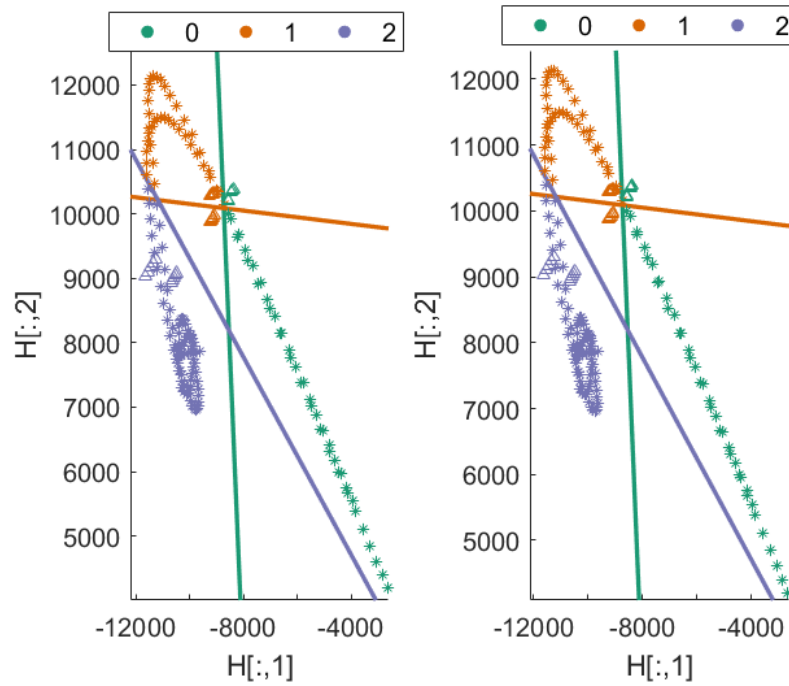


Figure 50: Training Phase of KBTL multi-class for the identification of the damage level

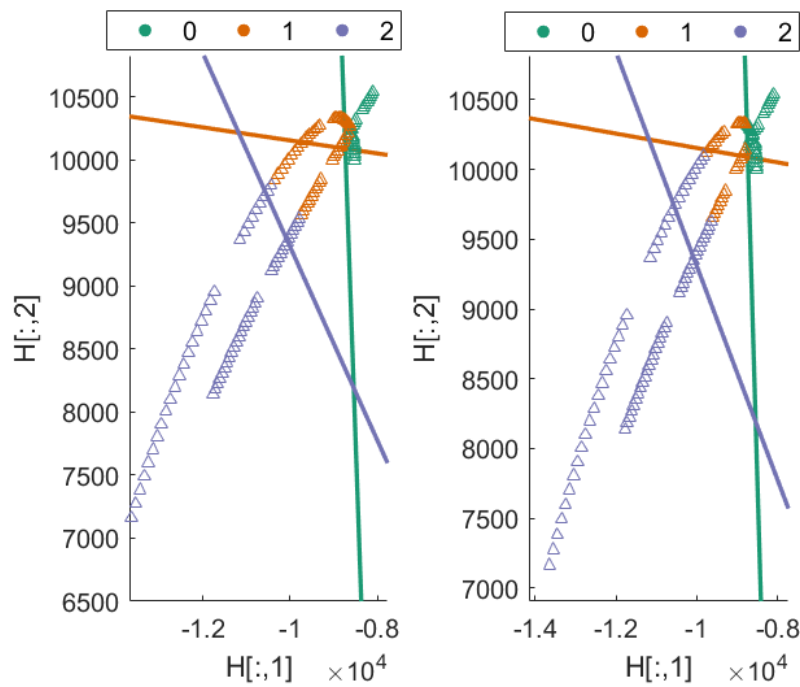


Figure 51: Test Phase of KBTL multi-class for the identification of the damage level

Since the ‘correct labels’ are available for all the data, for both training and test phase, the accuracy of the algorithm can be computed, and the values are shown in Table 13. What can be observed is that although few data for the Target Domain

have been provided to the algorithm in the training phase a quite good accuracy in the test phase is obtained, hence thanks to the presence of data from the Sanctuary of Vicoforte the algorithm is able to generalize well also for the data representative of the Church of Santa Caterina, indeed it is important to remember that the information about the limits of the classes are provided only by the Source Domain, but during the Test phase only data that belong to the Target Domain are provided, hence the algorithm is generalizing quite well even for the Target Domain.

<i>ACCURACY</i>		
<i>Domains</i>	<i>Training Phase</i>	<i>Test Phase</i>
Target <i>(Church of Santa Caterina)</i>	100.00 %	85.40 %
Source <i>(Sanctuary of Vicoforte)</i>	100.00 %	-

Table 13: Accuracy for the Target and Source Domains, during both the training and test phases for the identification of the damage level

In addition to the accuracies evaluated above, also the accuracy for the prediction of each single class can be computed, the results are reported in Table 14. From these results it can be noted that the medium damage is always classified in the correct way, while some mistakes are performed in the classification of the slight damage and the serious damage, indeed sometimes both are confused with a medium one. It is important to highlight that the accuracy of the serious damage is higher than the accuracy of the slight one and this is still something to point out, because it means that the algorithm makes more mistakes in classifying a slight damage as an medium damage than it does in classifying a serious damage as an medium one, but if a slight damage is classified as medium one the error is a *False Positive*, so it is in a safety condition, while if it confuses a serious one with a medium one a *False Negative* occurs. In any case a damage is present, hence in the reality additional check in site would be developed in particular to check if it is a medium or a serious damage.

<i>ACCURACY</i>		
<i>Target Domain (Church of Santa Caterina)</i>		
<i>Class 1 - label '0'</i> <i>(Slight damage)</i>	<i>Class 2 - label '1'</i> <i>(Medium damage)</i>	<i>Class 3 - label '2'</i> <i>(Serious damage)</i>
72.73%	100 %	85.14 %

Table 14: Accuracy for each class during the Test Phase for the identification of the damage level

Chapter 5

Transfer learning technique (KBTL) applied to oval masonry domes for the temperature states identification

5.1 Case study – Accuracy analysis

In this subchapter an accuracy analysis is presented. In the details, the variation of the accuracy in the predictions for the Target Domain, by varying the amount of data of the Source Domain is realized. For what concern the Target Domain, two cases are reported, the first regards a domain of more or less 300 observations, that can be representative of a period monitoring system, the second of a domain of 30 observations, strongly smaller than the previous one and therefore it can be representative of a una-tantum dynamic monitoring activity.

5.1.1 Experimental data from the monitoring system of the Sanctuary of Vicoforte

In *subchapter 4.1.1* the Dynamic Monitoring System of the Sanctuary of Vicoforte is described. Thanks to the recorded response of the structure to the environmental excitation the first seven frequencies of structure have been identified with an identification process. However, different *Not a Number (NaN)* are present for the highest frequencies, therefore only the first three natural frequencies (the first two

flexural modes and the first torsional mode) as function of the temperature changes are considered. In Figure 52 these relationships are shown.

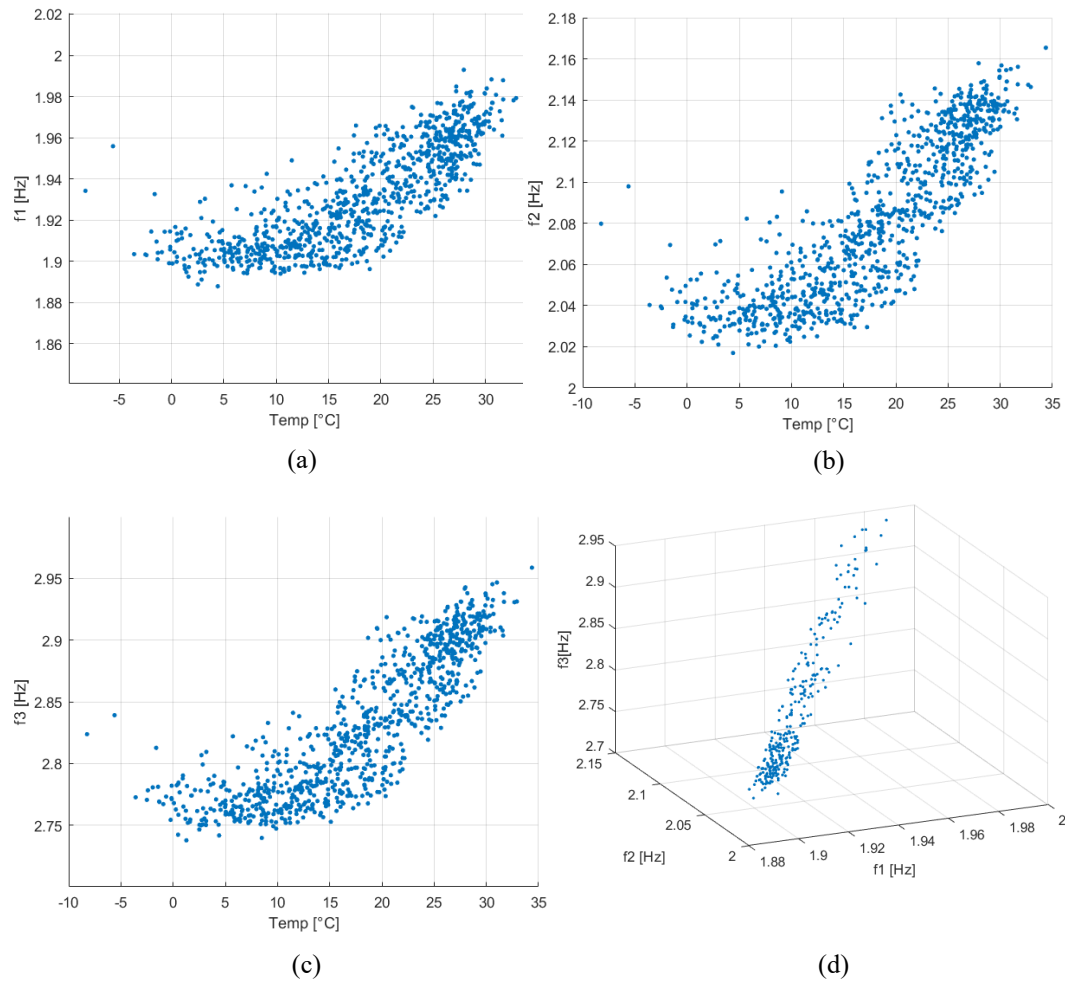


Figure 52: Frequency-temperature relationship for the Sanctuary of Vicoforte. (a) First bending mode f_1 , (b) First bending mode f_2 , (c) First torsional mode f_3 and (d) Spatial representation of these first three frequencies

5.1.2 ‘Semi-Experimental’ data for the Church of Santa Caterina

For this first analysis, ‘*semi-experimental*’ data are used. Where this term implies that the frequencies of the Church of Santa Caterina are obtained by a simulation based on three experimental observations. In this phase, only three observations of the first five natural frequencies of the Church are available, which have been obtained from an identification process on signal recorded on site for three different temperatures: 1.5°C , 6°C and 20°C . The three values related to the three temperatures for each of the five frequencies are reported in Table 15. While in

Figure 53, Figure 54, Figure 55, Figure 56 and Figure 57 the plots of these frequencies are shown.

Temperature	Frequencies				
	$f1$ [Hz]	$f2$ [Hz]	$f3$ [Hz]	$f4$ [Hz]	$f5$ [Hz]
1.5 °C	3.0540	3.4126	3.8420	4.0572	4.5109
6.0 °C	3.0457	3.4550	3.8835	4.0634	4.4928
20.0 °C	3.0719	3.4170	3.7713	4.0783	4.4310

Table 15: Frequencies for three temperature values from the signal recorded during the dynamic monitoring activities at the Church of Santa Caterina

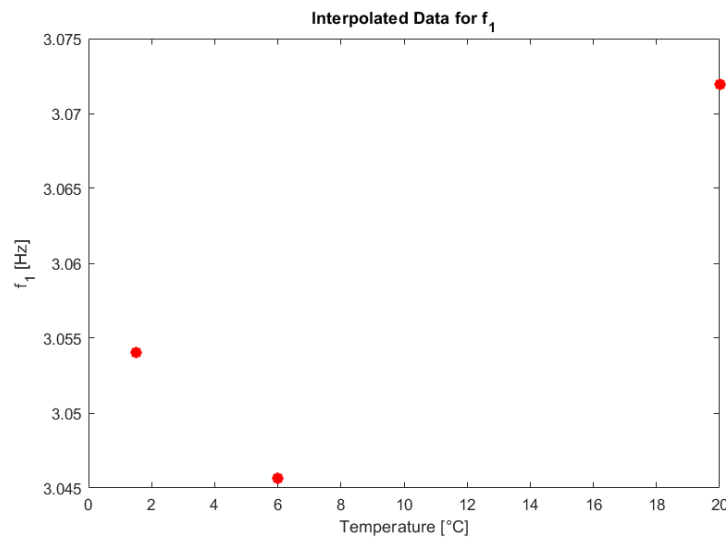


Figure 53: Interpolated data for f_1 of the Church of Santa Caterina

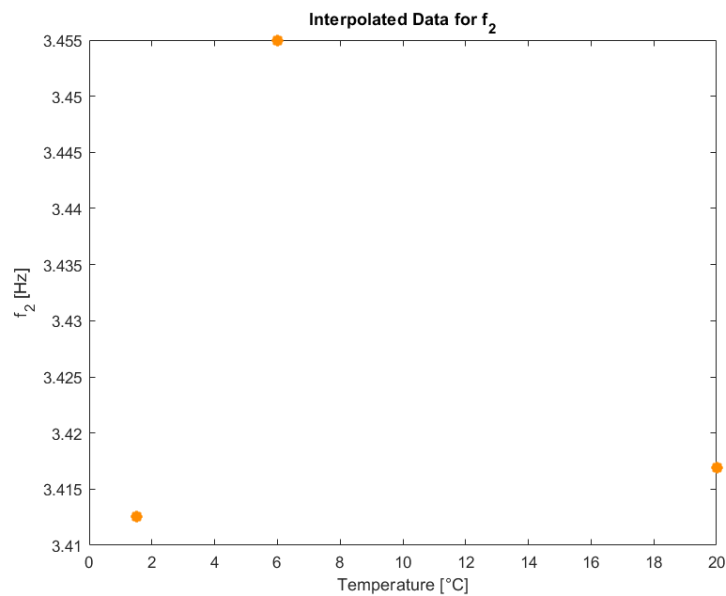


Figure 54: Interpolated data for f_2 of the Church of Santa Caterina

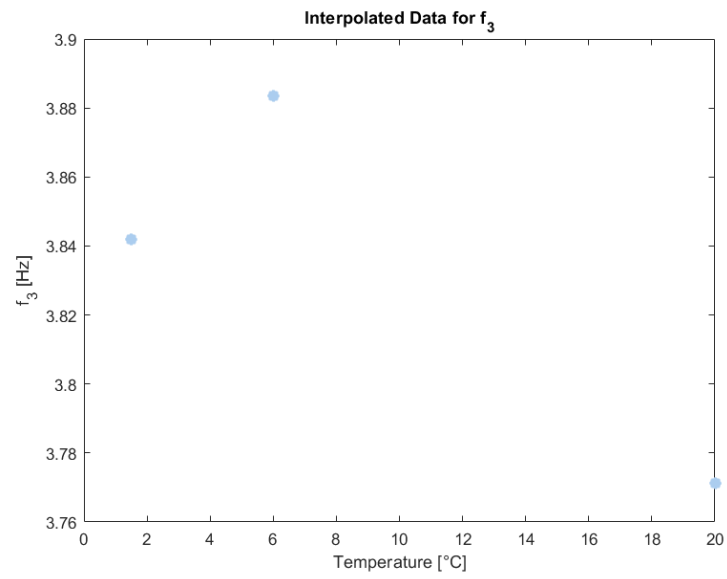


Figure 55: Interpolated data for f_3 of the Church of Santa Caterina

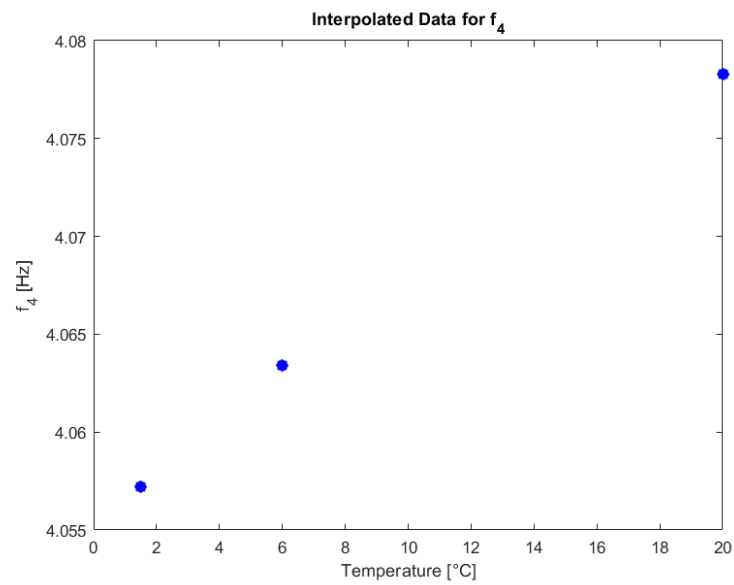


Figure 56: Interpolated data for f_4 of the Church of Santa Caterina

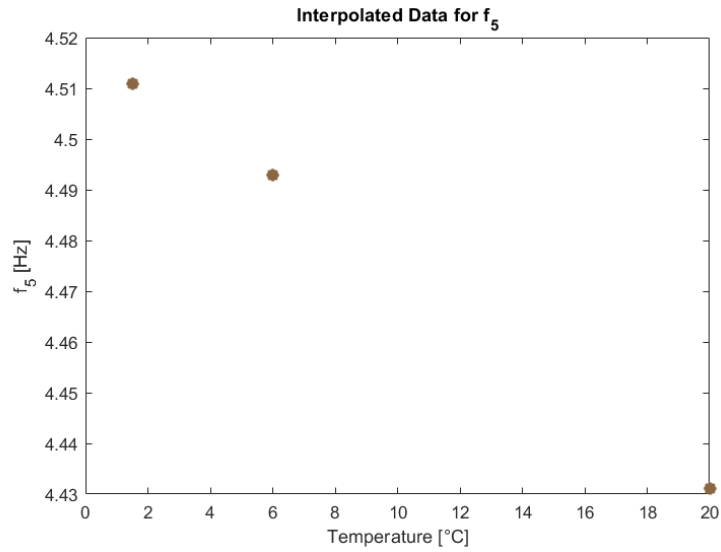


Figure 57: Interpolated data for f_5 of the Church of Santa Caterina

Since no experimental information are available for the negative temperature, in this first study the negative temperatures are not considered.

To obtain a distribution of each of these frequencies as the temperature changes, a linear interpolation of these three data is performed, also a quadric interpolation has been tested, but has been neglected as it adapts too much to the three data provided (overfitting problem). Then, to this linear interpolation a Gaussian noise is introduced, proportional to the standard deviation of the real measurements. In Figure 58, Figure 59, Figure 60, Figure 61 and Figure 62 the temperature-frequency relationship obtained from the linear interpolation of the three known values are shown. From these charts it is possible to note that only two frequencies show a quite evident variation with the temperature changes, in particular these frequencies are f_3 and f_5 , hence these two frequencies are used for the Target Domain. In addition to these two frequencies, also the first frequencies f_1 is considered since it is the more stable frequency. Additionally, it can be noted that the frequencies f_3 and f_5 show a descendant behavior with the increment of the temperature, while the first frequency f_1 has the opposite behavior even if it is very slight.

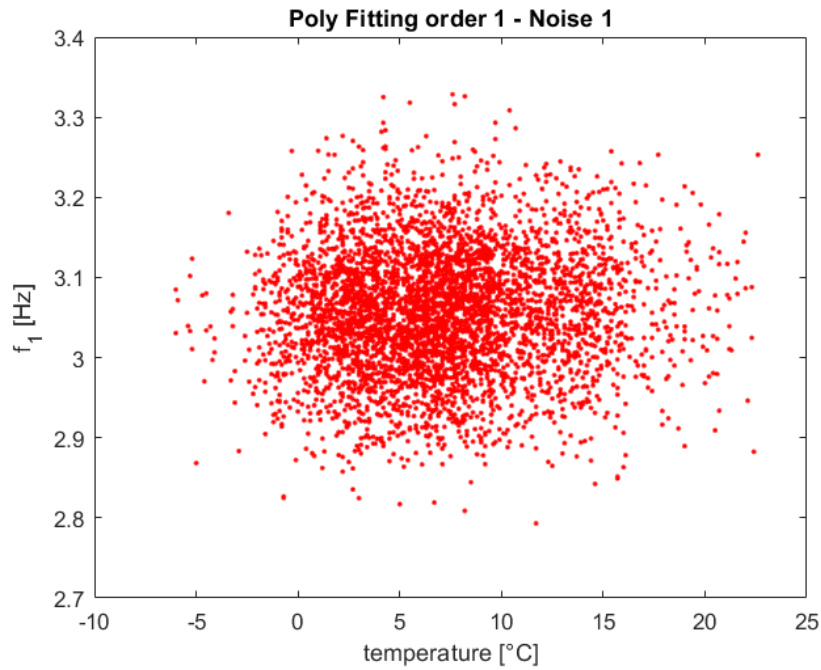


Figure 58: 'Semi-Experimental' relationship between f_1 [Hz] and Temperature [°C] for the Church of Santa Caterina

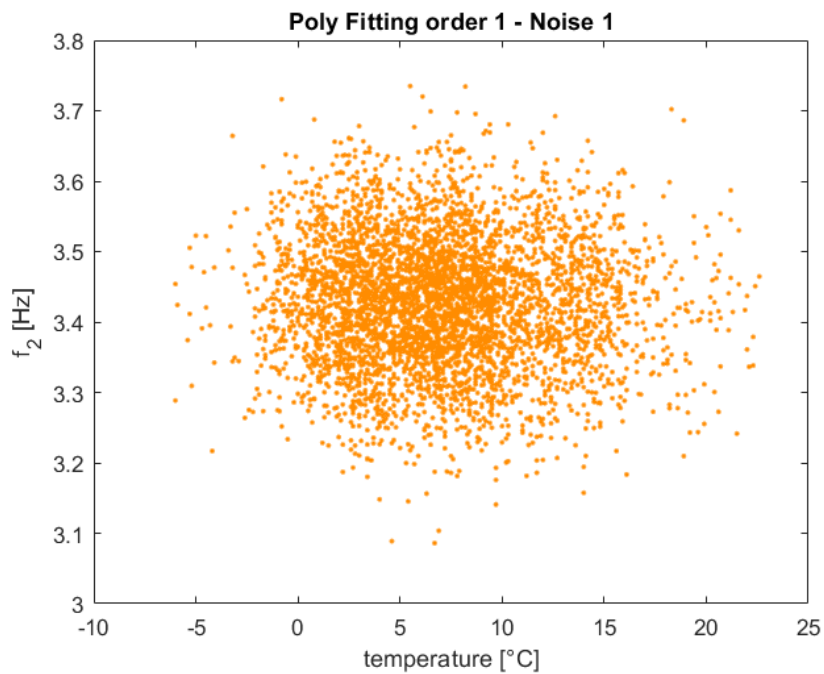


Figure 59: 'Semi-Experimental' relationship between f_2 [Hz] and Temperature [°C] for the Church of Santa Caterina

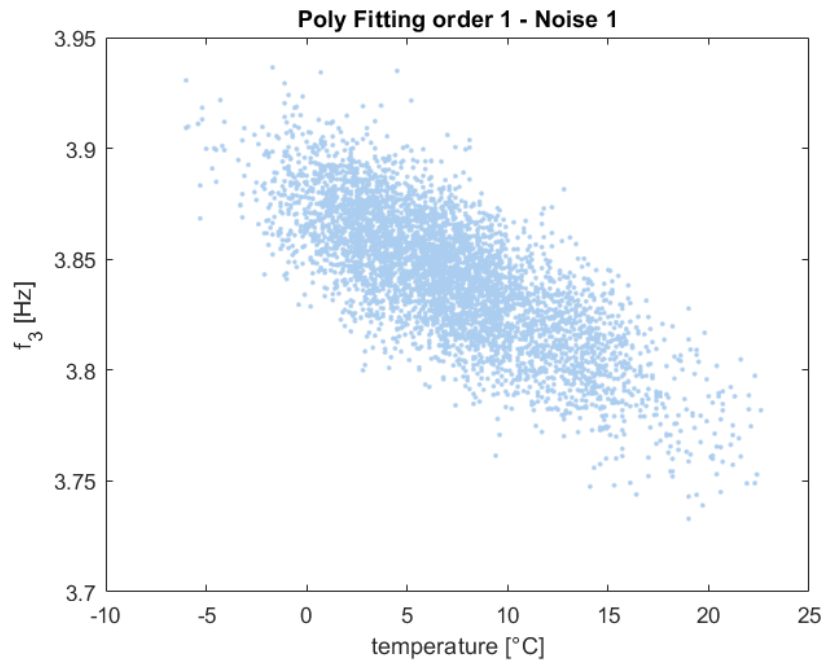


Figure 60: 'Semi-Experimental' relationship between f_3 [Hz] and Temperature [°C] for the Church of Santa Caterina

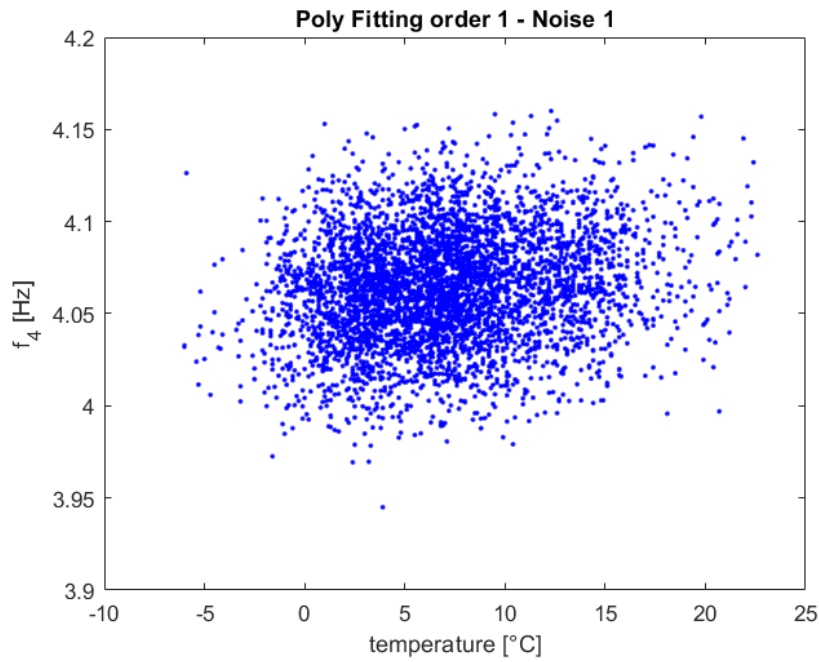


Figure 61: 'Semi-Experimental' relationship between f_4 [Hz] and Temperature [°C] for the Church of Santa Caterina

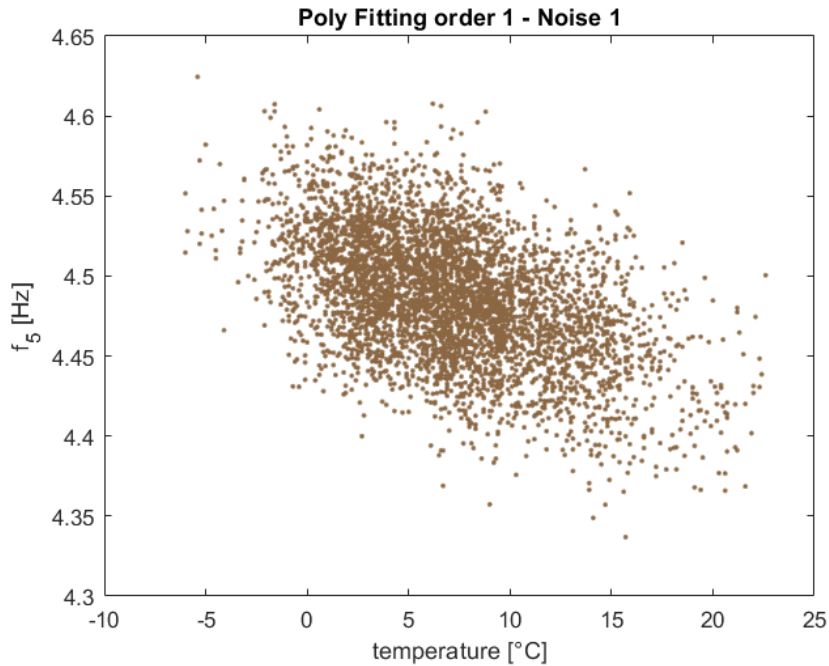


Figure 62: 'Semi-Experimental' relationship between f_5 [Hz] and Temperature [°C] for the Church of Santa Caterina

5.1.3 Domains and Labels

For this problem of classification, the following three classes of temperature are considered:

- ~ $0^{\circ}\text{C} \leq T < 10^{\circ}\text{C}$, to which *label '1'* is assigned.
- ~ $10^{\circ}\text{C} \leq T < 20^{\circ}\text{C}$, to which *label '2'* is assigned.
- ~ $T \geq 20^{\circ}\text{C}$, to which *label '3'* is assigned.

Two different Target Domains for the Training Phase are considered, one with 300 observations (*Target 1*, Figure 63(b)) and the other with 30 observations (*Target 2*, Figure 63(a)). In Table 16 the numbers of observations used during the training phase and the test phase for these two possible Target Domains are reported. These two domains can be considered as the results of two different monitoring activities, the richest one (Target 1) can be considered as results of a periodic monitoring activity, while the poorest one (Target 2) as results of a una-tantum dynamic test. The same classes are considered for the Source Domain. In order to understand how the accuracy on the predictions of data of the Church of Santa Caterina varies, three different Source Domains are considered, each of which is composed by a different amount of data representative of the three classes. In the details, there is '*VICO_300*'

a Source Domain composed by 300 observations (Figure 64 (a)), 'VICO_516' composed by 516 observations (Figure 64 (b)) and 'VICO_901' composed by 901 observations (Figure 64 (c)). From Figure 64 it can be observed how the three possible Source Domains have different amounts of data, but the limits of the classes are already visible from the smallest one, hence moving from one domain to another the only difference is the density of the points cloud. In Table 17 details about the number of observations for each class in each possible Source Domain are reported.

OBSERVATIONS for the Church of Santa Caterina

<i>Domains</i>	<i>Training Phase</i>			<i>Test Phase</i>		
	<i>Labels</i>			<i>Labels</i>		
	<i>y = 1</i>	<i>y = 2</i>	<i>y = 3</i>	<i>y = 1</i>	<i>y = 2</i>	<i>y = 3</i>
Target 1 <i>(Church of Santa Caterina)</i>	135	135	29	3083	921	6
Target 2 <i>(Church of Santa Caterina)</i>	10	10	10	3208	1046	25

Table 16: Number of Observations for the Training and Test Phases for the two types of Target Domains

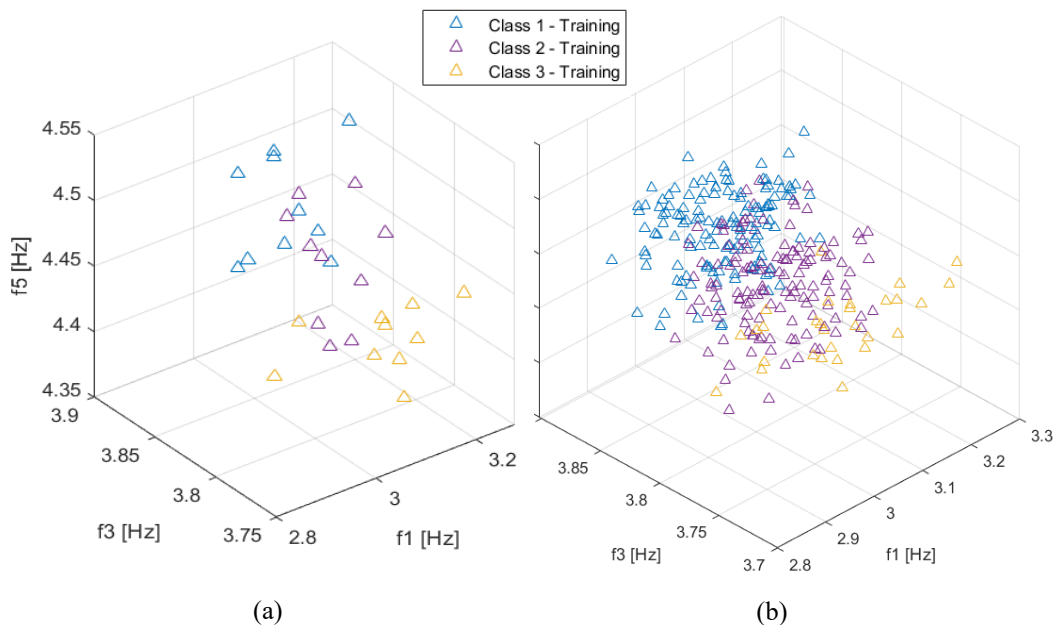


Figure 63: Different Target Domains for the Accuracy study, (a) Target 2 composed by 30 Observations and (b) Target 1 composed by 300 Observations

<i>OBSERVATIONS for the Sanctuary of Vicoforte</i>						
<i>Domains</i>	<i>Training Phase</i>			<i>Test Phase</i>		
	<i>Labels</i>			<i>Labels</i>		
	<i>y = 1</i>	<i>y = 2</i>	<i>y = 3</i>	<i>y = 1</i>	<i>y = 2</i>	<i>y = 3</i>
VICO_300 <i>(Sanctuary of Vicoforte)</i>	100	100	100	0	0	0
VICO_516 <i>(Sanctuary of Vicoforte)</i>	172	172	172	0	0	0
VICO_901 <i>(Sanctuary of Vicoforte)</i>	172	320	409	0	0	0

Table 17: Number of Observations for the different classes of the three possible Source Domains

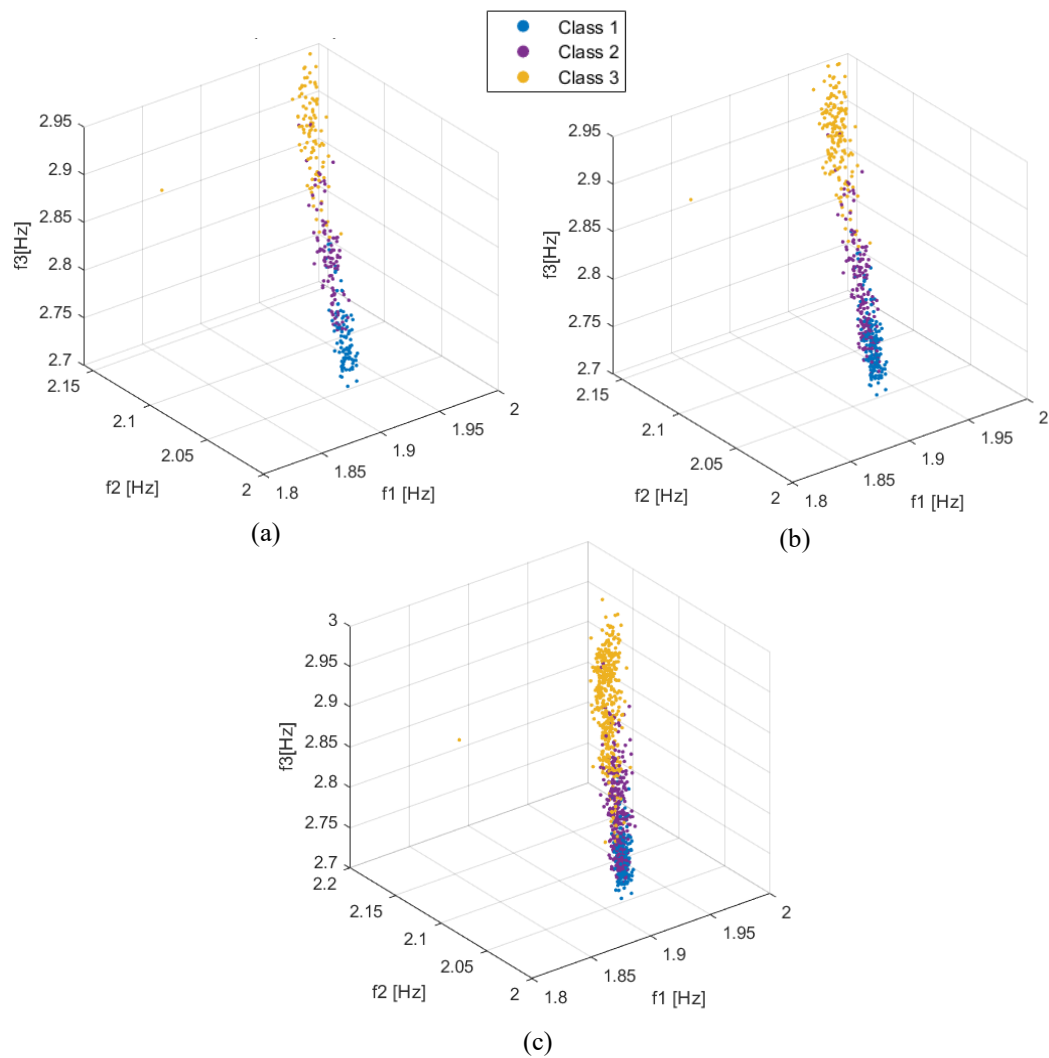


Figure 64: Different Source Domains for the Accuracy study, (a) VICO_300, (b) VICO_516 and (c) VICO_901

5.1.4 Accuracy study by varying the number of observations of the source domain, the case of Target 1

Before the application of DA techniques, a simple *Linear Discriminant ML algorithm* (from the *MATLAB Toolbox 'Classification Learner'*) is used to classify the states of temperature by using, during the training phase, only data of the Target Domain, in this condition an accuracy of 76.6% is reached during the training phase, while an accuracy of 78.8% during the test phase. Then three models with the KBTL are generated starting from different training datasets, each of which consists of the Target Domain 1 (300 data) and one of three Source Domains.

Model 1:

For this first model the domain Target 1 is used as representative of the Church of Santa Caterina, while as Source Domain *VICO_300* is used. It can be observed that the two domains have practically the same number of observations (299 one and 300 the other). In Figure 65 the training phase is shown, here it can be noted two plots, the one on the left represents the projection of the Source and Target Domains in the shared latent subspace, with the data colored as function of the predictions performed by the model (*'predicted labels'*), while in the one on the left the data projected in the same space are colored as function of the correct labels that are given to the algorithm as input data (*'correct labels'*). The Source and Target domains can be distinguished thanks to the different symbols used, the triangle Δ for the Target and the star $*$ for the Source, while the three classes of temperature can be distinguished with the three colors used, blue for *label '1'*, purple for *label '2'* and yellow for *label '3'*. In this phase an accuracy of 80.94 % is reached for the Target Domain.

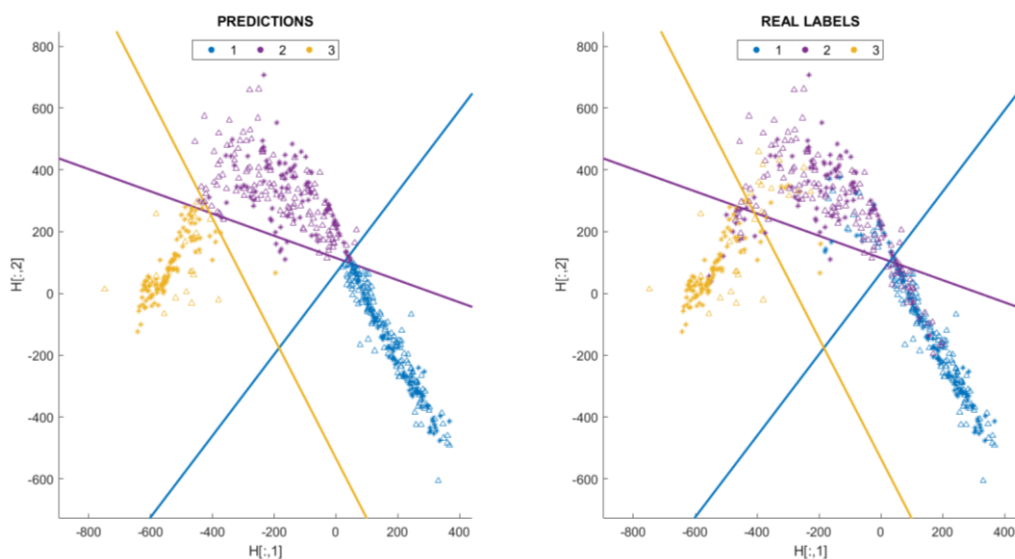


Figure 65: Training Phase of Model 1, on the left side the predictions of the algorithm are shown while on the right the correct labels

In Figure 66 the results of the test phase are shown. In this phase only data representative of the Target Domain are given to the algorithm and an accuracy of 77.58 % is reached for the predictions. Also this figure is divided into two plots, the one on the left with the '*predicted labels*' and the one on the right with the '*correct labels*'. In Table 18 details about the accuracy of each class are reported.

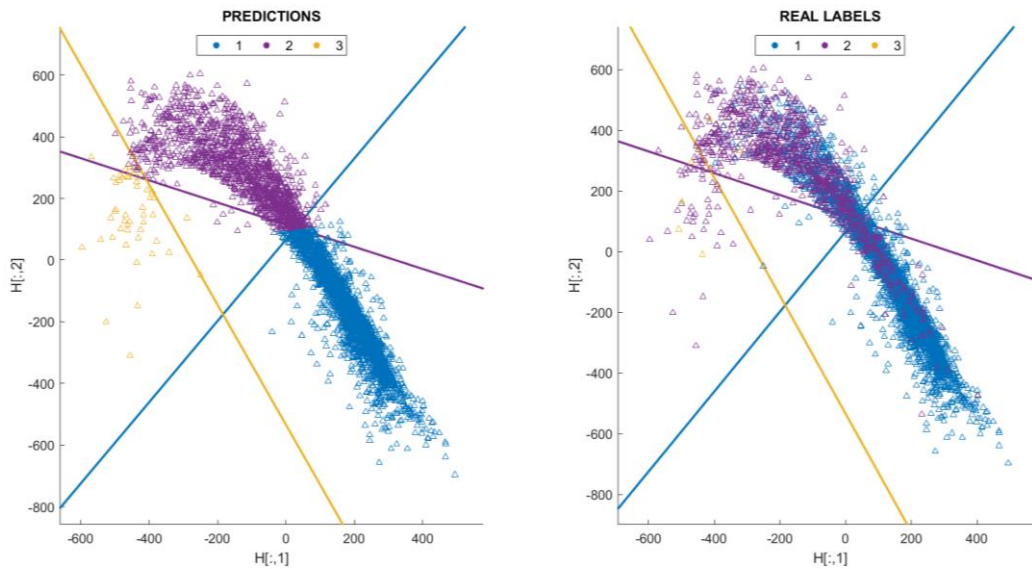


Figure 66: Test Phase of Model 1, on the left side the predictions of the algorithm are shown while on the right the correct labels

ACCURACY test phase Model 1

Target Domain (Church of Santa Caterina)

Class 1 - label '1' ($T \in [0,10]^{\circ}\text{C}$)	Class 2 - label '2' ($T \in [10,20]^{\circ}\text{C}$)	Class 3 - label '3' ($T \in [20, \infty)^{\circ}\text{C}$)
76.74%	80.46 %	66.67 %

Table 18: Accuracy for each class of temperature of the test phase of the Model 1

Model 2:

For this second model the domain Target 1 is used as representative of the Church of Santa Caterina, while as Source Domain *VICO_516* is used. In Figure 67 the training phase of this model is shown, and as before on the left the '*predicted labels*' are visible while on the right the '*correct labels*' are reported. In this phase an accuracy of 80.94 % is obtained. Then, in Figure 68 the test phase of this model is shown, only data representative of the Church of Santa Caterina are tested, and an accuracy of 77.21% is obtained. In Table 19 details about the accuracy of each class are reported.

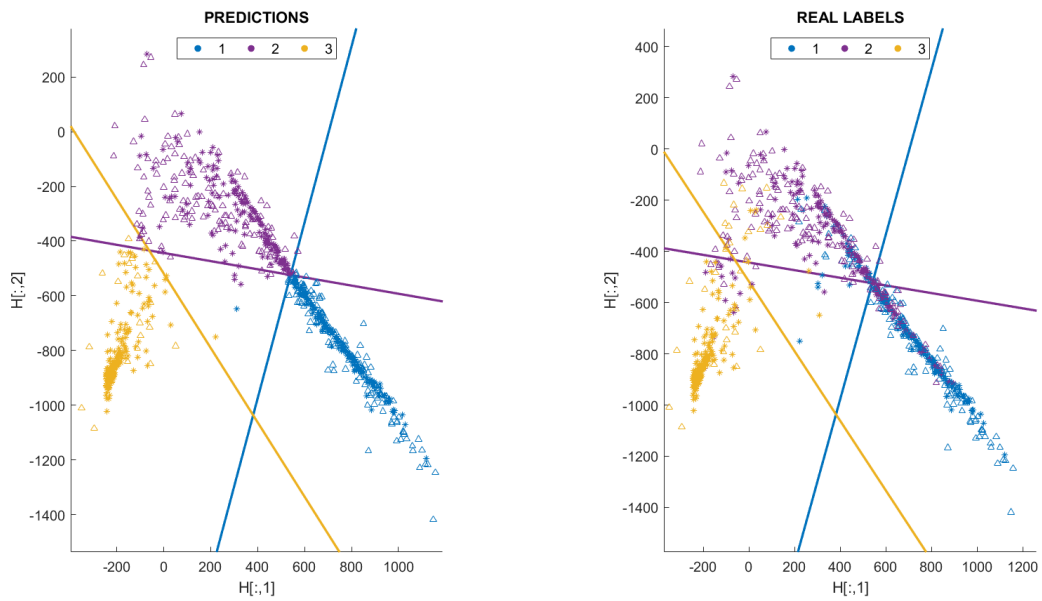


Figure 67: Training Phase of Model 2, on the left side the predictions of the algorithm are shown while on the right the correct labels

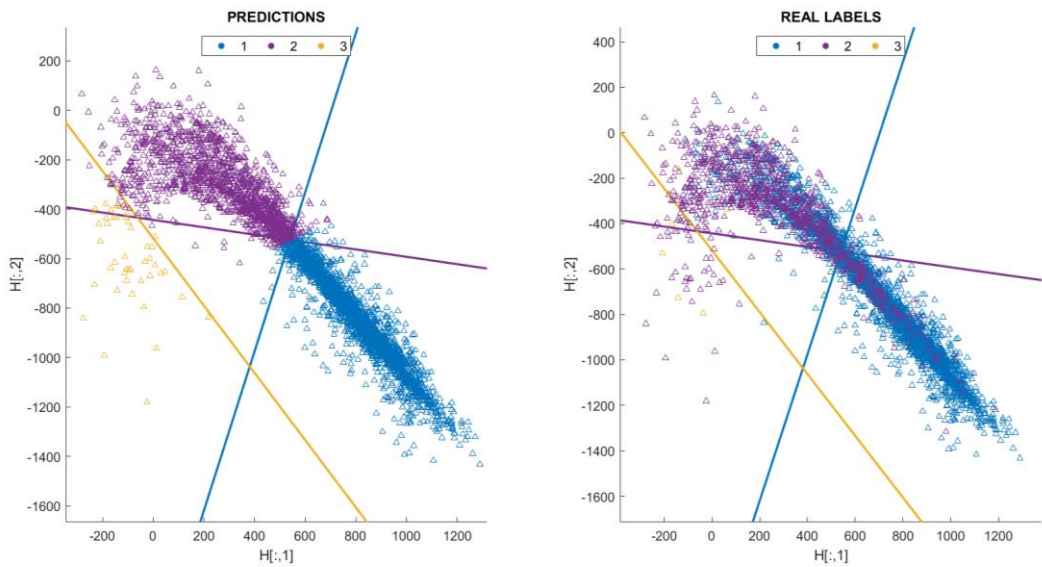


Figure 68: Test phase of Model 2, on the left side the predictions of the algorithm are shown while on the right the correct labels

<i>ACCURACY test phase Model 2</i>		
<i>Target Domain (Church of Santa Caterina)</i>		
<i>Class 1 - label '1'</i> <i>($T \in [0,10]^{\circ}C$)</i>	<i>Class 2 - label '2'</i> <i>($T \in [10,20]^{\circ}C$)</i>	<i>Class 3 - label '3'</i> <i>($T \in [20,\infty)^{\circ}C$)</i>
76.13%	80.89 %	66.67 %

Table 19: Accuracy for each class of temperature of the test phase of the Model 2

Model 3:

For this third model the domain Target 1 is used as representative of the Church of Santa Caterina, while as Source Domain *VICO_901* is used. In Figure 69 the training phase of this model is shown, and as before on the left the 'predicted labels' are visible while on the right the 'correct labels' are reported. In this phase an accuracy of 81.27 % is obtained. While, in Figure 70 the models applied to new data is presented (test phase), with predictions on the left and correct labels on the right, the accuracy reached in this phase is 77.68 %. In Table 20 details about the accuracy of each class are reported.

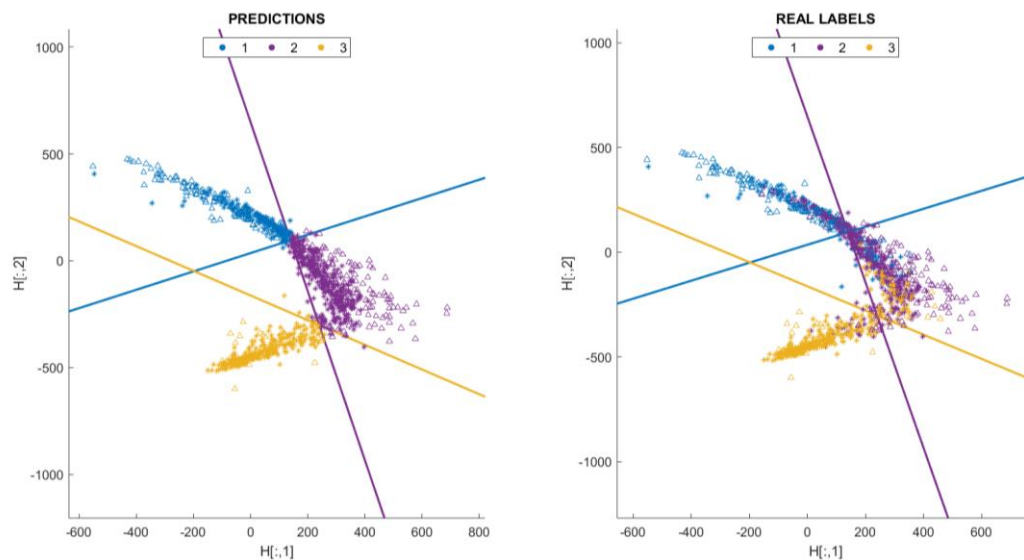


Figure 69: Training Phase of Model 3, on the left side the predictions of the algorithm are shown while on the right the correct labels

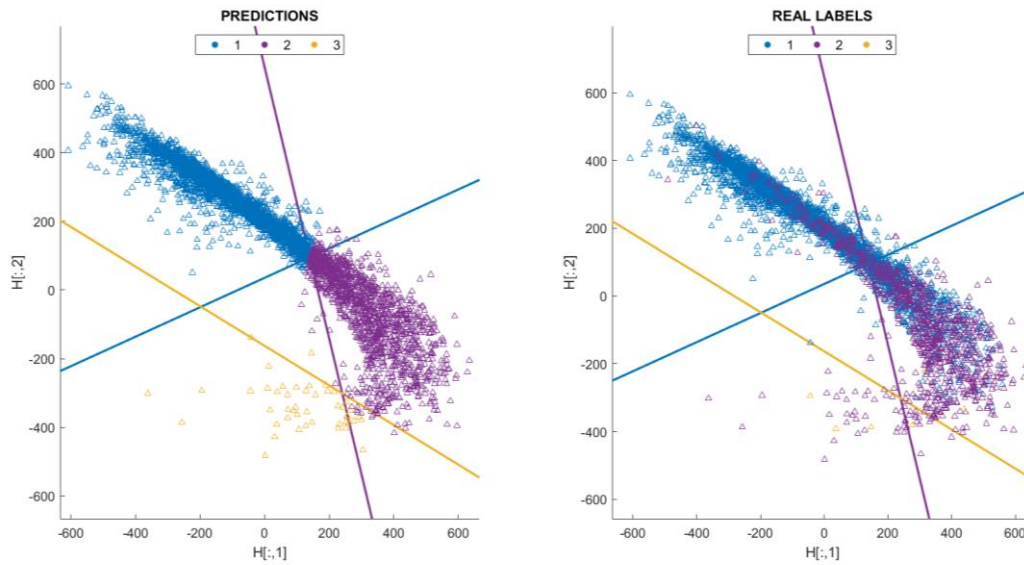


Figure 70: Test Phase of Model 3, on the left side the predictions of the algorithm are shown while on the right the correct labels

ACCURACY test phase Model 3

Target Domain (Church of Santa Caterina)

Class 1 - label '1' ($T \in [0,10]^{\circ}\text{C}$)	Class 2 - label '2' ($T \in [10,20]^{\circ}\text{C}$)	Class 3 - label '3' ($T \in [20,\infty)^{\circ}\text{C}$)
76.91%	80.35 %	66.67 %

Table 20: Accuracy for each class of temperature of the test phase of Model 3

In Table 21 and in Figure 71 the results, in terms of accuracy of the three models are summarized.

ACCURACY for the Church of Santa Caterina (Target Domain)

<i>Model</i>	<i>Training Phase</i>	<i>Test Phase</i>
Model 1	80.94 %	77.58 %
Model 2	80.94 %	77.21 %
Model 3	81.27 %	77.68 %

Table 21: Summary of the accuracies obtained during the accuracy analysis for the domain Target 1

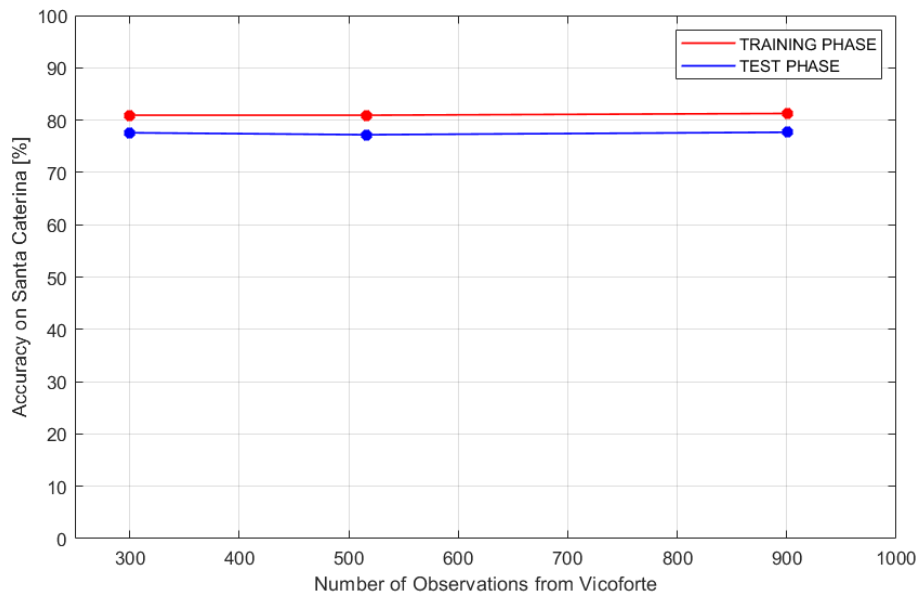


Figure 71: Accuracy trend on target domain predictions during the training phase (red) and test phase (blue)

From the results shown above, it can be highlight that, at least of some slight oscillations, the accuracy during both the phases (training and test) remain practically unvaried, this could be due to the fact that the information about the limits of the classes are already present from the smallest source domain, so adding more data the information, from a practical point of view of the algorithm, are not increasing. What can also be observed is that the accuracy reached with a simple linear ML is close to the ones obtained with KBTL, this is because 299 observations for the Church of Santa Caterina are available and are sufficient to generate a ML model that is able to generalize for new data.

5.1.5 Accuracy study by varying the number of observations of the source domain, the case of Target 2

In this case only the DA algorithm is used, since the number of observations available to perform a machine learning on data representative of the Church of Santa Caterina are only 30, that are too few to permit the generation of a model that will be able to generalize well on new data. Hence, in this case the use of data coming from a second structure (Sanctuary of Vicoforte) are necessary to ‘increase’ the training dataset in order to generate a model that will be able to predict in a proper way also for data that it has never seen before. Below, the three models created for the three different source domains are reported with all the results. As before, the Target Domain is identified by the tringle \triangle and the Source Domain by the star $*$, while the classes can be distinguished by the colors used, blue for

label '1', purple for label '2' and yellow for label '3'. Finally, as before all the model, for both training phase and test phase, are presented with two plots, the one on the left represents the '*predicted labels*' by the model, while the one on the right represents the '*correct labels*'. For the test phase only data representative of the Target domain are used.

Model 1:

For this first model the domain Target 2 is used as representative of the Church of Santa Caterina, while as Source Domain *VICO_300* is used.

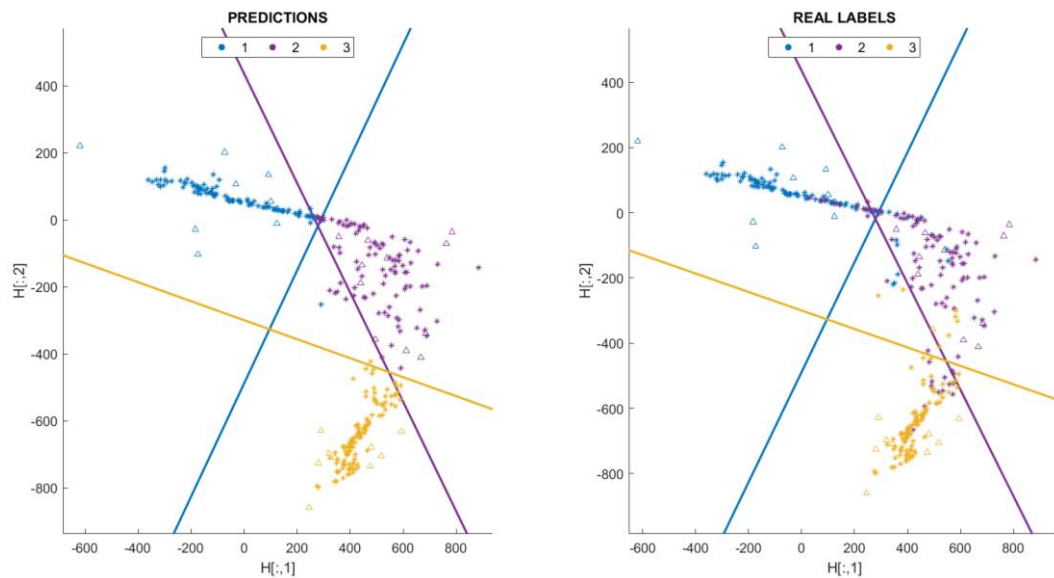


Figure 72: Training Phase of Model 1, on the left side the predictions of the algorithm are shown while on the right the correct labels

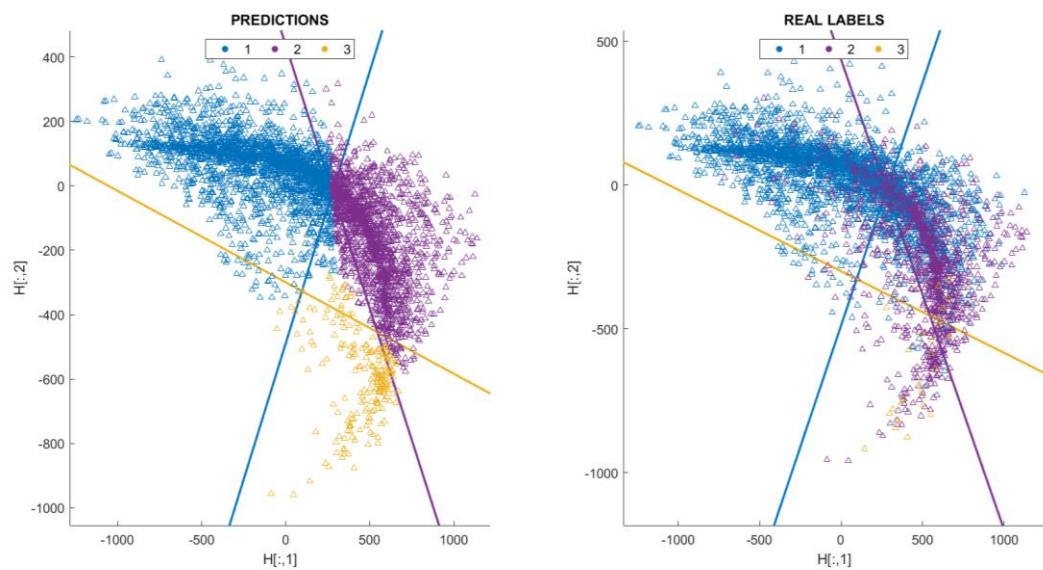


Figure 73: Test Phase of Model 1, on the left side the predictions of the algorithm are shown while on the right the correct labels

In Figure 72 and Figure 73 the training phase and the test phase are reported, respectively. With this model the accuracies shown in Table 23 are reached.

<i>ACCURACY for the Church of Santa Caterina (Target Domain)</i>		
<i>Model</i>	<i>Training Phase</i>	<i>Test Phase</i>
Model 1	96.67 %	68.64 %

Table 22: Accuracy of Model 1 with domain Target 2, during training and test phase

<i>ACCURACY test phase Model 3</i>		
<i>Target Domain (Church of Santa Caterina)</i>		
<i>Class 1 - label '1'</i> <i>($T \in [0,10)^\circ C$)</i>	<i>Class 2 - label '2'</i> <i>($T \in [10,20)^\circ C$)</i>	<i>Class 3 - label '3'</i> <i>($T \in [20, \infty)^\circ C$)</i>
68.67 %	68.45 %	72.00 %

Table 23: Accuracy for each class of Model 1 with domain Target 2, during test phase

What can be noted from now is the difference in the accuracy with respect to the previous case, indeed, since less data are given as input the accuracy in the training phase increases and tends to the 100 %, hence the algorithm generates a model that is able to classify all the 30 observations of the training. However, during the test phase a lot of new data are provided to the algorithm and in this phase a decrement in the accuracy is visible, this because only few data has been provided to the algorithm in the training phase to define a model, a model that is necessarily less general with respect to the previous case where a lot more data were available already in the training phase.

Model 2:

For this second model the domain Target 2 is used as representative of the Church of Santa Caterina, while as Source Domain *VICO_516* is used. In the two figures above the training phase and the test phase of the model are shown, while in Table 24 and Table 25, the results in terms of accuracies are reported.

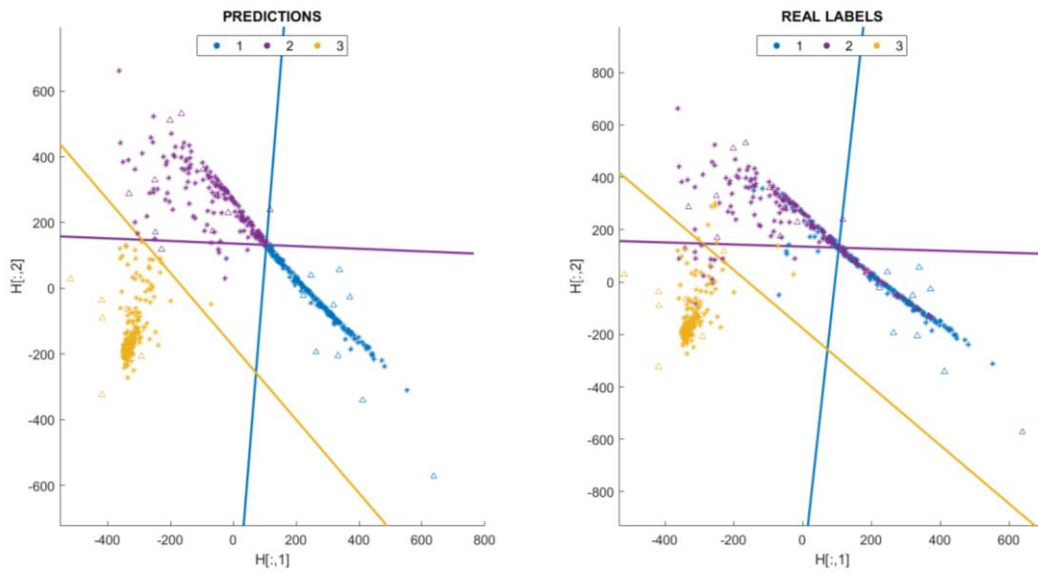


Figure 74: Training Phase of Model 2, on the left side the predictions of the algorithm are shown while on the right the correct labels

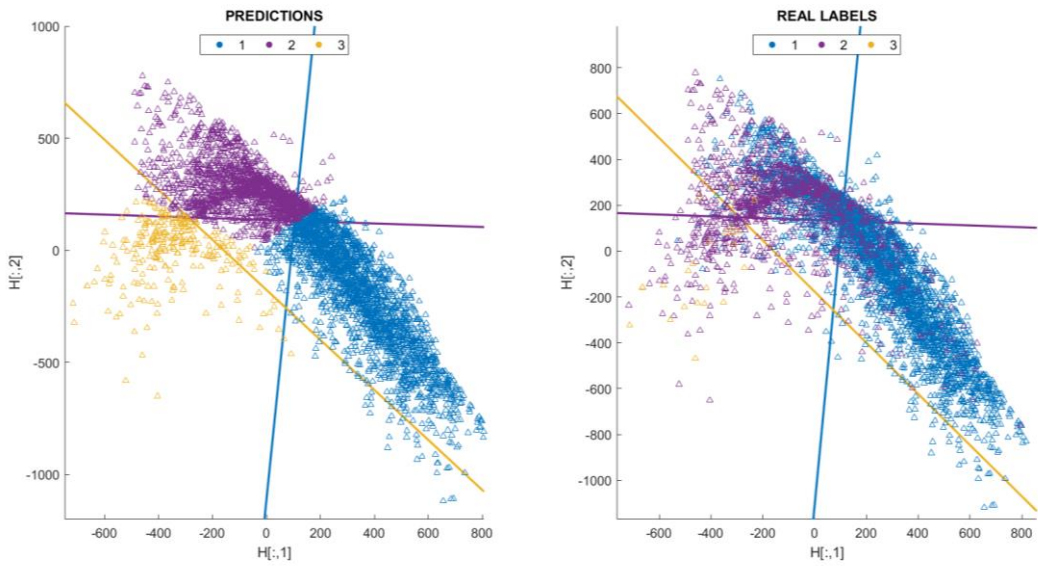


Figure 75: Test Phase of Model 2, on the left side the predictions of the algorithm are shown while on the right the correct labels

ACCURACY for the Church of Santa Caterina (Target Domain)

<i>Model</i>	<i>Training Phase</i>	<i>Test Phase</i>
Model 2	96.70 %	67.80 %

Table 24: Accuracy of Model 2 with domain Target 2, during training and test phase

ACCURACY test phase Model 2

Target Domain (Church of Santa Caterina)

<i>Class 1 - label '1'</i> <i>($T \in [0,10]^{\circ}\text{C}$)</i>	<i>Class 2 - label '2'</i> <i>($T \in [10,20]^{\circ}\text{C}$)</i>	<i>Class 3 - label '3'</i> <i>($T \in [20,\infty)^{\circ}\text{C}$)</i>
68.67 %	68.82 %	80.00 %

Table 25: Accuracy for each class of Model 2 with domain Target 2, during test phase

Model 3:

For this third model the domain Target 2 is used as representative of the Church of Santa Caterina, while as Source Domain *VICO_901* is used. In the two figures above the training phase and the test phase of the model are shown, while Table 26 in Table 27 and, the results in terms of accuracies are reported.

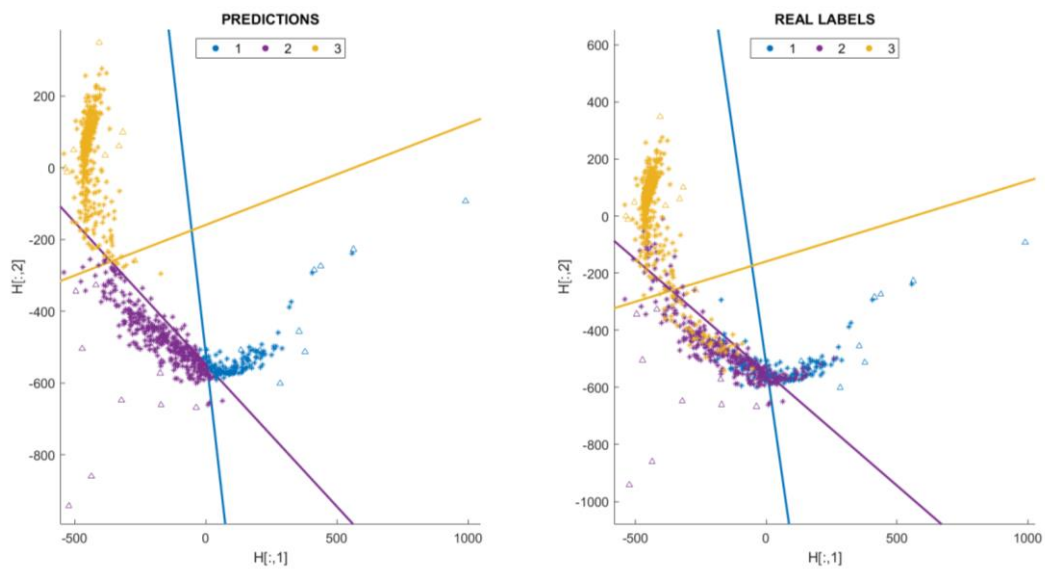


Figure 76: Training Phase of Model 3, on the left side the predictions of the algorithm are shown while on the right the correct labels

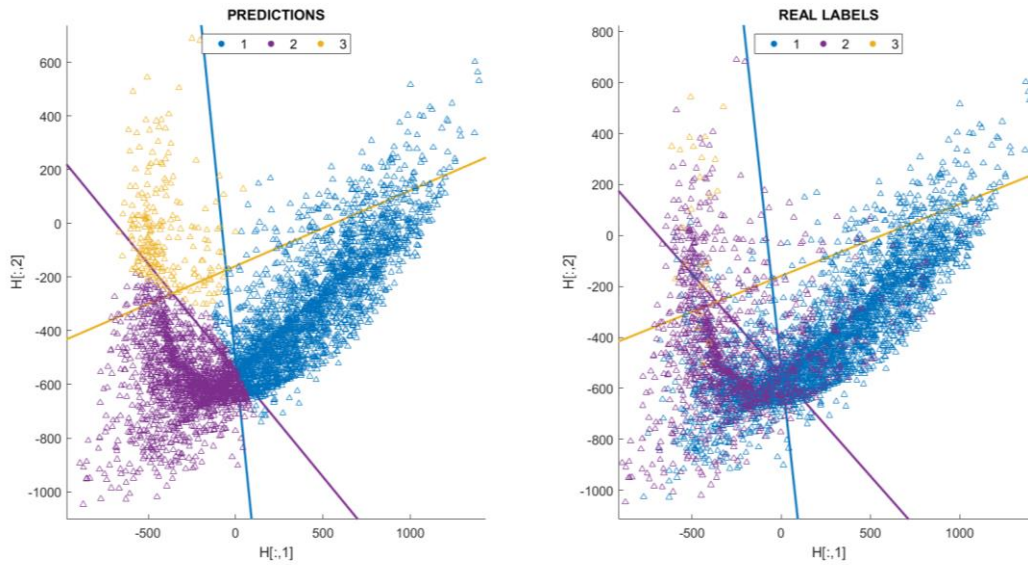


Figure 77: Test Phase of Model 3, on the left side the predictions of the algorithm are shown while on the right the correct labels

ACCURACY for the Church of Santa Caterina (Target Domain)

Model	Training Phase	Test Phase
Model 3	100 %	68.47 %

Table 26: Accuracy of Model 3 with domain Target 2, during training and test phase

ACCURACY test phase Model 3

Target Domain (Church of Santa Caterina)

Class 1 - label '1' ($T \in [0,10]^{\circ}C$)	Class 2 - label '2' ($T \in [10,20]^{\circ}C$)	Class 3 - label '3' ($T \in [20,\infty)^{\circ}C$)
69.33 %	65.49 %	84.00 %

Table 27: Accuracy for each class of Model 3 with domain Target 2, during test phase

Finally, it is possible to summarize the results, as reported in Table 28 and Figure 78, to understand the behavior of the accuracy by varying the amount of data of the Source Domain. From this chart it is possible to understand how, even if few data for the Target Domain are used for the training phase, the algorithm is able to generalize well for the new data provided during the test phase. The accuracy in this case is lower than the one of the previous case precisely because the model in this case is generated on the base of few data representative of the Church of Santa

Caterina and so the largest part of the training dataset is composed by information from the Sanctuary of Vicoforte, for this reason the accuracy in the test phase is smaller than case of Target 1, indeed the generated model generalizes worse for the data from the Church of Santa Caterina. At the same time, the accuracy for the data of the Church of Santa Caterina of the training phase is higher than the case of Target 1, this is due to the fact that in this phase the model has to classify only 30 observations, the same observation on which the model was generated. While, as before it can be observed how the accuracy remain practically unvaried even if the observations of the Source Domain increase, this is justifiable as previously, the information about the limits of the classes are already present from the smallest source domain, so adding more data the information, from a practical point of view of the algorithm, are not increasing.

<i>ACCURACY for the Church of Santa Caterina (Target Domain)</i>		
<i>Model</i>	<i>Training Phase</i>	<i>Test Phase</i>
Model 1	96.67 %	68.64 %
Model 2	96.70 %	67.80 %
Model 3	100 %	68.47 %

Table 28: Summary of the accuracies obtained during the accuracy analysis for the domain Target 2

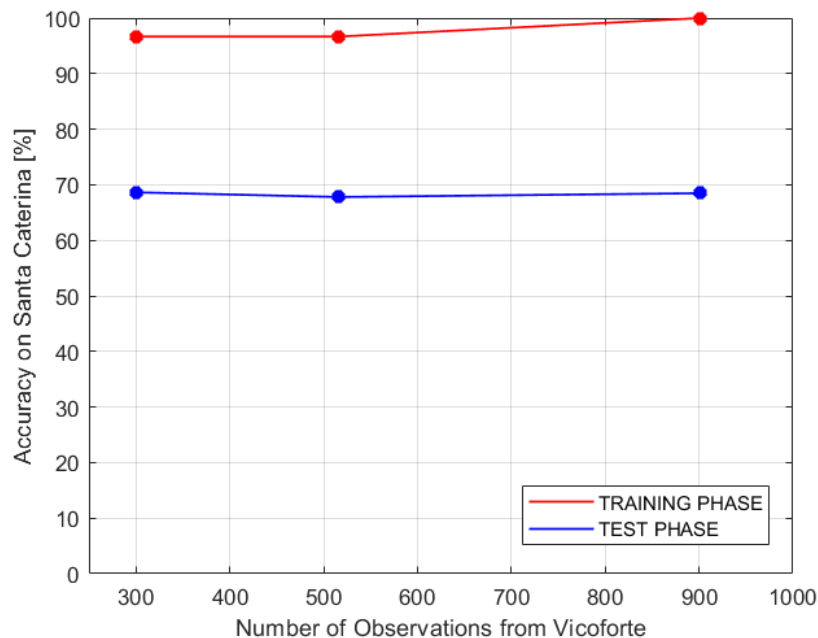


Figure 78: Accuracy trend on target domain predictions during the training phase (red) and test phase (blue)

5.2 Case study – Identification of four temperature classes

In this subchapter the problem of classification among four temperature classes is presented. Here, the natural frequencies of the Sanctuary of Vicoforte are used to implement the accuracy in the predictions for data of the Church of Santa Caterina. To increase the complexity of the problem, classes of temperature higher and lower than 0 degrees are considered. To demonstrate the improvement in the performance the same classification problem is performed firstly with a simple SVM ML and then with the KBTL, which is a domain adaptation algorithm in which the classifier used is conceptually a SVM classifier.

For what concern the frequencies of the Sanctuary of Vicoforte the same presented in *paragraph 5.1.1* are used here. While, for what concern the frequencies of the Church of Santa Caterina some additional considerations have to be performed in order to obtain realistic values of the frequencies also for the negative temperature.

5.2.1 ‘Semi-Experimental’ data for the Church of Santa Caterina

In this subchapter some details about the frequencies of the Church of Santa Caterina are reported. These frequencies are ‘*semi-experimental*’ values since they have been obtained starting from three known points in the plane temperature-frequency. From these three values the behavior of the first five frequencies of the Church f_1, f_2, f_3, f_4 and f_5 have been obtained, as reported in *paragraph 5.1.2*, with a linear interpolation (order of the polynomial $N = 1$) and with a Gaussian noise proportional to the standard deviation obtained from the three known measurements ($n = 1$). However, these three inputs information regard only positive temperatures, therefore the behavior defined starting from these three points cannot be used also for the negative temperatures, indeed what can be observed from the experimental frequencies of the Sanctuary of Vicoforte is that their behavior strongly change moving from negative temperatures to positive ones; to observe this behavior, please refer to *paragraph 2.1.3*, Figure 13. Thanks to different studies present in the literature it can be observed how the behavior of the frequencies for positive temperature can follow different path (descending or increasing), while for the negative temperature it has always been observed that with the increment of temperature the frequencies follow a descending path. This can be due to the fact that with the decreasing of temperature, more ice appears in the structure and introduce an increment in the structure rigidity (Coletta, Monitoring of architectural heritage with machine learning methods, 2022). From these observations, it is assumed a linear behavior also for the negative temperatures, which has the double

inclination with respect to the one of the positive temperatures and with a slope always negative. Then the points cloud is obtained with the same Gaussian noise used for the positive temperatures. In Figure 79 and Figure 80 the representation of the *frequency – temperature laws* obtained for the five natural frequencies is shown.

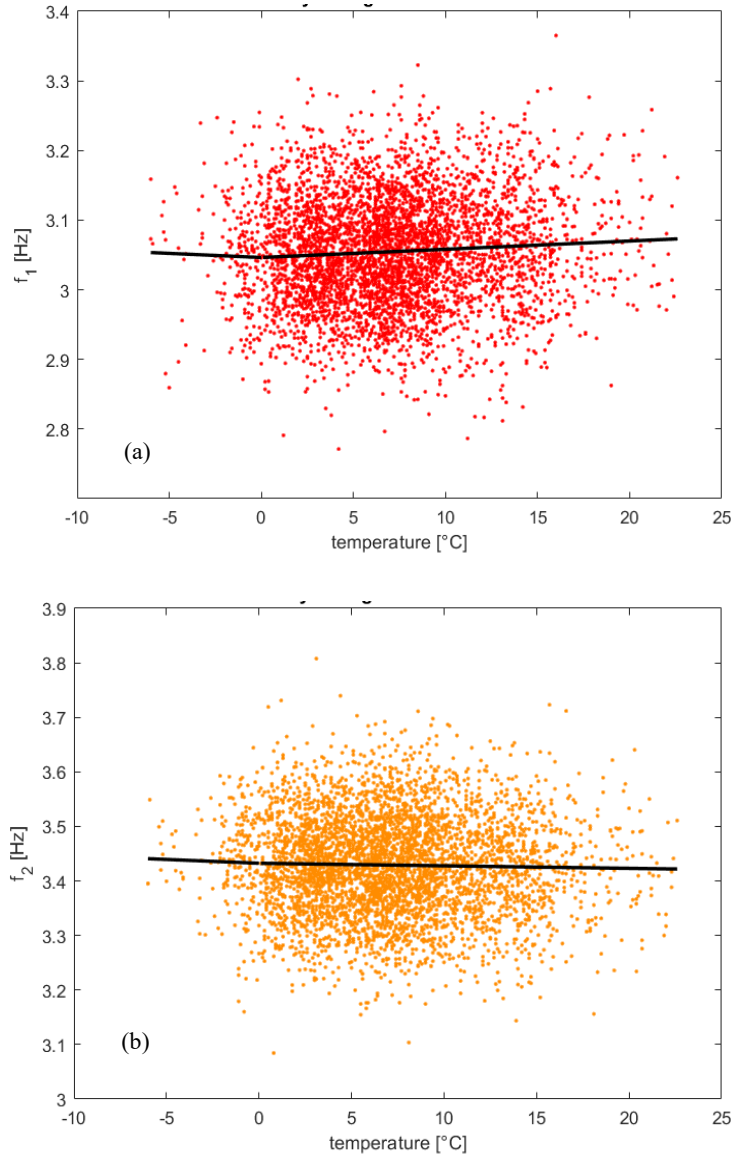


Figure 79: Simulated bi-linear frequency-temperature law for the natural frequencies of the Church of Santa Caterina, (a) f_1 and (b) f_2

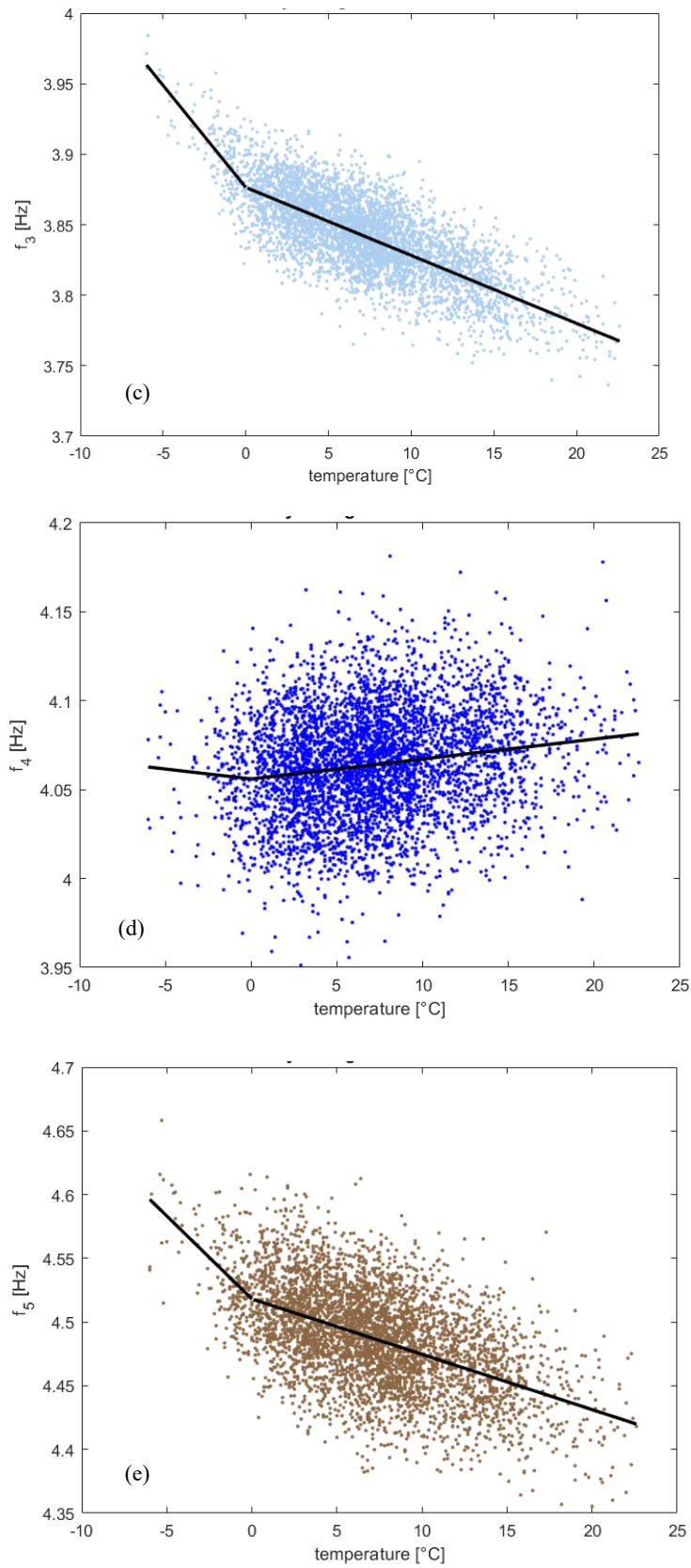


Figure 80: Simulated bi-linear frequency-temperature law for the natural frequencies of the Church of Santa Caterina, (c) f_3 , (d) f_4 and (e) f_5

5.2.2 Domains and Labels

For this classification problem the following classes of temperature T are considered:

- ~ Class 0: $-3^{\circ}\text{C} \leq T \leq -1^{\circ}\text{C}$ to which *label '0'* is assigned.
- ~ Class 1: $3^{\circ}\text{C} \leq T \leq 6^{\circ}\text{C}$ to which *label '1'* is assigned.
- ~ Class 2: $10^{\circ}\text{C} \leq T \leq 13^{\circ}\text{C}$ to which *label '2'* is assigned.
- ~ Class 3: $16^{\circ}\text{C} \leq T \leq 19^{\circ}\text{C}$ to which *label '3'* is assigned.

The Target Domain for the training phase is representative of the Church of Santa Caterina and it is composed by the three features f_1, f_3 and f_5 with five observations for each class. Only these three frequencies are considered since the first one is the most stable while the other two are the more sensible to the temperature variations. On the other hand, the Source Domain for the training phase is composed by the three features f_1, f_2 and f_3 , with 40 observations for class 1, class 2 and class 3 while no observations are introduced for the class 0, since all the frequency-temperature laws of the Sanctuary of Vicoforte present a ‘V’ shape in correspondence of the 0°C and therefore there is an overlapping between the frequencies that represent a positive temperatures and those representing the negative ones, hence this class will only confuse the algorithm. In Table 29 and Table 30 a summary of the classes and the number of observations used for the training phase of the two possible algorithms are reported.

OBSERVATIONS-TRAINING PHASE				
<i>for SVM (ML)</i>				
DOMAIN	Labels			
	$y = 0$	$y = 1$	$y = 2$	$y = 3$
Target (Church of Santa Caterina)	5	5	5	5

Table 29: Number of observations for each class for the Domain of the Church of Santa Caterina used for the Training Phase of a simple ML algorithm, the SVM

OBSERVATIONS-TRAINING PHASE				
<i>for KBTL</i>				
DOMAINS	Labels			
	$y = 0$	$y = 1$	$y = 2$	$y = 3$
Target (Church of Santa Caterina)	5	5	5	5
Source (Sanctuary of Vicoforte)	0	40	40	40

Table 30: Number of observations for each class for the dataset used for the Training Phase of the KBTL, the dataset is here composed by two Domains, Target and Source

For the test phase only data representative of the Church of Santa Caterina are used to verify the increment of the performance for the predictions; in Table 31 the number of observations for each classes are reported.

OBSERVATIONS-TEST PHASE				
<i>(for both SVM and KBTL)</i>				
<i>DOMAIN</i>	<i>Labels</i>			
	<i>y = 0</i>	<i>y = 1</i>	<i>y = 2</i>	<i>y = 3</i>
<i>Target</i> <i>(Church of Santa Caterina)</i>	60	60	60	60

Table 31: Number of observations for each class for the test phase of both the algorithm, SVM and KBTL

In Figure 81 and Figure 82 the training and test domains from the Church of Santa Caterina are visible, indeed the points circled in red represent the training dataset, while all the other the test dataset.

In Figure 83 and Figure 84 the additional information obtained from the Sanctuary of Vicoforte and used for the training of the KBTL are shown.

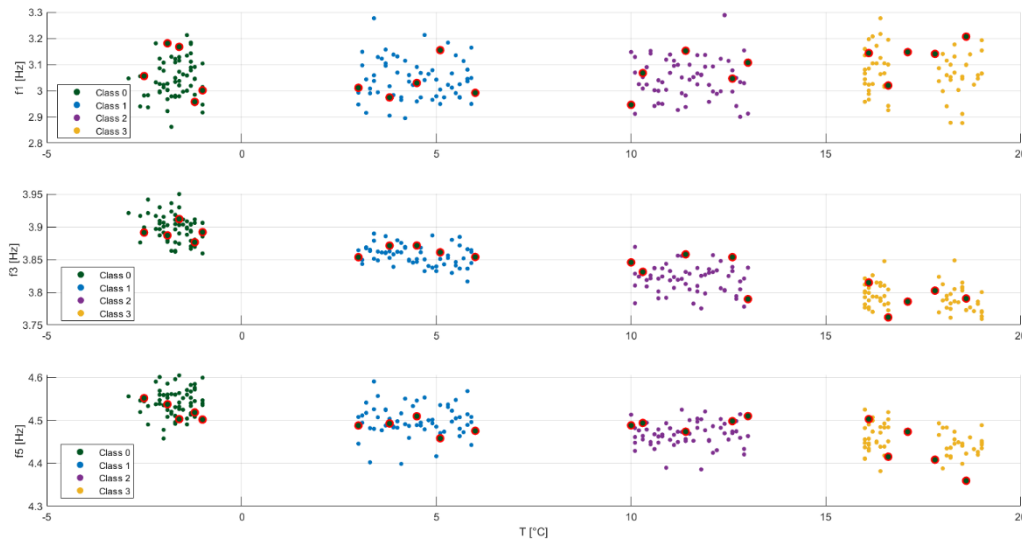


Figure 81: Training and Test dataset for the Church of Santa Caterina in the planes frequency-temperature, the points circled in red are data used for the training of the algorithms, all the other are part of the test dataset

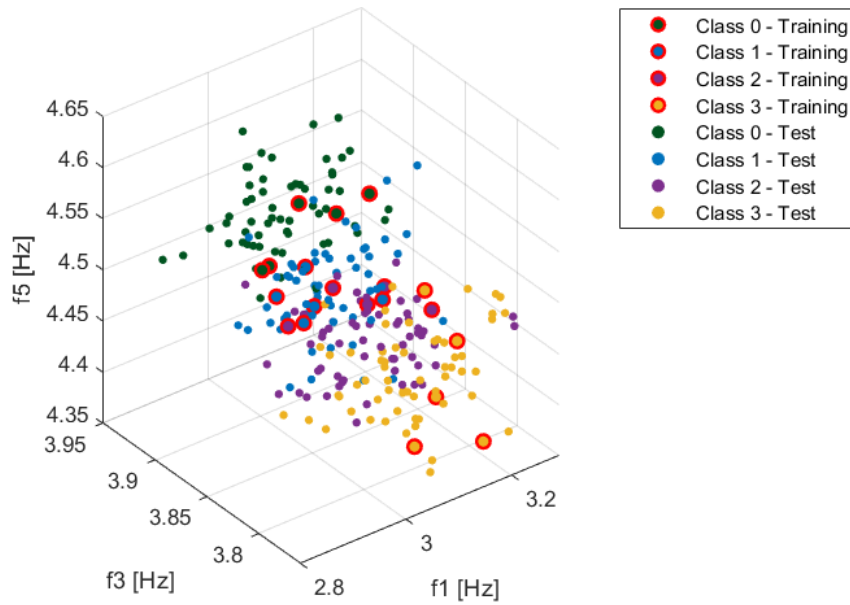


Figure 82: Training and Test dataset for the Church of Santa Caterina

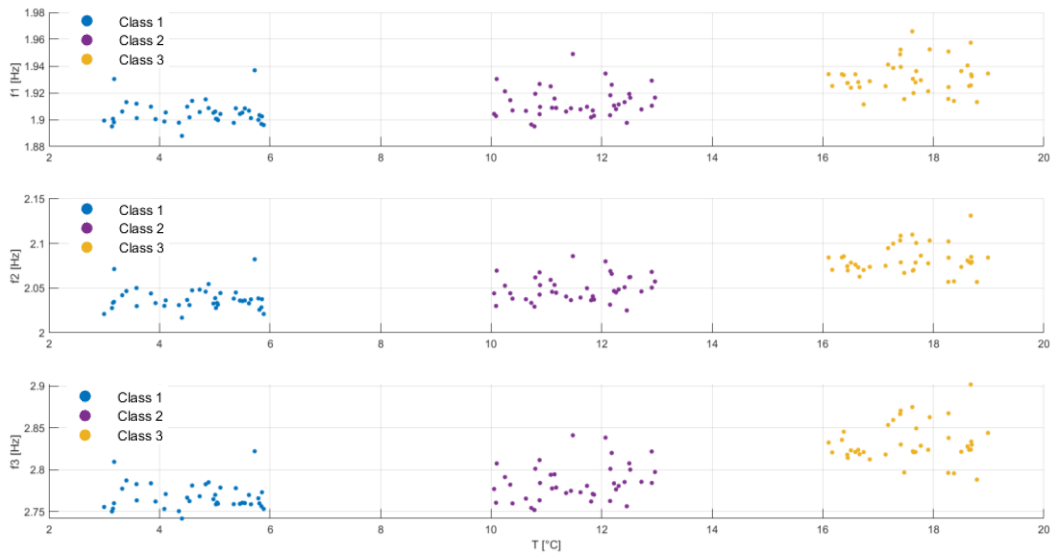


Figure 83: Source Domain (Sanctuary of Vicoforte), plotted in the planes frequency-temperature, used for the training phase of the KBTL

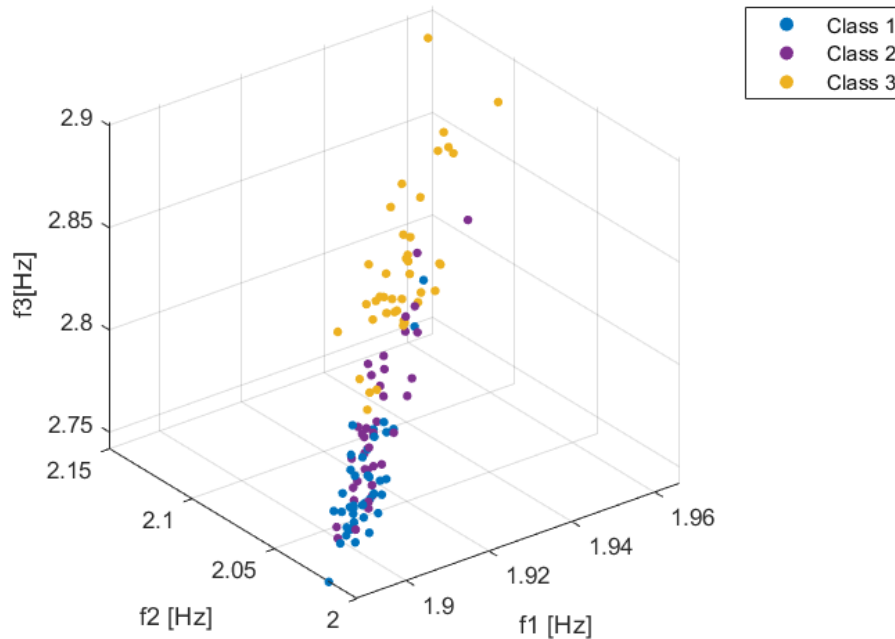


Figure 84: Source Domain plotted in the space f_1 - f_2 - f_3 used for the training of the KBTL

5.2.3 Results

Firstly, a SVM algorithm is used to classify the data of the Church of Santa Caterina, by training it only on the twenty observations available for the training phase (five for each class). The SVM algorithm used is the one present in the *MATLAB Toolbox* ‘*Classification Learner*’ that tries to define different linear margins to separate the four classes presented in the training phase, in order to use them later for classification of new data. With this model an accuracy of 55.00 % is reached during the training phase, and an accuracy of 67.50 % is reached with the test phase. In Table 32 the confusion matrix of the test phase is presented, from which it is possible to evaluate the accuracy of the prediction for each class. From the confusion matrix it is possible to observe how the model tends to favor the *class 0*, performing poorly on the other classes where several errors become apparent, hence only the *class 0* reaches a good accuracy, all the other reach too small values. In this condition, it can be understood that this model does not perform in a proper way, hence another AI technique must be used in order to improve the performance of the model predictions.

0	56	4	0	0
1	9	33	18	0
2	0	14	38	8
3	0	1	24	35
	0	1	2	3

Predicted Class

Table 32: Confusion Matrix of the Test Phase of the SVM model, obtained with the MATLAB Toolbox Classification Learner

For the reason declared above, the KBTL is applied with a training dataset composed by the twenty observations from the Church of Santa Caterina (Target Domain) and those, without *class 0*, from the Sanctuary of Vicoforte (Source Domain). Several models have been developed by varying the hyper-parameters within the interval $[10^{-3}, 10^{-1}]$ due to the small sample sizes in the two domains. Among all the tested sets of hyper-parameters, the one used for the final model implies the highest computed accuracy, for the prior of the optimal projection matrix the hyper-parameters used are $(\alpha_\lambda, \beta_\lambda) = (10^{-1}, 10^{-1})$, for the prior of the weights vector are $(\alpha_\eta, \beta_\eta) = (10^{-1}, 10^{-1})$ and for the prior of the bias parameter are $(\alpha_\gamma, \beta_\gamma) = (10^{-1}, 10^{-1})$. Then, 1500 iterations are performed, a standard deviation of the shared latent subspace σ_h equal to 0.15 is used and the non-negative margin ν is fixed equal to 0. In Figure 85 the training phase is plotted, in this figure two plots of the domains in the shared latent subspace are visible, the one on the left shows the data of the domains colored with color representative of the '*predicted labels*', while the one on the right shows the data colored with color representative of the '*correct labels*'. The two structures can be distinguished thanks to the two different symbols used, the star * for the Source Domain and the triangle Δ for the Target one, while the four classes can be distinguished by the different colors used, green for *label '0'*, blue for *label '1'*, purple for *label '2'* and

yellow for *label '3'*. Subsequently, in Figure 86 the test phase is shown, the plot is composed in the same way of the training phase, '*predicted labels*' on the left and '*correct labels*' on the right. With this model an accuracy of the 80.00 % is reached during the training phase and an accuracy of 75.00% is reached during the test phase. In Table 33 the confusion matrix of the KBTL test phase is shown.

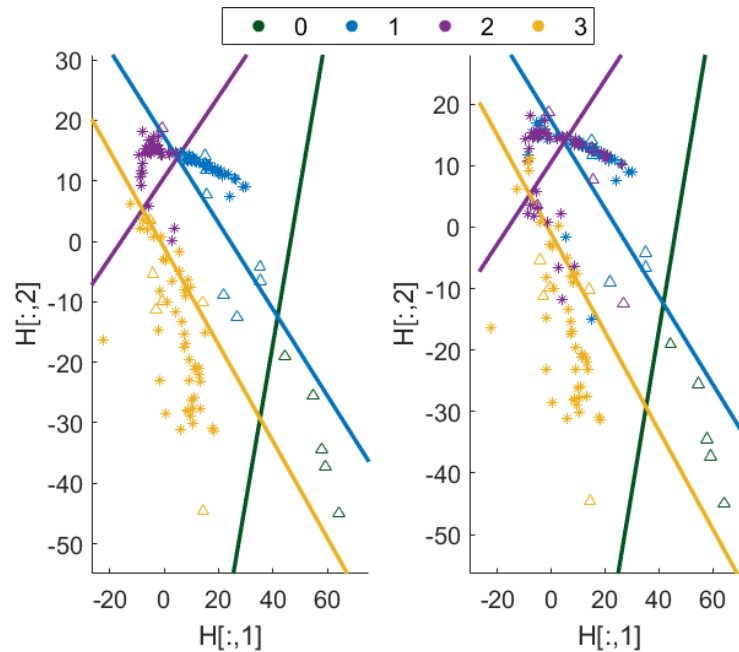


Figure 85: Training Phase of the KBTL model for the classification of four different temperature states

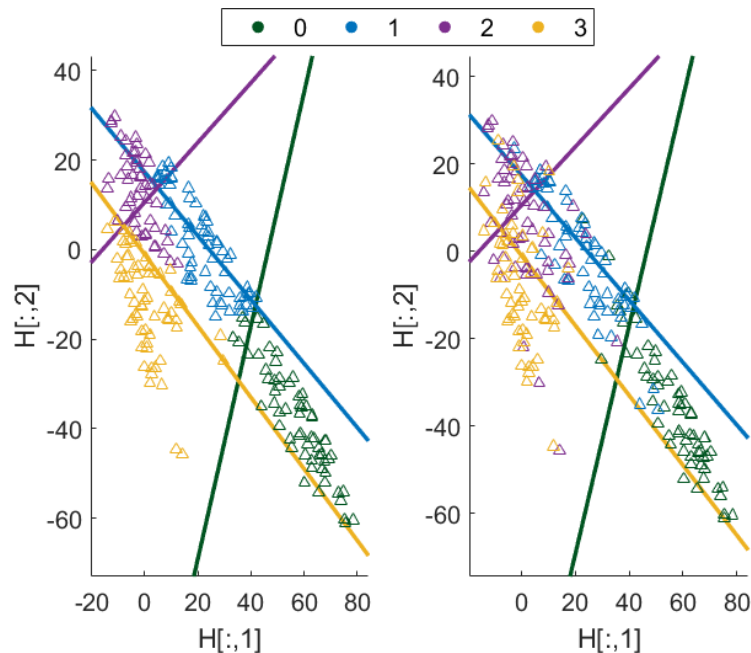


Figure 86: Test Phase of the KBTL model for the classification of four different temperature states

0	54	6	1	0
1	5	49	9	2
2	0	4	32	13
3	1	1	18	45
	0	1	2	3

Table 33: Confusion Matrix of the Test Phase of the KBTL model

In Table 34 the comparison between the accuracies obtained with SVM and those obtained with KBTL is shown. From this table it is possible to identify an increment in the accuracy, during the test phase, of 7.50 percentage points, passing from a simple SVM to the KBTL. From a practical point of view the KBTL can be described as a SVM model inferred in a shared latent subspace obtained with a dimensionality reduction and projection of the original domains by using a Domain Adaptation approach; hence, performing previously a simple SVM in the original space of the domain of the Church of Santa Caterina and then in a space that has been obtained with a DA, this increment in the accuracy of the test phase can be read as the increment induced by the process of domain adaptation. In this way it is shown how the knowledge of the Sanctuary of Vicoforte can be useful in implementing that of the Church of Santa Caterina, despite the fact that the two churches present different dynamic responses. In addition, also an improvement of the accuracy of the training phase is visible passing from SVM model to the KBTL model, this increase is quite high, 25 percentage points, but is less important with respect to the increment of the test phase. Indeed, we are more interest in an improvement of the test accuracy instead of the training one, since during the test phase data that were never seen by the algorithm are provided to it in order to perform predictions.

At the same time, some variation in the accuracy on the prediction of each class are visible. Firstly, it can be observed how the accuracy of the different classes are more

homogenous in the KBTL model with respect to those of the SVM model, indeed three classes reach a quite good accuracy ($\geq 75.00\%$) and only one results as lower; while in the SVM model only the *class 0* reaches a very high accuracy while all the other are strongly lower ($\leq 63.30\%$). Therefore, the KBTL not only provides higher accuracy in the test phase, but also results in better homogeneity in the accuracies of individual classes, so there is not one class preponderating over the others. However, even in this case one class, *class 2*, remains an underdog with an accuracy of 53.33 %, which is prevalently confused with *class 1* and *class 3*.

<i>ACCURACIES</i>						
<i>MODEL</i>	<i>TRAINING</i>	<i>TEST</i>	<i>Test Phase</i>			
			<i>class 0</i>	<i>class 1</i>	<i>class 2</i>	<i>class 3</i>
<i>SVM</i>	55.00%	67.50%	93.30%	55.00%	63.30%	58.30%
<i>KBTL</i>	80.00%	75.00%	90.00%	81.67%	53.33%	75.00%
<i>Δacc</i>	25.00%	7.50%	-3.30%	26.67%	-9.97%	16.70%

Table 34: Comparison of the accuracies obtained in the training and test phases of the two models (*SVM* and *KBTL*)

Conclusions

In recent years, the field of Structural Health Monitoring has increasingly moved towards the use of artificial intelligence to implement and facilitate the detection of a suffer state of the structure. Machine Learning algorithms can be useful, where the dataset is labelled, to solve classification or regression problems. However, finding a labelled dataset is not a matter of course, especially if the label to which data needs to be associated is representative of a damage, since it is not possible to purposely damage a structure to obtain data representative of that damage in order to create an AI model that can predict it. It is with this in mind that the world of research has started to move towards Transfer Learning algorithms, specifically the ones with Domain Adaptation (DA) approaches. With these techniques one tries to exploit the knowledge of a better-known structure (Source Domain) to implement that of a less-known one (Target Domain), where these two structures must have some similarities and depending on these, the domains can define a homogeneous or a heterogenous population. The transfer of knowledge is developed at level of the diagnostic characteristics, also defined as features, that are characteristics extrapolated from the results of the monitoring activities, static or dynamic. Since the dynamic activities are less invasive and more representative of the global response and global integrity of the structure, the diagnostic characteristics are often the natural frequencies obtained with an identification process on the signal recorded on site, which are representative of the dynamic response of the structure to environmental excitations.

In literature several examples of DA can be found, where knowledge is transferred between fairly regular structures, such as shear-frames whose seismic response is well known and similar, while there are few cases in which these techniques are applied to full-scale structure health monitoring systems.

In this thesis applications of transfer learning techniques to data from full-scale structure health monitoring systems have been developed, where the structures under consideration are churches characterized by oval domes, but with strongly distinct plan and elevation developments, thus generating a heterogeneous population. In a first phase, only data simulated on the FEM of the structures have been used in order to understand if the transfer of knowledge from the domain of the Sanctuary of Vicoforte to the domain of the Church of Santa Cateria is possible for the damage detection and the identification of the damage level. What has been observed is that this transfer of knowledge is possible and that it is also possible to perform a sort of *meta-optimization* of the algorithm in such a way to obtain a model that among all the errors has the highest percentage of false positive instead of false negative. Indeed, it is well known that it is practically impossible to obtain a model that has a prediction accuracy of 100%, so it is necessary to accept the presence of

errors. However, when we are dealing with the identification of a damaged or healthy condition, it can be seen how it is detrimental to confuse a damaged condition with a healthy one (false negative error), while it is far less problematic to confuse a healthy condition with a damaged one (false positive error). Therefore, if we know that the error will be present it is necessary to try to govern the algorithm, by managing the hyper-parameters, in order to obtain a model that will tend to provide as few errors as possible, and that among these errors there are more false positives than false negatives. Hence, it can be concluded, from this first study, how the control of the algorithm hyper-parameters is important not only to minimize the percentage of error but also to govern these same mistakes to really improve the performance of the model. This problem of meta-optimization will be of fundamental importance when the identification of the damage with AI will be applied in practice on real structures, as a real support to engineers for the maintenance over time of the structure and the consequent design of the improvement or retrofitting interventions.

Even if the effectiveness of the transfer of knowledge and the government of the hyper-parameters to improve the performance of a model have been demonstrated with this first study on simulated data, a second study, more connected to the reality, is necessary in order to approach more and more to the objective of permitting the transfer of knowledge between data deriving from different real structures. Indeed the simulated data are “cleaner” than any data obtained from the monitoring activities on the real structure, this because the model, however calibrated, is a simplification of the reality as many environmental factors are difficult to be inserted in it. Therefore, a second study has been presented to generate a transfer of knowledge between the experimental data of the Sanctuary of Vicoforte and the 'semi-experimental' data, as obtained from three data identified in field, of the Church of Santa Caterina. However it is important to highlight that, unlike the previous case, here the data are representative of states of temperatures since the two real structures are currently in a healthy state. Anyway, in this phase the ability of the KBTL to improve the performance of the classifier has been demonstrated compared to the case in which the simple SVM classifier (ML method) has been applied exclusively to the Target Domain, the one of the less known structure, the Church of Santa Caterina. Since the classifier within the KBTL code is analogous to an SVM classifier, it can be concluded that the improvement that occurs with the application of the KBTL is due to the fact that in the training phase not only the same data of the Target Domain provided to the simple SVM, but also all the data of the Source Domain (Sanctuary of Vicoforte) have been provided to the algorithm. Therefore, “*the cause*” of the increase in predictive capabilities of the model obtained with KBTL can be associated with the presence of data from the Sanctuary of Vicoforte and consequently it can be understood how the transfer of knowledge

is not only feasible also between data obtained from the two real structures but results in an increase in the prediction accuracy of 7.5 percentage points.

In conclusion, in this thesis the effectiveness of the transfer of knowledge between two quite different structures has been demonstrate together with the importance in the control of the errors to obtain a model that can reduce false negatives compared to false positives. However, further analyses and tests are required, specifically the first analysis that will be necessarily developed is practically the same of the study case developed for the temperatures states but using in the training phase the real experimental data of the Church of Santa Caterina, that are currently under a clustering process. Then additional researches will be necessary to overcome the obstacle represented by the lack of labelled data; in this view the hybrid approaches may be useful as they could allow the compensation of the lack of knowledge about damaged conditions from the real structure by obtaining such data from its FE model appropriately calibrated, but in this case the problem of the fluctuation of the natural frequencies induced by the environmental agents, such as temperature and humidity, must be kept in consideration since a pathological variation cannot be confused with a physiological one (false negative error), in this view the regression model could be useful.

List of Abbreviations

AHS: Architectural Heritage Structure
AI: Artificial Intelligence
CH: Cultural Heritage
DA: Domain Adaptation
FE: Finite Element
FEM: Finite Element Model
FN: False Negative
FP: False Positive
KBTL: Kernelized Bayesian Transfer Learning
ML: Machine Learning
PBSHM: Population-Based Structural Health Monitoring
RBF: Radial-Basis Function
RKHS: Reproducing Kernel Hilbert Space
RVM: Relevance Vector Machine
SD: Source Domain
SHM: Structural Health Monitoring
SVM: Support Vector Machine
TCA: Transfer Component Analysis
TD: Target Domain
TL: Transfer Learning
TN: True Negative
TP: True Positive

References

- Ceravolo, R. (2022). Structural and seismic monitoring of historical and contemporary buildings: general principles and applications. *Assembly of the class of mathematical, physical and natural sciences*.
- Ceravolo, R., Coletta, G., Miraglia, G., & Palma, F. (2021). Static correlation between environmental time series and data from long-term monitoring of buildings. *Mechanical Systems and Signal Processing*, 152, 107460. doi:<https://doi.org/10.1016/j.ymssp.2020.107460>
- Ceravolo, R., De Lucia, G., Miraglia, G., & Pecorelli, M. (2020). Thermoelastic finite element model updating with application to monumental buildings. *Computer-Aided Civil and Infrastructure Engineering*, 35(6), 628-642. doi:<https://doi.org/10.1111/mice.12516>
- Ceravolo, R., De Marinis, A., Pecorelli, M., & Zanotti Fragonara, L. (2017). Monitoring of masonry historical constructions: 10 years of static monitoring of the world's largest oval dome. *Structural Control and Health Monitoring*, 24(10).
- Ceravolo, R., Lenticchia, E., Miraglia, G., & Scussolini, L. (n.d.). Calibration of dynamical models for the seismic upgrading of historical buildings: application to the church of Santa Caterina in Casale Monferrato (in press). *IJAH*.
- Ceravolo, R., Pistone, G., Zanotti Fragonara, L., Masetto, S., & Abbiati, G. (2016). Vibration-Based Monitoring and Diagnosis of Cultural Heritage: A Methodological Discussion in Three Examples. *International Journal of Architectural Heritage*, 10(4), 375-395. doi:[10.1080/15583058.2013.850554](https://doi.org/10.1080/15583058.2013.850554)
- Classificatore vs Regressione quale usare? Machine learning esempi pratici*. (n.d.). Retrieved from *Intelligenza Artificiale Italiana*: <https://www.intelligenzaartificialeitalia.net/post/classificatore-vs-regressione-quale-usare-machine-learning-esempi-pratici>
- Coletta, G. (2022). *Monitoring of architectural heritage with machine learning methods*. Doctoral Program in Architectural and Landscape Heritage (34th Cycle), Torino.
- Coletta, G., Miraglia, G., Gardner, P., Ceravolo, R., Surace, C., & Worden, K. (2021). A Transfer Learning Application to FEM and Monitoring Data for Supporting the Classification of Structural Condition States. In *European Workshop on Structural Health Monitoring - Special Collection of 2020 Papers - Volume 1* (pp. 947-957). Springer International Publishing. doi:https://doi.org/10.1007/978-3-030-64594-6_91

-
- Delua, J. (2021, March 12). *Supervised vs. Unsupervised Learning: What's the Difference?* Retrieved from IBM blog: <https://www.ibm.com/blog/supervised-vs-unsupervised-learning/>
- Farrar, C. R., & Worden, K. (2012). *Structural Health Monitoring, A Machine Learning Perspective*. John Wiley & Sons. doi:10.1002/9781118443118
- Gardner, P., Bull, L. A., Dervilis, N., & Worden, K. (2022). On the application of kernelised Bayesian transfer learning to population-based structural health monitoring. *Mechanical Systems and Signal Processing*, 167, 108519. doi:<https://doi.org/10.1016/j.ymsp.2021.108519>.
- Gardner, P., Bull, L. A., Gosliga, J., Dervilis, N., & Worden, K. (2020, october 28). Towards population-based structural health monitoring, Part IV : heterogeneous populations, transfer and mapping. In *Model Validation and Uncertainty Quantification, Volume 3: Proceedings of the 38th IMAC, A Conference and Exposition on Structural Dynamics 2020* (pp. 187-199). Springer International Publishing. doi:https://doi.org/10.1007/978-3-030-47638-0_20
- Gönen, M., & Margolin, A. (2014). Kernelized Bayesian Transfer Learning. *Proceedings of the AAAI Conference on Artificial Intelligence*, 28(1). doi:<https://doi.org/10.1609/aaai.v28i1.8948>
- Gosliga, J., Gardner, P. A., Bull, L. A., Dervilis, N., & Worden, K. (2021). Foundations of Population-based SHM, Part II: Heterogeneous - Graphs, networks, and communities. *Mechanical Systems and Signal Processing*, 148, 107144. doi:<https://doi.org/10.1016/j.ymsp.2020.107144>
- Gretton, A., Sejdinovic, D., Strathmann, H., Balakrishnan, S., Pontil, M., Fukumizu, K., & Sriperumbudur, B. K. (2012). Optimal kernel choice for large scale two-sample tests. *Advances in neural information processing systems*, 25, 1205-1213.
- GT, R. (2016, Giugno 1). *Piemonte barocco, alla scoperta del santuario di vicoforte, la basilica dei record*. Retrieved from Gazzetta di Torino: https://www.gazzettatorino.it/wordpress/santuario_di_vicoforte/
- ICOMOS. (2003). Recommendations For The Analysis, Conservation And Structural Restoration Of Architectural Heritage.
- Khan, S., Asim, M., Chelloug, S. A., Abdelrahiem, B., Khan, S., & Musyafa, A. (2023, May 28). A Novel Cluster Matching-Based Improved Kernel Fisher Criterion for Image Classification in Unsupervised Domain Adaptation. *Symmetry*, 15(6), 1163. doi:<https://doi.org/10.3390/sym15061163>
- Kundu, R. (2022, July 1). *Domain Adaptation in Computer Vision: Everything You Need to Know*. Retrieved from v7labs: <https://www.v7labs.com/blog/domain-adaptation->

guide#:~:text=Domain%20Adaptation%20is%20a%20technique,special%20case%20of%20transfer%20learning.

La Chiesa. (2021). Retrieved from Santa Caterina Onlus - Casale Monferrato: <https://www.santacaterinacasalemonferrato.it/>

Machine Learning with ML.NET – Complete Guide to Clustering. (n.d.). Retrieved from Rubik's Code - Building smart apps: <https://rubikscore.net/2021/02/08/machine-learning-with-ml-net-complete-guide-to-clustering/>

MathWorks. (n.d.). *Overfitting*. Retrieved from MathWorks: <https://it.mathworks.com/discovery/overfitting.html>

Nellihela, P. (2022, July 1). *What is K-fold Cross Validation?* Retrieved from Towards Data Science: <https://towardsdatascience.com/what-is-k-fold-cross-validation-5a7bb241d82f>

Rossi, M., & Bournas, D. (2023). Structural Health Monitoring and Management of Cultural Heritage Structures: A State-of-the-Art Review. *Applied Sciences*, 13(11), 6450. doi:<https://doi.org/10.3390/app13116450>

Yang, Y., Zhang, Y., & Tan, X. (2021). Review on Vibration-Based Structural Health Monitoring Techniques and Technical Codes. *Symmetry*, 13(11), 1998. doi: <https://doi.org/10.3390/sym13111998>

I would like to express my gratitude to Professor Rosario Ceravolo and to the researchers Giorgia Coletta, Gaetano Miraglia and Linda Scussolini for guiding me in the development of this work.

I want to express my thanks to my colleagues, Ilie, Marco and Matteo for their support, laughter and company of this past year.

I would like to say thank you to Rosario for being close to me during these five years, for understanding and supporting me, and for always being there.

I want to express my thank to my aunt, Sabrina, for supporting me on this path and for her good-luck messages before each exam.

And finally, I wish to thank my Mum, the woman who raised me and made me the person I am, who inspired me and always supported me.

Thanks also to Niche for sleeping in my arms during the preparation of all the exam sessions.